

This is the author's peer reviewed, accepted manuscript. However, the online version of record will be different from this version once it has been copyedited and typeset.

PLEASE CITE THIS ARTICLE AS DOI: 10.1063/5.0031138

Flow and thermal characteristics of three-dimensional turbulent wall jet

Priyesh Kakka¹ and Kameswararao Anupindi^{1,a)}

*Department of Mechanical Engineering, Indian Institute of Technology Madras, Chennai,
TN - 600036, India*

In the present work, a three-dimensional turbulent wall jet is simulated using large-eddy simulation (LES) to characterize its flow and thermal characteristics. The solver is first validated for streamwise velocity decay, wall-normal and spanwise spread rates, and mean and second-order flow statistics using reference experimental data from the literature. The mean vorticity transport equation (VTE) for the streamwise component is analyzed to identify the dominant terms that contribute to the large spanwise spread of the jet. The terms that contain Reynolds normal stresses are identified as major contributors towards a large mean streamwise component of vorticity. The mean streamwise and wall-normal components of vorticity are studied for their evolution and contribution towards the spanwise spread. It was found that both these components together aid in the large spanwise spread of the jet. The heat transfer characteristics are studied for the jet flow on a heated isothermal wall. The profiles of mean and fluctuating temperatures, the evolution of Nusselt number and turbulent heat flux characteristics are studied. The streamwise evolution of Nusselt number behavior is explained using instantaneous vortical structures. A significant drop in heat transfer is observed in the potential core region. Further, the turbulent heat flux contours show the transport of heat in the streamwise direction is different from that of the plane wall jet. A peculiar turbulent heat transport was found in the analysis of the spanwise heat flux. The heat transfer characteristics noted for the three-dimensional wall jet may help in the design and analysis of film-cooling applications.

⁵ **Keywords:** Large-eddy simulation (LES), turbulent wall jet, heat transfer, vorticity

^{a)}kanupindi@iitm.ac.in

This is the author's peer reviewed, accepted manuscript. However, the online version of record will be different from this version once it has been copyedited and typeset.

PLEASE CITE THIS ARTICLE AS DOI: 10.1063/5.0031138

NOMENCLATURE

| | |
|-----------------|---|
| C | Model coefficients |
| L | Length of the domain |
| Nu | Nusselt number |
| $^{10} Pr$ | Prandtl number |
| Re | Reynolds number |
| S | Strain rate tensor |
| T | Temperature |
| U_o | Jet inlet velocity |
| $^{15} \Omega$ | Vorticity |
| h | Jet inlet height |
| p | Pressure |
| q | Heat flux |
| t | Time |
| $^{20} u, v, w$ | Instantaneous velocity |
| u_τ | Friction velocity in streamwise direction |
| w_τ | Friction velocity in spanwise direction |
| y^+ | Inner-scaled wall normal length |

Abbreviations

| | |
|-------------|---------------------------------|
| $^{25} DNS$ | Direct Numerical Simulation |
| LDV | Laser Doppler Velocimetry |
| LES | Large-Eddy Simulation |
| LESIQ | LES Index of resolution Quality |
| PIV | Particle Image Velocimetry |
| $^{30} POD$ | Proper Orthogonal Decomposition |
| RANS | Reynolds-averaged Navier-Stokes |

This is the author's peer reviewed, accepted manuscript. However, the online version of record will be different from this version once it has been copyedited and typeset.

PLEASE CITE THIS ARTICLE AS DOI: 10.1063/5.0031138

| | |
|-----|------------------------------|
| SGS | Sub-Grid Scale |
| VTE | Vorticity Transport Equation |

Subscripts

| | | |
|----|-----------|-------------------------|
| 35 | i, j, k | Free indices |
| | k | Total kinetic energy |
| | rms | Root mean square |
| | sgs | Sub-grid scale quantity |
| | t | Turbulent quantity |
| 40 | x, y, z | Directions |

Greek symbols

| | | |
|----|----------|---------------------|
| | α | Thermal diffusivity |
| | Δ | Grid size |
| | δ | Kronecker delta |
| 45 | ν | Kinematic viscosity |
| | τ | SGS stress tensor |

Superscripts

| | | |
|----|------------------------|------------------------|
| | $\langle \phi \rangle$ | Time averaged quantity |
| | $\bar{\phi}$ | Filtered quantity |
| 50 | ϕ' | Fluctuating quantity |

This is the author's peer reviewed, accepted manuscript. However, the online version of record will be different from this version once it has been copyedited and typeset.

PLEASE CITE THIS ARTICLE AS DOI: 10.1063/5.0031138

I. INTRODUCTION

Three-dimensional turbulent wall jets display several interesting features and as a result attracted the attention of researchers. Some of these features include higher spanwise spread rate when compared to wall-normal spread rate, establishment of mean secondary flow, and a composite wall-bounded and free shear layer behavior. Turbulent wall jets can be found in several engineering applications such as drying¹, car defrosters², film-cooling of gas turbine and combustor liners³, occupational ventilation systems⁴, to name a few. Due to the numerous application of the jets as described, various studies with a focus on the development of the jet in different scenarios like the confined jet impingement⁵, counter flowing jet⁶, and the dynamics in the submerged offset jet⁷ etc., have been carried out. Similarly, three-dimensional jets have been extensively researched where, one of the earliest experimental measurements for three-dimensional wall jets were conducted by Sforza and Herbst⁸. They concluded that sufficiently far downstream the spread rate of the jet in the wall-normal direction and the centerline velocity decay of the jet are independent of the shape of the nozzle-exit through which the jet is issued. Newman *et al.*⁹ considered a sufficiently long domain to obtain a fully developed flow and performed measurements. They found the wall-normal spread rate in three-dimensional wall jet to be smaller when compared to planar wall jet, however, the streamwise turbulence intensity is noted to be higher in the former case. They further concluded that the spread rate in the spanwise direction to be higher than in the wall-normal direction for three-dimensional wall jet. Rajaratnam and Pani¹⁰ experimentally investigated the effects of nozzle exit shapes on the flow characteristics such as the growth rate of the jet, turbulent shear stress profiles, and jet centerline velocity decay. Later, Sun and Ewing¹¹ studied the effects of the inflow conditions on the development of three-dimensional wall jets for circular jet exit Reynolds numbers of 65000 and 10800. They noted that the various inflow conditions that were used have no effect on the jet growth rate, mean velocity profiles, Reynolds stress profiles and mean stream-wise velocity contours. Hall and Ewing¹² performed experiments for rectangular wall jets with different aspect ratio. They concluded that the characteristic crescent-shaped structure can be used to identify the far-field region of the jet. Further, Agelin-Chaab and Tachie¹³ investigated the three-dimensional wall jet using particle image velocimetry (PIV). They considered three circular jet exit Reynolds numbers of 5000, 10000 and 20000 and found that the centerline velocity decay, the wall-normal and the spanwise spread rates are independent of the Reynolds number in the region defined by $52 \leq x/d \leq 100$. They obtained self-similar turbulence intensity profiles by $x/h \approx 65$

This is the author's peer reviewed, accepted manuscript. However, the online version of record will be different from this version once it has been copyedited and typeset.

PLEASE CITE THIS ARTICLE AS DOI: 10.1063/5.0031138

for a Reynolds number of 5000, whereas by $x/h \approx 40$ for the other two Reynolds numbers. Owing to a disparity in background turbulence levels, they observed higher turbulence intensities when compared to the then existing experimental results available in the literature. Padmanabham and Lakshmana Gowda¹⁴, Abrahamsson, Johansson, and Löfdahl¹⁵ and Law and Herlina¹⁶, Law *et al.*¹⁷ also experimentally investigated turbulent wall jet flows. Ai *et al.*¹⁸ compared vortex characteristics and its development due to different shaped nozzles in the free jets while, Godi, Pattamatta, and Balaji^{19,20} performed experiments and RANS simulations for three-dimensional wall jets at different nozzle exit Reynolds numbers as well as nozzle shapes to study their effects on the Nusselt number.⁹⁰

In one of the earliest review work Launder and Rodi²¹ performed a comprehensive review of turbulent wall jets and provided estimates for wall-normal and spanwise growth rates. Further, the spanwise spread rate was noted to be approximately 5.5 times the wall-normal spread rate and this was attributed to the presence of a mean secondary flow. In a later work, Launder and Rodi²² further pointed out the presence of strong sustained stream-wise vorticity as the primary reason for the prevailing mean secondary flow. Further insights into the evolution of stream-wise vorticity were obtained by analyzing the various terms of the mean stream-wise component of vorticity transport equation, given as follows:

$$\frac{\partial \langle \Omega_x \rangle}{\partial t} + \underbrace{\langle u \rangle \frac{\partial \langle \Omega_x \rangle}{\partial x} + \langle v \rangle \frac{\partial \langle \Omega_x \rangle}{\partial y} + \langle w \rangle \frac{\partial \langle \Omega_x \rangle}{\partial z}}_{A} = \underbrace{\langle \Omega_x \rangle \frac{\partial \langle u \rangle}{\partial x} + \langle \Omega_y \rangle \frac{\partial \langle u \rangle}{\partial y} + \langle \Omega_z \rangle \frac{\partial \langle u \rangle}{\partial z}}_{B} + \underbrace{\nu \left(\frac{\partial^2 \langle \Omega_x \rangle}{\partial y^2} + \frac{\partial^2 \langle \Omega_x \rangle}{\partial z^2} \right)}_{F}, \\ + \underbrace{\frac{\partial^2 \langle v'^2 \rangle}{\partial y \partial z} - \frac{\partial^2 \langle w'^2 \rangle}{\partial y \partial z}}_{D1} - \underbrace{\frac{\partial^2 \langle w'^2 \rangle}{\partial y \partial z}}_{D2} + \underbrace{\frac{\partial^2 \langle v'w' \rangle}{\partial z^2} - \frac{\partial^2 \langle v'w' \rangle}{\partial y^2}}_{E1} - \underbrace{\frac{\partial^2 \langle v'w' \rangle}{\partial y^2}}_{E2} + \nu \left(\frac{\partial^2 \langle \Omega_x \rangle}{\partial y^2} + \frac{\partial^2 \langle \Omega_x \rangle}{\partial z^2} \right), \quad (1)$$

where $\langle u \rangle$ is the mean (time-averaged) stream-wise velocity, $\langle \Omega_x \rangle$, $\langle \Omega_y \rangle$ and $\langle \Omega_z \rangle$ indicate the mean vorticity components in the x , y and z -directions respectively, v' and w' indicate the fluctuating velocity components in the y and z -directions respectively, and ν indicates the viscosity of the fluid, x , y and z denote the three Cartesian directions and t indicates time. The term enclosed by B is responsible for vortex stretching of the mean vorticity, and the two terms represented by C are responsible for vortex line bending. Vorticity production is obtained because of the Reynolds stress terms enclosed by D and E, and the terms enclosed by F are responsible for the diffusion of vorticity¹⁰⁵.

This is the author's peer reviewed, accepted manuscript. However, the online version of record will be different from this version once it has been copyedited and typeset.

PLEASE CITE THIS ARTICLE AS DOI: 10.1063/5.0031138

due to viscosity. In the analysis the authors make an assumption that the line bending term along with the Reynolds stress terms are important for the generation of vorticity and contribute to the spanwise spread of the wall jet. Craft and Launder²³ investigated various terms in the mean stream-wise vorticity transport equation (VTE) using a laminar three-dimensional wall jet and concluded
110 that vortex line bending (term-C) does not contribute significantly to the spanwise spreading, and therefore, the terms containing Reynolds stresses (terms D and E) must be responsible for the higher spanwise spread of the wall jet.

Further, Namgyal and Hall²⁴ investigated the near-field region of three-dimensional wall jets with circular inlet, using proper orthogonal decomposition (POD) and studied the effect of stream-wise vortex structures on the mean secondary flow. They found that the vortex structures closer to the wall are primarily responsible for the spanwise spread and the secondary flow in three-dimensional wall jets. In a subsequent work, Namgyal and Hall²⁵ extended the earlier work done by Craft and Launder²³ to characterize the Reynolds stress terms in the mean stream-wise VTE. They found that the Reynolds normal stress terms, $\langle v'^2 - w'^2 \rangle$, given by term-D in eq. 1, are indeed
120 dominant when compared to the Reynolds shear stress terms, $\langle v'w' \rangle$, given by term-E in eq. 1, in a magnitude sense. They, however, could not calculate the required second spatial derivatives to evaluate the terms D and E; owing to the large oscillations that may arise while evaluating second derivatives for the measurements near the walls. Panidis, Schwab, and Pollard²⁶ extended the earlier work on free jets by Vouros *et al.*²⁷ to a rectangular wall jet with an aspect ratio of 10.
125 Unlike previous experimental works, Panidis, Schwab, and Pollard²⁶ tried to study the effects of each of the terms of eq. 1 on the flow behavior. In studying these effects the authors used vorticity budgets and analyzed the effect of the presence of wall by comparing them with those obtained using free jets. Similar to Namgyal and Hall²⁵, Panidis, Schwab, and Pollard²⁶ also found that the Reynolds normal stresses have a larger magnitude, however, they missed to obtain the relevant data
130 required for evaluating term-E in eq. 1, and therefore they recommended further investigations to be performed to evaluate the term-E. They found that the Reynolds stresses have a larger magnitude but missed the data on the term-E in eq. 1 and hence, recommended that an investigation should be carried out based on the missing terms. Most of the aforementioned experiments focused on the flow physics of three-dimensional wall jet, and as experiments might be uncertain while
135 calculating double spatial gradients of the terms involved in eq. 1 as differentiation amplifies the noise present as suggested by Namgyal and Hall²⁵. Moreover, many experiments were unable to capture near-wall characteristics because of inheriting difficulties in the measurement process.

This is the author's peer reviewed, accepted manuscript. However, the online version of record will be different from this version once it has been copyedited and typeset.

PLEASE CITE THIS ARTICLE AS DOI: 10.1063/5.0031138

Therefore, Panidis, Schwab, and Pollard²⁶ suggested to perform numerical simulations to evaluate the several terms involved in the mean stream-wise VTE – and this is one of the motivations of the
140 present study – which will further help in understanding the effects of stream-wise vorticity on the spanwise flow development of wall jets.

Wall jets are a commonplace in film-cooling of gas-turbine blades. Intricate shapes of the gas-turbine blades and parametric sweeps of the designs require accurate numerical simulations to analyze the heat transfer characteristics and performance of the blade designs. Towards this
145 end, Naqavi, Tyacke, and Tucker^{28, 29} analyzed the flow and heat transfer characteristics for a planar wall jet using direct numerical simulation (DNS) based on the experiments performed by Rostamy *et al.*³⁰. Further Ahlman, Brethouwer, and Johansson³¹ did similar analysis on planar jet for passive scalar at lower Reynolds number, and the study was extended for non-isothermal jets with different co-flow combinations^{32, 33}. As DNS requires prohibitive computational resources, researchers in
150 the past instead used large-eddy simulation (LES). Dejoan and Leschziner³⁴ performed LES for planar wall jet and analyzed the resulting flow characteristics. Kakka and Anupindi³⁵ assessed the effects of different subgrid-scale (SGS) models that are used in LES. They evaluated different SGS models in terms of their capability to accurately predict flow and thermal characteristics. They concluded that Smagorinsky model coupled with van-Driest near-wall damping function accurately
155 predicts the near-wall thermal characteristics. Coming to the three-dimensional wall jets, Zhang, Law, and Zhao³⁶ performed LES using Smagorinsky model and also compared the results with those obtained using two different Reynolds-averaged Navier-Stokes (RANS) models. Further, they analyzed the behavior of various terms in the scalar transport equation to demonstrate the capabilities of LES. However, they did not provide a comprehensive analysis of heat transfer and
160 other thermal properties.

A review of the experimental and computational studies suggests that there are only a few studies that focused on thermal characterization of three-dimensional wall jets. Therefore, the present work aims to perform a comprehensive analysis of flow and heat transfer characteristics for three-dimensional wall jets using LES. As mentioned earlier, another contribution of the present
165 work is to characterize each of the terms in the mean stream-wise VTE, eq. 1, and study their near-wall behavior.

The remainder of the paper is organized as follows. The relevant governing equations, details of the numerical methods, geometry and the mesh used along with the appropriate boundary and initial conditions are discussed in Section II. Section III presents the grid sensitivity study,

This is the author's peer reviewed, accepted manuscript. However, the online version of record will be different from this version once it has been copyedited and typeset.

PLEASE CITE THIS ARTICLE AS DOI: 10.1063/5.0031138

- ¹⁷⁰ validation of the solver and the main results. Detailed analysis of mean stream-wise VTE, wall shear stresses, spanwise and wall-normal profiles of mean and second-order statistics for both flow and thermal quantities, and profiles of Nusselt number are also discussed in this section. The paper is concluded in Section IV and some directions for future work are suggested.

¹⁷⁵ II. GOVERNING EQUATIONS AND NUMERICAL METHODS

A. Details of the domain and boundary conditions

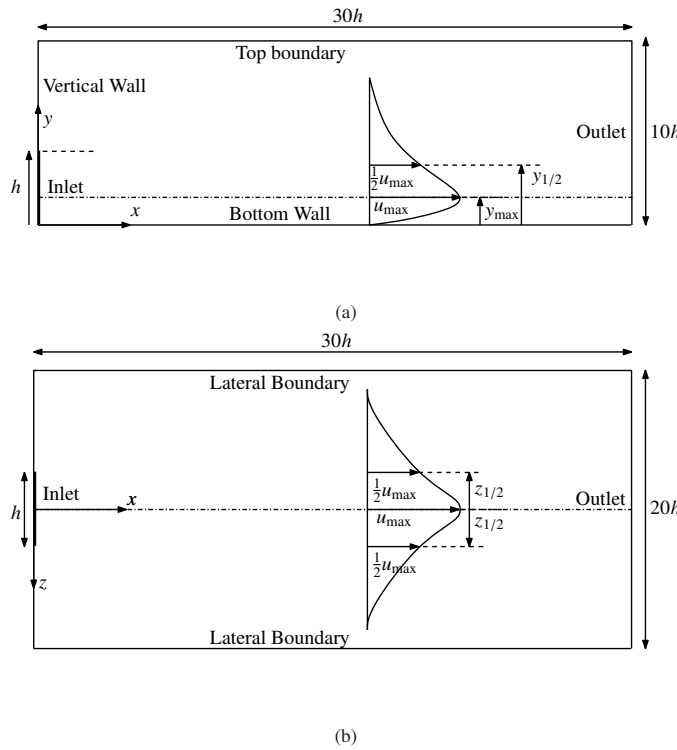


FIG. 1. Schematic of domain together with boundary conditions (a) front view (b) top view.

The domain used in the present simulations is shown in frames (a) and (b) of figure 1 for front view and top view respectively. The computational domain extends \$30h\$ in the \$x\$-direction, \$10h\$

in the y -direction, and $20h$ in the z -directions, where h is the side of the square shaped nozzle
¹⁸⁰ exit through which the jet is issued. The x , y and z directions are also referred as stream-wise,
 wall-normal and spanwise directions respectively. Figure 1 also depicts the typical mean velocity
 profiles for the x -component of velocity as functions of y and z in frames (a) and (b) respectively.

The top view is plotted on xz -plane at a height of $y = y_{max}$. The location y_{max} corresponds to
¹⁸⁵ a height where a local maximum for streamwise component of velocity, u_{max} is obtained. While
 the location $y_{1/2}$ is the height at which the local streamwise component of velocity, u is half that
 of the local maximum streamwise component of velocity, u_{max} . With reference to this figure, on
 the Inlet boundary a uniform mean velocity profile together with random fluctuations with 0.25%
 intensity are used.

A non-reflective boundary condition is applied on the Outlet boundary as shown in eq. 2, where
¹⁹⁰ u_n is the velocity normal to the boundary (convection speed) and n denotes the unit normal vector
 to the boundary. Considering a physical quantity represented by ϕ , the non-reflective boundary
 condition or advective boundary condition can be written as follows,

$$\frac{\partial \phi}{\partial t} + u_n \frac{\partial \phi}{\partial n} = 0. \quad (2)$$

An impermeable and no-slip boundary condition for velocity is applied on the Bottom Wall, which
 can be written as, $u_i = 0$, where u_i denotes the velocity vector. On the Top Boundary a zero-
¹⁹⁵ gradient boundary condition for velocity is applied, which can be represented as, $\frac{\partial u_i}{\partial n} = 0$, where
 n is the unit normal vector to the Top Boundary. On the Vertical Wall boundary, a no-slip and
 impermeable boundary condition for velocity, represented by $u_i = 0$, and an adiabatic boundary
 condition for temperature, represented by $\frac{\partial T}{\partial n} = 0$, are applied. Zero-gradient boundary condition
²⁰⁰ $\frac{\partial p}{\partial n} = 0$ for pressure is used at the Inlet and on all the walls. In the spanwise direction periodic
 boundary conditions are applied for all variables on the Lateral Boundary shown in frame (b).

B. Large-eddy simulation (LES) equations

The governing equations pertinent to the problem under consideration are the filtered incompressible continuity, Navier-Stokes and the energy equations obtained from Pope³⁷ are given as follows:

$$\frac{\partial \overline{u_i}}{\partial x_i} = 0, \quad (3)$$

This is the author's peer reviewed, accepted manuscript. However, the online version of record will be different from this version once it has been copyedited and typeset.

PLEASE CITE THIS ARTICLE AS DOI: 10.1063/5.0031138

205

$$\frac{\partial \bar{u}_i}{\partial t} + \frac{\partial}{\partial x_j} (\bar{u}_i \bar{u}_j) = -\frac{\partial((\bar{p}/\rho)\delta_{ij} + \tau_{ij})}{\partial x_j} + \nu \frac{\partial^2 \bar{u}_i}{\partial x_j \partial x_i}, \quad (4)$$

where \bar{u}_i is the filtered velocity, \bar{p} is the filtered pressure, ρ is the fluid density, ν is the kinematic viscosity and $\tau_{ij} = \bar{u}_i \bar{u}_j - \bar{u}_i \bar{u}_j$ is the SGS stress tensor and t denotes time. The SGS stress tensor is modeled using Boussinesq hypothesis and can be expressed as follows

$$\tau_{ij} = -2\nu_t \bar{S}_{ij} + \frac{1}{3}\tau_{kk}\delta_{ij}, \quad (5)$$

where δ_{ij} is the Kronecker delta function, ν_t is the turbulent viscosity, and \bar{S}_{ij} is the filtered strain rate tensor given by $\frac{1}{2} \left(\frac{\partial \bar{u}_i}{\partial x_j} + \frac{\partial \bar{u}_j}{\partial x_i} \right)$. The filtered energy equation can be written as follows:

$$\frac{\partial \bar{T}}{\partial t} + \frac{\partial}{\partial x_j} (\bar{T} \bar{u}_j) = \alpha \frac{\partial^2 \bar{T}}{\partial x_j \partial x_i} + \frac{\partial q_j}{\partial x_j}, \quad (6)$$

where $q_j = \bar{T} \bar{u}_j - \bar{T} u_j$ is the turbulent heat flux that needs to be modeled. In the present work an eddy-diffusivity model is used that models the turbulent heat flux similar to eddy-viscosity. Using this model, the turbulent heat flux can be defined as $\bar{q}_j = \alpha_t \frac{\partial \bar{T}}{\partial x_j}$, where α_t is the eddy diffusivity and is evaluated using turbulent Prandtl number and turbulent viscosity as $\alpha_t = \frac{\nu_t}{Pr_t}$. On the other hand, the molecular diffusivity is defined as $\alpha = \frac{\nu}{Pr}$. In the present study the Prandtl number Pr is taken as 0.71 for air. The values of α_t are calculated based on the values of ν_t and Pr_t . The turbulent Prandtl number, Pr_t , is taken to be a constant value and is equal to 0.85. Further, the values of ν_t are obtained using a particular SGS model. In the present work the constant coefficient Smagorinsky model is used. According to this model ν_t can be obtained using filtered velocity field as follows,

$$\nu_t = \left(C_s \Delta^2 \right) |\bar{S}|, \quad (7)$$

where $|\bar{S}|$ is the magnitude of filtered strain rate tensor given by $|\bar{S}| = \sqrt{2\bar{S}_{ij} \bar{S}_{ij}}$, Δ is the filter width, and C_s is the constant of the model which is taken as 0.168 in the present work. The filter width, Δ , used in the present LES calculations is taken to be equal to cube-root of the volume of each cell given by, $(\Delta_x \Delta_y \Delta_z)^{1/3}$, where Δ is the grid size, and the subscript denotes the corresponding direction. One of the shortcomings of the constant coefficient Smagorinsky model is that the turbulent viscosity, ν_t , does not decay to zero as one approaches the wall. In order to address this problem, near wall van-Driest damping function was used. This damping function modifies

This is the author's peer reviewed, accepted manuscript. However, the online version of record will be different from this version once it has been copyedited and typeset.

PLEASE CITE THIS ARTICLE AS DOI: 10.1063/5.0031138

the definition of the local filter-width, Δ , which further properly damps the turbulent viscosity. The definition of Δ is modified by choosing a minimum of $\frac{\kappa y}{C_s} D$ and Δ where the value of D is calculated as, $D = 1 - \exp\left(\frac{-y^+}{A^+}\right)$. The coefficients used are $A^+ = 26$, $C_s = 0.1$ and $\kappa = 0.41$.

C. Details of the solver and numerical methods

In the present work, OpenFOAM^{38,39} version 5.0 is used to integrate the LES equations. The incompressible, filtered, unsteady Navier-Stokes equations together with the energy equation are discretized and solved using an implicit pressure-based PIMPLE algorithm. Second-order accurate central differencing schemes are used to discretize all the spatial derivatives and second-order accurate Crank-Nicolson scheme is used for time integration.

The jet exit Reynolds number, Re , is defined based on the magnitude of the uniform velocity profile at the jet exit, u_{max} , and the width of the square nozzle, h , and is equal to 7500. The length of the domain, $30h$, used in the present study is deemed to be sufficient as self-similar profiles are observed beyond $x \approx 20h$. A time scale t^* is introduced using L/u_o . Here, L is the domain length in the streamwise direction and u_o is the average inlet velocity. Hence, the non-dimensional time step $(\Delta t)/t^*$ used to integrate the equations comes out to be 0.0038 and the dimensional time step (Δt) used is 10^{-4} seconds. All the statistics presented in this work are collected for a period of $50t^*$, after discarding an initial transient time of $11t^*$.

The domain is discretized using 10.54 million cells with a distribution of $250 \times 222 \times 190$ cells in each of the streamwise, wall-normal and spanwise directions respectively. About 100 cells are used to accurately resolve the flow in the wall-normal direction in the region enclosed by $0 \leq y/h \leq 1$. The first cell-centroid away from the wall is ensured to satisfy the condition $y^+ \leq 1$. To capture the jet spread accurately in the spanwise direction, the mesh is made finer near the nozzle exit (inlet to the domain) and is made coarser as one moves away further downstream. A structured, orthogonal and non-uniform mesh with grid-stretching away from the inlet is used for all the simulations. All the contours plots and the three-dimensional figures in the present manuscript are produced using Paraview⁴⁰ software and the line plots are produced using gnuplot⁴¹ software.

This is the author's peer reviewed, accepted manuscript. However, the online version of record will be different from this version once it has been copyedited and typeset.

PLEASE CITE THIS ARTICLE AS DOI: 10.1063/5.0031138

III. RESULTS AND DISCUSSION

The primary focus of this work is to assess the capability of LES in capturing the spread of three-dimensional wall jet, quantify and study the effect of streamwise and wall-normal components of vorticity on the spanwise spread of the jet and discuss the effect of its flow dynamics on the heat transfer characteristics.

A. Grid sensitivity study

1. Grid sensitivity study

In this section, the grid sensitivity of the solver is established. Three different mesh resolutions consisting of 8.32 million, 10.54 million and 12.21 million cells are considered. The profile of mean u velocity as a function of y is shown in figure 2(a). In this figure, the mean u velocity is normalized using the local maximum u velocity, and the y coordinate is normalized using $y_{1/2}$.

The values used for normalization of u , y and z for different grids are shown in Table I.

TABLE I. The values used for normalizing u , $y_{1/2}$ and $z_{1/2}$ for each grid.

| Grid size | $u_{max}(m/s)$ | $y_{1/2}(m)$ | $z_{1/2}(m)$ |
|---------------|----------------|--------------|--------------|
| 12.21 million | 4.47 | 0.017 | 0.032 |
| 10.54 million | 4.52 | 0.014 | 0.030 |
| 8.32 million | 4.37 | 0.02 | 0.028 |

The profile of mean turbulent kinetic energy, $\langle k \rangle$, as a function of y is shown in figure 2(b) for the three mesh resolutions considered. From these two figures it can be noted that there are no appreciable changes in the results for mean velocity and for mean turbulent kinetic energy as the mesh is made finer. In the near-wall region, all the meshes shows a good overlap for mean u velocity. Away from the wall, the finest mesh shows some deviation in results in the range of $1.2 \leq y/y_{1/2} \leq 2$ when compared to the other two mesh resolutions. However, as the near-wall mesh is the region of interest in the present study, the effect of these slight deviations could be neglected. The profiles of mean u velocity and mean turbulent kinetic energy, $\langle k \rangle$, as a function of the spanwise coordinate, z , are shown in figures 3(a) and 3(b) respectively. From these two figures it can be noted that the mesh resolutions considered show a good overlap. To strike a balance between an optimum grid size and capturing all the necessary features, the mesh resolution with

This is the author's peer reviewed, accepted manuscript. However, the online version of record will be different from this version once it has been copyedited and typeset.

PLEASE CITE THIS ARTICLE AS DOI: 10.1063/5.0031138

10.54 million cells is selected to perform all further analysis.

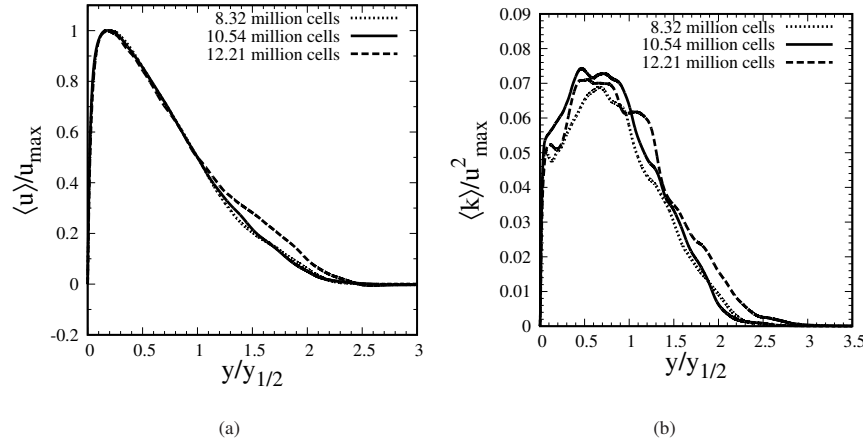


FIG. 2. Mean profiles of (a) streamwise velocity (b) turbulent kinetic energy, as a function of y extracted at the location $x/h = 20$ and $z = 0$ for three different mesh resolutions considered.

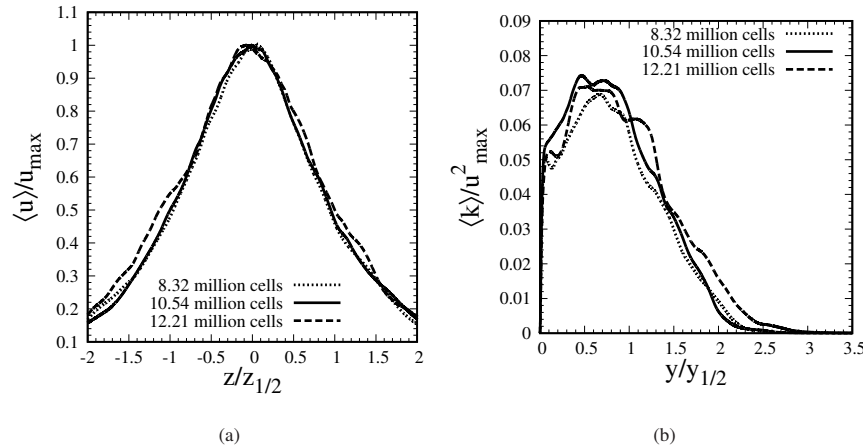


FIG. 3. Mean profiles of (a) streamwise velocity (b) turbulent kinetic energy, as a function of z extracted at the location $x/h = 20$ and $y = y_{\max}$ for three different mesh resolutions considered.

2. LES index of resolution quality

The quality of mesh used for LES can be further checked based on the fraction of turbulent energy that the mesh resolves. According to Pope³⁷, in an LES, approximately 80 percent of the total energy in the flow should be resolved by the grid employed. Based on this criteria, a metric to quantify the mesh used was suggested by Celik, Klein, and Janicka⁴² in terms of LES index of resolution quality (IQ). Celik, Klein, and Janicka⁴² define $LESIQ_v$ based on the kinematic viscosity of the fluid, ν , and the total effective viscosity, $\nu_{t,eff}$ of the fluid, as follows:

$$LESIQ_v = \left[1 + \alpha_v \left(\frac{\langle \nu_{t,eff} \rangle}{\nu} \right)^n \right]^{-1}. \quad (8)$$

According to Celik, Klein, and Janicka⁴², a mesh is said to be well resolved when $LESIQ_v$ for that particular mesh is above 0.8 in most of the domain where there is a presence of turbulent flow. The $LESIQ_v$ metric is computed for the mesh size of 10.54 million cells and is shown in figures 4(a) and 4(b) for xz and xy -planes respectively. From these figures it can be noted that the values of $LESIQ_v$ in the entire domain are more than 0.9, which indicates that the mesh with 10.54 million cells sufficiently resolves the turbulent energy. The values of α_v and n are taken as 0.05 and 0.53 in the present work.

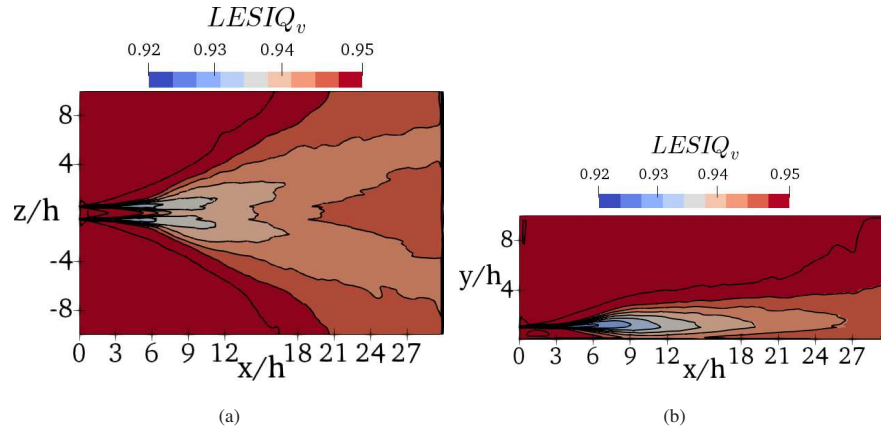


FIG. 4. Contours of $LESIQ_v$ a) on xz -plane at a height $y = 0.5h$ b) on xy -plane on the jet centerline.

This is the author's peer reviewed, accepted manuscript. However, the online version of record will be different from this version once it has been copyedited and typeset.

PLEASE CITE THIS ARTICLE AS DOI: 10.1063/5.0031138

B. Flow properties and their validation

Next, the flow solver is validated for three-dimensional wall jet. The parameters such as the velocity decay, spread rate, profiles of Reynolds stresses are compared for the present results and reference experimental data. The streamwise evolution of maximum u velocity along the jet centerline is shown in figure 5 for the present simulations as well for the results obtained by Sun and Ewing¹¹ and Namgyal and Hall²⁵. The maximum u velocity is normalized using the inlet u velocity, u_0 . It can be noted that as one moves downstream the maximum u velocity decays closely following the indicated experimental results.

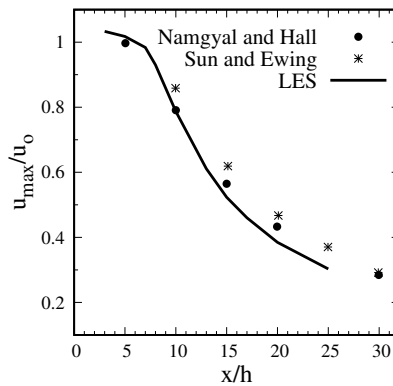


FIG. 5. Streamwise evolution of maximum u velocity along the jet centerline $z/h = 0$.

The spread rate of the jet can be measured by looking at the evolution of half-widths in the wall-normal and spanwise directions. The wall-normal half-width, $y_{1/2}$, at any streamwise location on the jet centerline, $z = 0$, is defined as the y location where the local u velocity is half the maximum u velocity along the y line at that location. Similarly, the spanwise half-width, $z_{1/2}$, at any streamwise location on the $y = y_{max}$ line is defined as the location where the local u velocity is half the maximum u velocity along the z line at that location. The streamwise evolution of wall-normal and spanwise spread rates are shown in figures 6(a) and 6(b) respectively for the present results and for the experimental results^{11,25}. From these figures it can be noted that the spread rates (slope of the $y_{1/2}$ and $z_{1/2}$ lines) follow the ones reported by experiments. The wall-normal spread rate, $\frac{\Delta y_{1/2}}{\Delta x}$, for the present simulations calculated for the region $15 \leq x/h \leq 25$ is 0.0443.

This is the author's peer reviewed, accepted manuscript. However, the online version of record will be different from this version once it has been copyedited and typeset.

PLEASE CITE THIS ARTICLE AS DOI: 10.1063/5.0031138

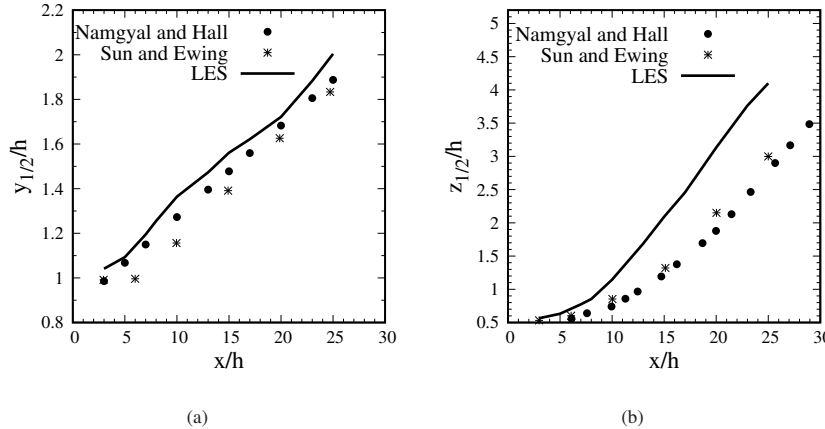


FIG. 6. Streamwise evolution of (a) wall-normal (b) spanwise spread rates.

- 310 The wall-normal spread rate obtained by Namgyal and Hall²⁵ and Launder and Rodi²² are 0.041 and 0.048 respectively. It can be noted that the value obtained from present simulations lies in between the values reported by reference experiments^{22,25}. The values of spanwise spread rate, $\frac{\Delta z_{1/2}}{\Delta x}$, for the present simulations calculated for the region $15 \leq x/h \leq 25$ is 0.2271. The spanwise spread rate reported by Namgyal and Hall²⁵ is 0.2296 and this matches with the value obtained
315 in the present simulations. One of the most interesting features of three-dimensional wall jets is their large spanwise spread rate when compared to the wall-normal spread rate. Agelin-Chaab and Tachie¹³ pointed out a wide range of values being reported in the literature for the ratio of spanwise to wall-normal spread rates. The range of values reported in the literature¹³ for this ratio are 3.7 to 7.1. The ratio calculated for the present simulations is 5.12 and it lies within the range of values
320 mentioned in the literature¹³.

Next, a comparison of the mean and second-order statistics for the flow variables has been discussed. The mean u velocity profile as a function of the wall-normal direction on the jet centerline $z/h = 0$ is shown in figure 7(a) for the present results and for the experimental data reported by Agelin-Chaab and Tachie¹³ and Sun and Ewing¹¹. Similarly, the mean u velocity profile as a function of the spanwise direction at a height of $y = y_{max}$ is shown in figure 7(b) for the present results and for the reference data. From these two figures it can be noted that mean u velocity profiles are self-similar beyond $x/h = 20$ as the two profiles obtained for locations $x/h = 20$ and
325

This is the author's peer reviewed, accepted manuscript. However, the online version of record will be different from this version once it has been copyedited and typeset.

PLEASE CITE THIS ARTICLE AS DOI: 10.1063/5.0031138

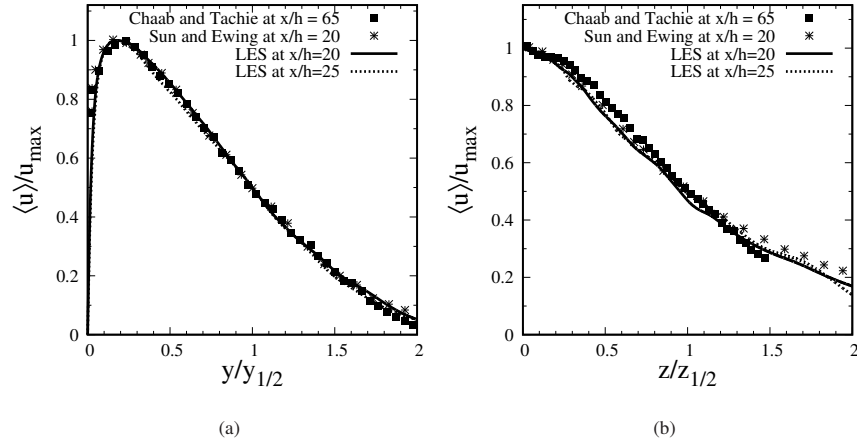


FIG. 7. Mean u velocity profile as a function of the (a) wall-normal direction on the jet centerline $z/h = 0$ (b) spanwise direction at a height of $y = y_{max}$, for the present results and for the indicated reference experiments.

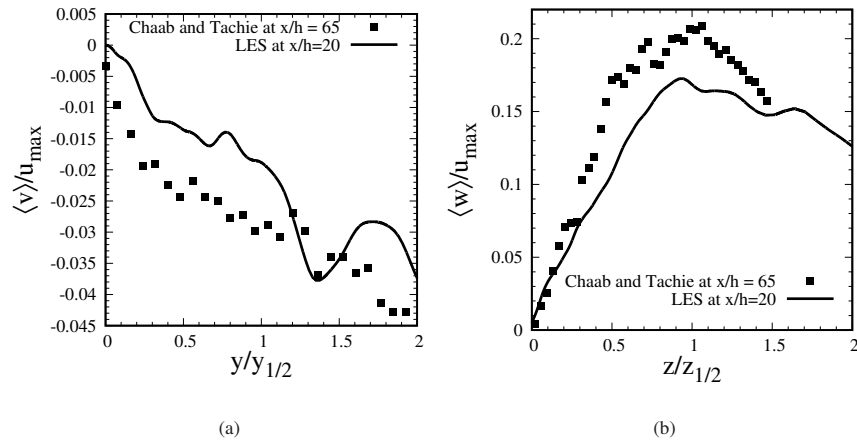


FIG. 8. (a) Mean v velocity profile as a function of y on the jet center line, $z/h = 0$ (b) mean w velocity profile as a function of z at a height of $y = y_{max}$; for the present simulation results at $x/h = 20$ and for the reference experimental data^[13].

$x/h = 25$ overlap. Further, it can be noted that a good match is observed between the present results and the reference experimental data^[11,13] for both the wall-normal and spanwise profiles. The mean

This is the author's peer reviewed, accepted manuscript. However, the online version of record will be different from this version once it has been copyedited and typeset.

PLEASE CITE THIS ARTICLE AS DOI: 10.1063/5.0031138

³³⁰ v velocity profiles as a function of the wall-normal direction on the jet centerline, $z/h = 0$, are shown in figure 8(a) for the present simulations and for the experiments reported by Agelin-Chaab and Tachie¹³. From this figure, it can be noted that the present results agree well with the data obtained by reference experiments. The v velocity profile indicates that as one approaches the wall in the y direction the v component of velocity is always directed towards the wall, in $0 < y/y_{1/2} \leq 2$
³³⁵ region, and its magnitude decreases and eventually reaches a zero value on the wall. The mean w velocity profile as a function of the spanwise direction at a height of $y = y_{max}$ is shown in figure 8(b) for the present simulations and for the reference experiments¹³. The w velocity is zero on the centerline, $z/h = 0$, and increases as one moves away from the centerline (in either direction), reaches a peak value around $z = z_{1/2}$ and thereafter starts to decrease. A good match
³⁴⁰ between the present results and reference data¹³ can be noted. Further, it can be observed that the w component of velocity are an order of magnitude larger than the v component of velocities at the same location.

Finally, as part of the validation, second-order statistics are compared. Mean Reynolds normal stress profiles as a function of the wall-normal and spanwise directions are shown in figures 9(a) and 9(b) respectively for the present results and for the reference experimental data reported by Sun and Ewing¹¹. The Reynolds normal stresses show an excellent match with the reference data. For the profiles in the wall-normal direction, it can be noted that, all the Reynolds normal stress components, $\langle u'u' \rangle$, $\langle v'v' \rangle$, and $\langle w'w' \rangle$ reach a value of zero near the wall and their maximum values are of the same order of magnitude. All the components start to decay beyond $y \geq y_{1/2}$.
³⁵⁰ Further it can be noted that $\langle u'u' \rangle$, and $\langle w'w' \rangle$ show sharp near-wall gradients when compared to $\langle v'v' \rangle$. For the profiles in the spanwise direction, shown in figure 9(b), a symmetry of the profiles about the jet centerline, $z/h = 0$, can be noted. All the components show a plateau till about $z \approx 0.7 \times z_{1/2}$ and start to decay thereafter. It can be noted that, $\langle u'u' \rangle$ profile shows the largest magnitude followed by $\langle w'w' \rangle$, whereas the $\langle v'v' \rangle$ show lowest magnitude throughout the
³⁵⁵ domain depicted. The mean Reynolds shear stress profiles as a function of the wall-normal and spanwise directions are shown in figures 10(a) and 10(b) respectively for the results obtained using the present simulations and the reference data obtained by Namgyal and Hall²⁵. It can be noted that $\langle u'v' \rangle$ profile shows the largest magnitude in the wall-normal direction profiles and $\langle u'w' \rangle$ profile shows the largest magnitude in the spanwise direction profiles. Overall, all the profiles
³⁶⁰ qualitatively show a good match with the reference data²⁵. However, there are also some deviations in resolving the peak values of these two shear stresses. The deviations in the magnitude of these

This is the author's peer reviewed, accepted manuscript. However, the online version of record will be different from this version once it has been copyedited and typeset.

PLEASE CITE THIS ARTICLE AS DOI: 10.1063/5.0031138

two shear stress components could be because of the background turbulence level present during the experiments, as pointed out by Agelin-Chaab and Tachie¹³. The nature of the profiles in the wall-normal and spanwise directions show similar trends to that of the experimental results²⁵, this
 365 is essential in the analysis of vorticity budgets that is performed in section III C 2.

As expected, all the Reynolds shear stress components approach zero as one approaches the wall, $y = 0$. The Reynolds shear stress profiles in the spanwise direction, however, are not symmetric about $z = 0$ unlike the Reynolds normal stress components as observed before. The Reynolds shear stress profiles display are not symmetric about the jet centerline, $z = 0$. In the wall-normal direction, the two Reynolds shear stress components, namely, $\langle v'w' \rangle$ and $\langle u'w' \rangle$ are of similar order of magnitude and are quite small compared to the $\langle u'v' \rangle$ component.
 370

In the spanwise direction, the three Reynolds shear stress components can be clearly ordered based on their relative magnitude. The component $\langle u'w' \rangle$ shows the largest magnitude followed by $\langle u'v' \rangle$ and finally $\langle v'w' \rangle$ component is the smallest in magnitude through out the domain depicted.
 375 Having validated the present solver for three-dimensional wall jet, the analysis of results using vorticity contours, streamwise evolution of vorticity using vorticity budgets, evolution of wall shear stresses, and finally thermal characteristics is discussed.

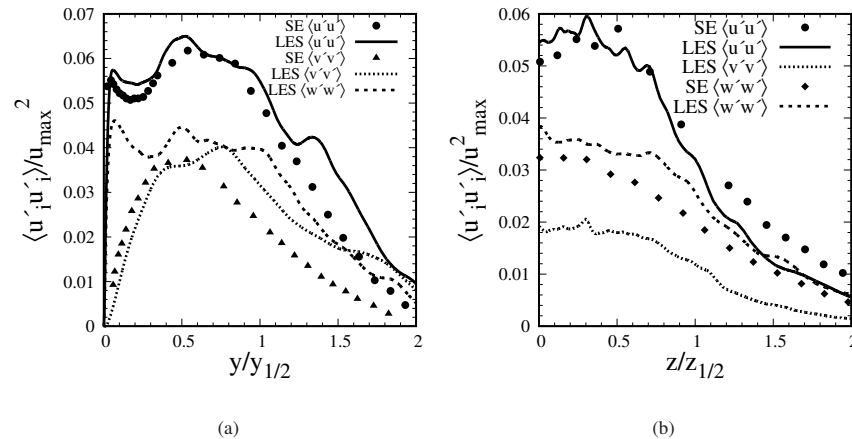


FIG. 9. Mean Reynolds normal stresses, extracted at streamwise location, $x/h = 20$, as a function of (a) wall-normal direction on the jet centerline, $z/h = 0$ (b) spanwise direction at a height of $y = y_{max}$; for the present simulations and for the experimental data reported by Sun and Ewing¹¹ (SE).

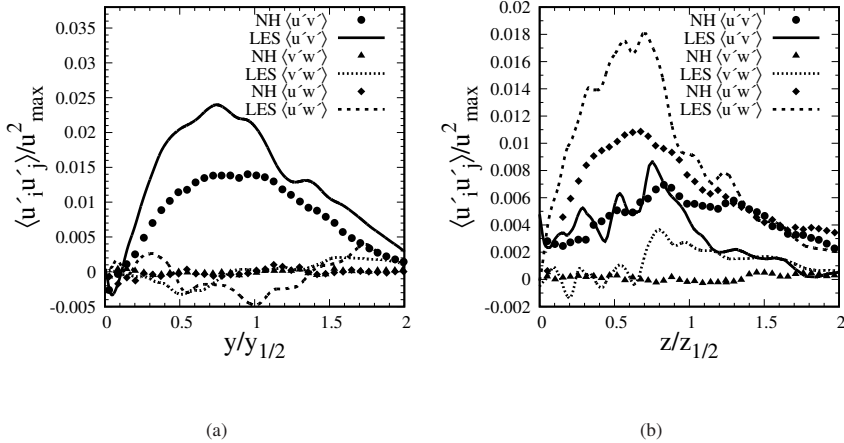


FIG. 10. Mean Reynolds shear stresses, extracted at a streamwise location, $x/h = 20$, as a function of (a) wall-normal direction on the jet centerline, $z/h = 0$ (b) spanwise direction at a height of $y = y_{max}$; for the present simulations and for the experimental data reported by Namgyal and Hall²⁵ (NH).

³⁸⁰ C. Vorticity

1. Vorticity contours

To understand the disparity in the spanwise and the wall-normal spreading rates, the evolution of streamwise and wall-normal components of mean vorticity is studied. The mean streamwise component of vorticity, $\langle \Omega_x \rangle$, is plotted on yz -plane at two different streamwise locations $x/h = 10$ and $x/h = 20$ in figures 11(a) and 11(b) respectively. It can be noted that apart from the region very near to the wall, where the experiments were not able to capture the profile below $y/y_{0.5} \leq 0.1$, the $\langle \Omega_x \rangle$ contours obtained are similar to those obtained using experiments by Namgyal and Hall²⁵ and Sun and Ewing¹¹. A pair of oppositely rotating vortices can be noted in the $0.1 \leq y/y_{1/2} \leq 0.6$ region in figure 11(a). Another pair of oppositely rotating vortices can be observed in the $0.6 \leq y/y_{1/2} \leq 1.2$ region. In this figure, positive values of $\langle \Omega_x \rangle$ indicate a counter-clockwise rotation and a negative value indicates a clockwise rotation. As one moves downstream to $x/h = 20$, the magnitude of these vortices gets reduced as shown in figure 11(b).

To obtain a full picture of these coherent vortices, contours of $\langle \Omega_x \rangle$ are plotted on xz -plane

This is the author's peer reviewed, accepted manuscript. However, the online version of record will be different from this version once it has been copyedited and typeset.

PLEASE CITE THIS ARTICLE AS DOI: 10.1063/5.0031138

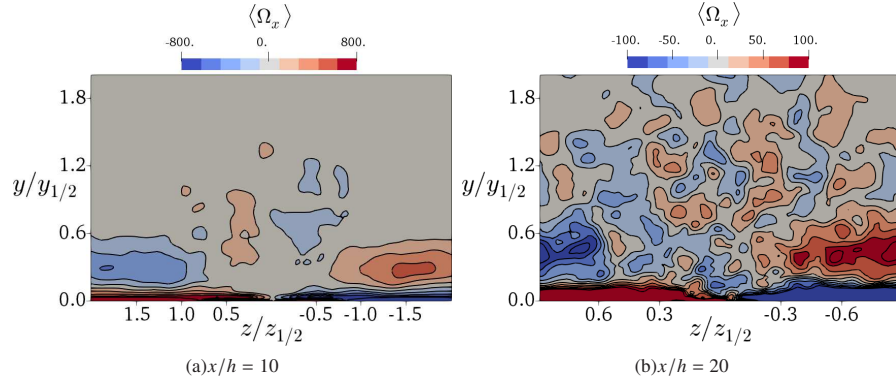


FIG. 11. Contours of mean streamwise component of vorticity, $\langle \Omega_x \rangle$, on yz -plane at (a) $x/h = 10$ and (b) $x/h = 20$.

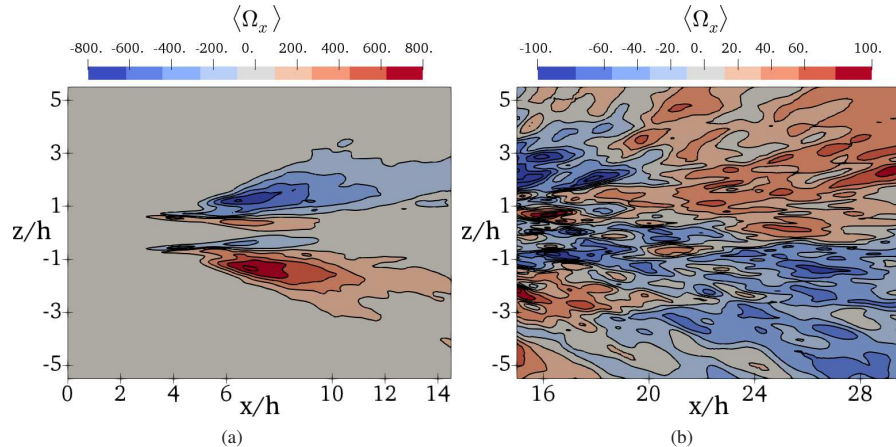


FIG. 12. Contours of mean streamwise component of vorticity, $\langle \Omega_x \rangle$, on xz -plane at a height of $y = y_{max}$, (a) for $0 \leq x/h \leq 15$ (b) for $15 \leq x/h \leq 29$.

at a height of $y = y_{max}$ obtained for $x/h = 20$ in figures 12(a) and 12(b) respectively. In figure 12(a) the two pairs of oppositely rotating coherent vortices can be observed and they reduce in magnitude in figure 12(b). With very large averaging in time, there is a possibility that these smaller magnitude vortices at the center might disappear further downstream, creating an anti-symmetric mean streamwise vorticity contours about the jet center line. The coherent vortices that are observed at $x/h = 10$ create strong entrainment of the flow in the region while inhibiting the

This is the author's peer reviewed, accepted manuscript. However, the online version of record will be different from this version once it has been copyedited and typeset.

PLEASE CITE THIS ARTICLE AS DOI: 10.1063/5.0031138

400 spread of the jet to certain extent. The pair of opposite streamwise vortices away from the center lines, as plotted in figure 11(a) and 11(b), are responsible for the stronger secondary flow, pushing the fluid away from the center plane.

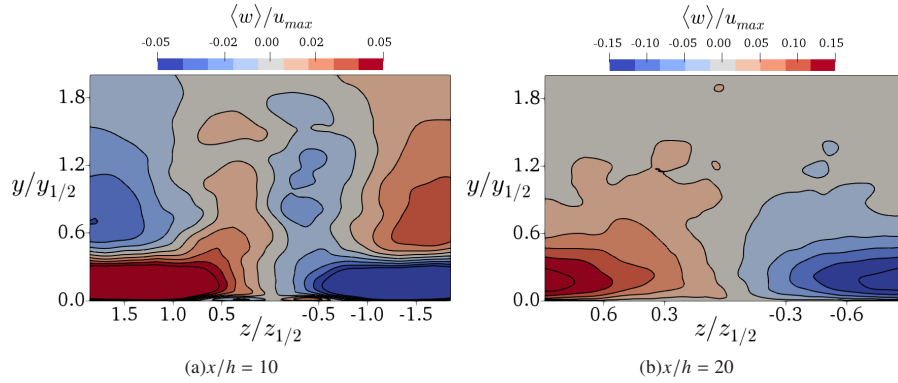


FIG. 13. Contours of mean spanwise component of velocity, $\langle w \rangle$, on yz -plane at (a) $x/h = 10$ and (b) $x/h = 20$.

To visualize the entrainment caused by these vortices, contour for mean spanwise component of velocity, $\langle w \rangle$ is plotted, on yz -plane at two different streamwise locations $x/h = 10$ and $x/h = 20$ 405 in figures 13(a) and 13(b) respectively. At $x/h = 10$, anti-symmetric pattern of contours of $\langle w \rangle$ can be noted about the jet centerline, that is $z = 0$. In the left-half of figure 13(a), that is the region enclosed by $z \geq 0$ for all y a large negative region of $\langle w \rangle$ values can be noted in the region enclosed by $0.5 \geq y/y_{1/2}$ and a small positive region of $\langle w \rangle$ in the region enclosed by $0 \leq y/y_{1/2} \leq 0.5$. The negative contours of $\langle w \rangle$ indicate entrainment of the fluid towards the jet centerline, this region 410 also happens to be in between the negative and positive $\langle \Omega_x \rangle$ vortices observed in the left-half of figure 11(a). These negative (clockwise rotating) and positive (counter-clockwise rotating) vortices drive the flow inwards as observed in the $\langle w \rangle$ contours. Similar observations can be for flow in the right-half of figure 13(a). The small positive region of $\langle w \rangle$ near the wall in the left-half of figure 13(a) indicates the fluid moving away from the jet centerline. Further downstream, at $x/h = 20$, 415 only one pair of positive and negative contours of $\langle w \rangle$ can be observed as shown in figure 13(b). This indicates that by $x/h = 20$, the entrainment of the fluid towards the jet centerline, $z = 0$, is absent and the fluid predominantly moves away from the jet centerline, which is nothing but the spread of the jet in the spanwise direction. As pointed out by Namgyal and Hall²⁴, the lateral

(spanwise) flow away from the jet centerline can be observed in the near wall contour plots of mean spanwise velocity as shown in figures 13(a) and 13(b). Further, it can be noted that the maximum $\langle w \rangle$ velocity is three-times larger at $x/h = 20$ when compared to that at location $x/h = 10$. In the

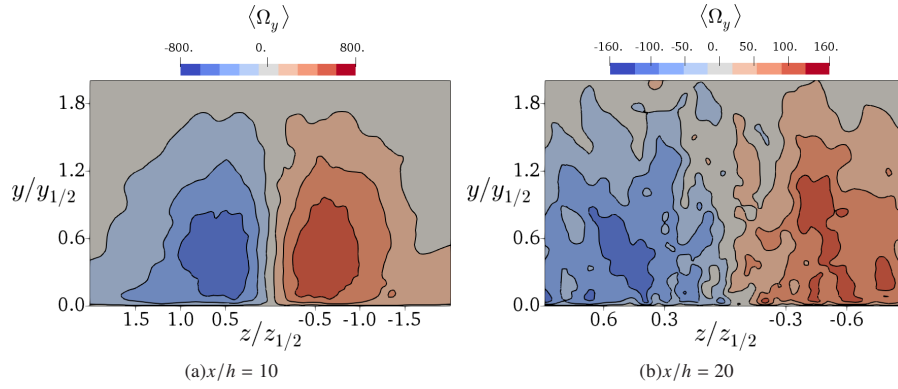


FIG. 14. Contours of mean wall-normal component of vorticity on yz -plane at (a) $x/h = 10$ (b) $x/h = 20$.

literature, the spanwise spread of the jet was studied using the evolution of streamwise component of vorticity. However, the wall-normal component of vorticity also contributes to the spanwise spread of the jet, and this is not explored in the existing literature^{23,25}. Therefore, next, the impact of the wall-normal component of vorticity, Ω_y on the spanwise spread of the jet is discussed. The contours of $\langle \Omega_y \rangle$ on yz -plane at two different streamwise locations of $x/h = 10$ and $x/h = 20$ are shown in figures 14(a) and 14(b) respectively. At $x/h = 10$ a pair of oppositely rotating $\langle \Omega_y \rangle$ vortices can be noted and at $x/h = 20$ the vortices breakdown. From figures 14(a), the direction of rotation for the vortices could be established as follows. The positive contours indicate a counter-clockwise rotating vortex about the y -axis and the negative contours indicate a clockwise rotating vortex. Therefore, the flow can be visualized as being entrained towards the jet centerline, $z/h = 0$, from the outer edges ($z/h \pm 1.5$) and being pushed out helping the spread. The $\langle \Omega_x \rangle$ vortices discussed earlier, were noted to help the spanwise spread of the jet while rotating about the x -axis, the Ω_y vortices discussed here will also help in the spanwise spread of the jet while rotating about the y -axis. As one moves to further downstream to $x/h = 20$, the $\langle \Omega_y \rangle$ diffuses (as can be noted from the magnitude) while breaking down into several smaller vortices.

As discussed above, the streamwise and wall-normal components of mean vorticity have profound effect on the spanwise spread of the three-dimensional wall jet. It would then be interesting

This is the author's peer reviewed, accepted manuscript. However, the online version of record will be different from this version once it has been copyedited and typeset.

PLEASE CITE THIS ARTICLE AS DOI: 10.1063/5.0031138

to look at the wall-normal distribution of mean vorticity components by comparing them to those obtained using a planar wall jet, for which there is no spanwise spread, at the same inlet Reynolds number. In order to make such a comparison the data obtained by Kakka and Anupindi³⁵ for planar turbulent wall jet is used. The profiles of mean vorticity components, $\langle \Omega_x \rangle$, $\langle \Omega_y \rangle$, and $\langle \Omega_z \rangle$ as a function of the wall-normal direction, y , are shown in figures 15(a), 15(b) and 15(c) respectively for the planar jet results³⁵ and for the present three-dimensional wall jet results, at two streamwise locations $x/h = 10$ and $x/h = 20$ and at two spanwise locations $z/h = 0$ and $z/h = 2.5$. All the components of mean vorticity are normalized using $\kappa_\Omega = \frac{u_{max}}{y_{1/2}}$, where u_{max} and $y_{1/2}$ are obtained respective streamwise locations. From figures 15(a) and 15(b), it can be observed that $\langle \Omega_x \rangle$ and $\langle \Omega_y \rangle$ are negligible throughout the wall-normal direction for planar jet, as expected. For the three-dimensional jet, the mean vorticity values obtained at the off-center location, $z/h = 2.5$, are consistently higher than those obtained at jet centerline, $z/h = 0$. This could be due to vortices on the sides of jet center line leading to spanwise spread. Coming to the $\langle \Omega_z \rangle$ profile, a reverse trend in the nature of the profiles can be noted when compared to the x and y components. The values obtained for plane jet are consistently larger, followed by those obtained at the jet centerline for the three-dimensional jet, followed by those obtained at the off-center location. The $\langle \Omega_z \rangle$ component of vorticity aids in the wall-normal spread of the jet and consistent with the larger values obtained for the planar jet in comparison to the three-dimensional jet. Hence, turbulent planar wall jets display a larger wall-normal spread rate when compared to three-dimensional wall jets.

This is the author's peer reviewed, accepted manuscript. However, the online version of record will be different from this version once it has been copyedited and typeset.

PLEASE CITE THIS ARTICLE AS DOI: 10.1063/5.0031138

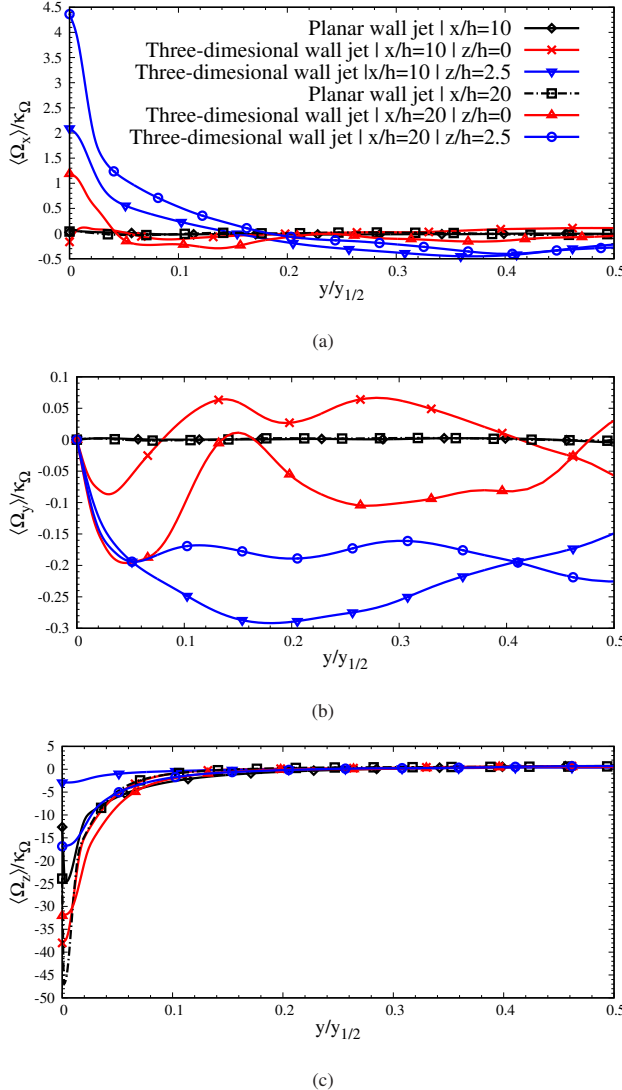


FIG. 15. Profiles of (a) mean streamwise component of vorticity, $\langle \Omega_x \rangle$, (b) mean wall-normal component of vorticity, $\langle \Omega_y \rangle$, and (c) mean spanwise component of vorticity, $\langle \Omega_z \rangle$; for planar wall jet and for three-dimensional wall jet at indicated streamwise locations and spanwise locations.

460 2. Vorticity budgets

Next, the influence of each of the terms occurring in the mean streamwise VTE, eq. 1, on the evolution of streamwise vorticity in the three-dimensional wall jet is evaluated. To verify that each of the terms evaluated are correct, the term-A (the convection term) is compared with the sum of all the terms on the right-hand-side of eq. 1 (term-B through term-F). The wall-normal profiles of term-A and sum of terms B through F are shown in figures 16(a) and 16(b) on the jet centerline, $z/h = 0$, at streamwise locations of $x/h = 10$ and $x/h = 20$ respectively. The magnitudes of these terms are non-dimensionalized using $\left(\frac{u_{max}}{y_{1/2}}\right)^2$, where u_{max} and $y_{1/2}$ are obtained corresponding to the particular x location indicated. From these two figures, a good match can be noted in most of the wall-normal region except close to the wall. These plots sufficiently verify that the individual terms are indeed accurate and they can now be used to analyze for their contribution in the spanwise spread of the jet.

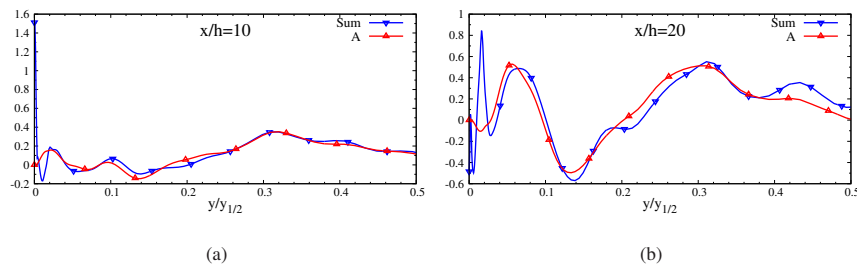


FIG. 16. Wall-normal profiles of term-A and the sum of terms B through F, indicated in the mean streamwise VTE given by eq. 1, on the jet centerline at streamwise locations (a) $x/h = 10$ (b) $x/h = 20$.

Next, the individual terms from the mean streamwise VTE, eq. 1, are plotted as a function of the wall-normal direction. The wall-normal profiles of terms B through F on the jet centerline, $z/h = 0$, at streamwise locations of $x/h = 5$ through $x/h = 25$ are shown in figures 17(a) through 17(e). The wall-normal profiles of terms B through F, on the off-center spanwise location of $z/h = 2.5$ at the same streamwise locations of $x/h = 5$ through $x/h = 25$ are shown in figures 18(a) through 18(e). At all the streamwise and spanwise locations, it can be noted that vorticity diffusion, term-F, has a large magnitude close to the wall and quickly decays to a zero value by $y \leq 0.1y_{1/2}$. This behavior can be attributed to the large second order derivatives in the wall-normal and spanwise directions of $\langle \Omega_x \rangle$ near the wall. The near-wall oscillations of term-F in figures 17(b) and 17(d) can

This is the author's peer reviewed, accepted manuscript. However, the online version of record will be different from this version once it has been copyedited and typeset.

PLEASE CITE THIS ARTICLE AS DOI: 10.1063/5.0031138

be understood by observing the $\langle \Omega_x \rangle$ contours on the yz -plane at locations $x/h = 10$ and $x/h = 20$ discussed earlier using figures 11(a) and 11(b). From the contours of $\langle \Omega_x \rangle$ in figure 11(a) in addition to the two pairs of counter rotating vortices another relatively flat pair of vortices, in the $0 \leq y/y_{1/2} \leq 0.1$ region, can be observed very close to the wall. These vortices together with
485 the upper counter rotating vortices, in the $0.1 \leq y/y_{1/2} \leq 0.6$ region, contribute the behavior of term-F observed in figures 17(b) and 17(d). It can further be noted that the vortex stretching term, term-B, and the vortex line bending term, term-C, have insignificant values in most of the wall-normal region, for all streamwise and spanwise locations. This shows that the terms B and C do not play a significant role in the spread of the three-dimensional wall jet. This corroborates
490 with the observations made earlier by Craft and Launder²³.

The terms that dominate in the mean streamwise VTE, that are responsible for the spanwise spread of the jet are the terms D and E that contain the second derivatives of the Reynolds stresses. It can be noted that beyond $x/h = 5$, for all streamwise and spanwise locations, these two terms have relatively larger magnitude. It can be noted that magnitude of terms D and E are lower
495 on the jet off-center when compared to the jet centerline at any given streamwise location. This trend indicates that the contribution of the terms D and E to the spanwise spread decreases as one moves away from the jet centerline. In the near nozzle exit region, that is near $x/h = 5$, term-D is dominant near the wall and the term-E is negligible, this can be noted from figures 17(a) and 18(a). In all other downstream locations, $x/h \geq 10$, the terms D and E are of comparable magnitude and
500 are out of phase with each other with respect to their profile in the wall-normal direction. Further, it can be observed that in most of the regions, the absolute magnitude of the term-D is larger when compared to the term-E. To quickly observe this, the sum of the terms D and E is shown in all the figures using label 'D+E' and this profile mostly follows the profile of term-D. The domination of term-D is in accordance with what was proposed in the literature by Namgyal and Hall²⁵. However,
505 in their work²⁵ they postulated it based on the sheer dominance in magnitude of $\langle v'^2 - w'^2 \rangle$ over $\langle v'w' \rangle$, but not based on their actual second derivatives of these Reynolds stress components as they appear in the mean streamwise VTE. In the present work, by completely evaluating the terms D and E the dominance of the terms containing the Reynolds normal stresses (term-D), over the terms containing the Reynolds shear stresses (term-E) is established. This further indicates that
510 some RANS models that capture the trends of the Reynolds stresses relatively well could provide good estimates for the spanwise spread.

This is the author's peer reviewed, accepted manuscript. However, the online version of record will be different from this version once it has been copyedited and typeset.

PLEASE CITE THIS ARTICLE AS DOI: 10.1063/5.0031138

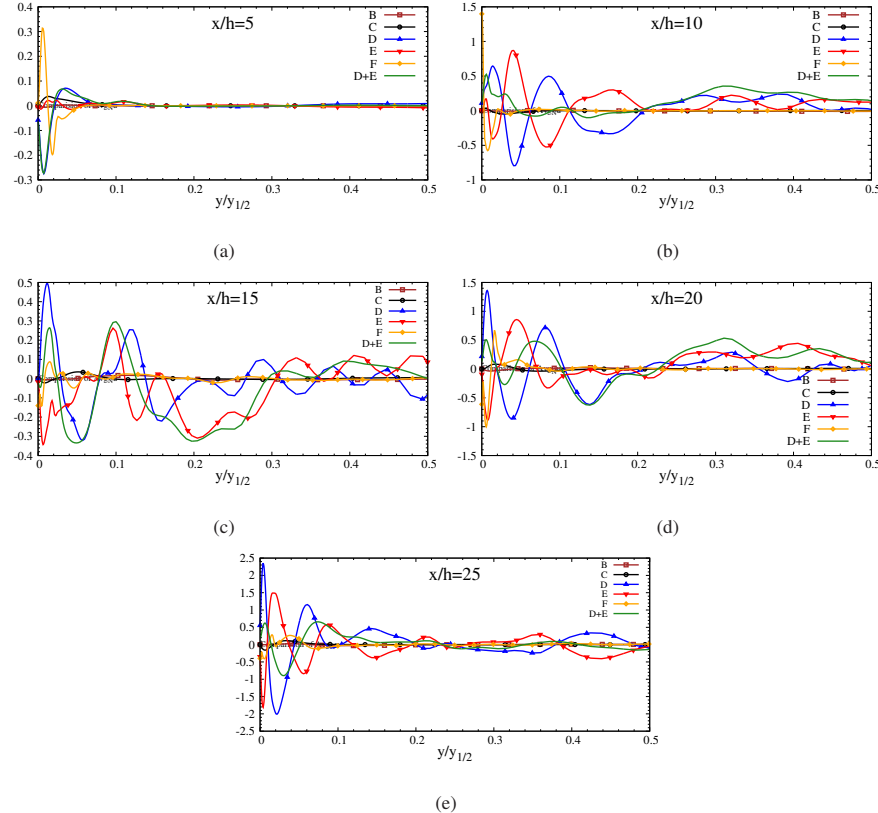


FIG. 17. Wall-normal profiles of terms B through F of the mean VTE, eq. 1, on the jet centerline, $z/h = 0$ at different streamwise locations; (a) $x/h = 5$ (b) $x/h = 10$ (c) $x/h = 15$ (d) $x/h = 20$ and (e) $x/h = 25$.

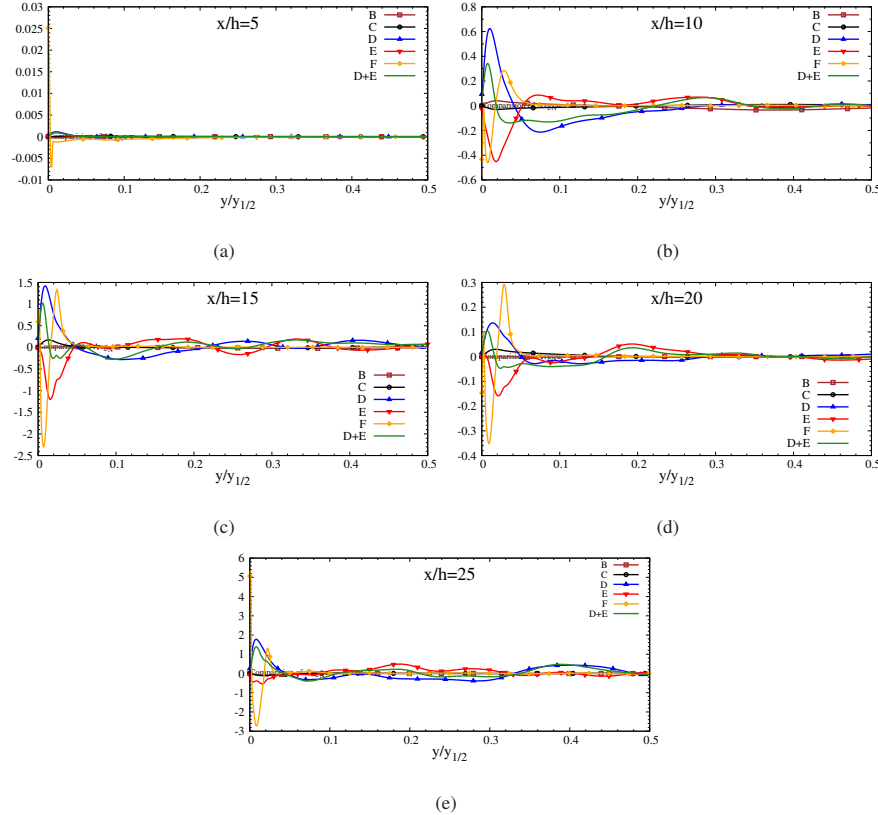


FIG. 18. Wall-normal profiles of terms B through F of the mean VTE, eq. 1, on the off-center location, $z/h = 2.5$ at different streamwise locations; (a) $x/h = 5$ (b) $x/h = 10$ (c) $x/h = 15$ (d) $x/h = 20$ and (e) $x/h = 25$.

As indicated in the mean streamwise VTE, eq. 1, the terms D and E further comprise of individual components labeled as D₁, D₂ and E₁, E₂. It should be emphasized here that there is a negative sign for the terms D₂ and E₂ in the mean streamwise VTE, eq. 1, therefore, term-D = ₅₁₅ term-D₁ - term-D₂ and term-E = term-E₁ - term-E₂. Therefore the same convention needs to be used in the following discussion. Next, in order to further identify which two terms out of these four terms are dominant, the wall-normal profiles of the terms D, E, and their components D₁, D₂, E₁ and E₂ are shown in figures 19(a) and 19(b) for locations $x/h = 10$ and $x/h = 20$ respectively.

From these figures it can be noted that D2 and E2 terms contribute larger to D and E respectively than D1 and E1. Further, the profiles of D2 and E2 are out of phase and these two components are mostly responsible for the large spanwise spread of the three-dimensional wall jet.

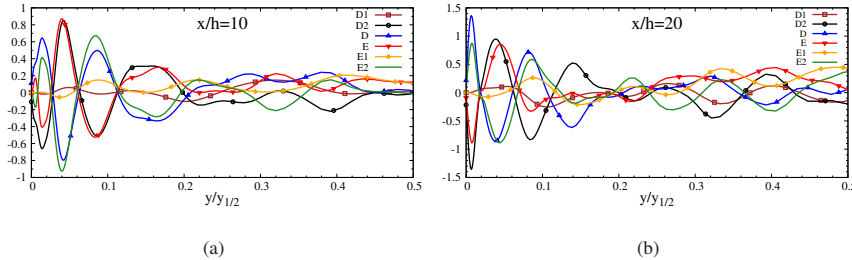


FIG. 19. Wall-normal profiles of the terms D, D1, D2, E, E1 and E2 indicated in the mean VTE, eq. 1, on the jet centerline, $z/h = 0$, at streamwise locations (a) $x/h = 10$ and (b) $x/h = 20$.

D. Shear stress

Next, the effect of streamwise vorticity on the wall shear stress and its self-similarity are studied. In section III B, it was noted that the wall-normal profiles of mean u velocity become self-similar by a streamwise location of $x/h = 20$. Similarly, the spanwise profiles of wall shear stress also become self-similar when non-dimensionalized using appropriate quantities. Rajaratnam and Pani¹⁰ provided the self-similar profile of the wall shear stress obtained from their experiments. The self-similar profiles of shear stress as a function of non-dimensional spanwise distance are shown in figure 20 for the present results and for the experimental results¹⁰. In this figure, the streamwise shear stress, τ , is non-dimensionalized using the shear stress at the jet centerline, τ_o , and the spanwise distance, z , is non-dimensionalized using h_τ , where h_τ is the half-length which is defined as the location on the z -axis where $\tau = \frac{1}{2}\tau_o$. From this figure, a good match can be noted between the present results and the experimental data¹⁰. The wall shear stress has a maximum value at the jet centerline and it decreases as one moves away from the centerline. The profiles at $x/h = 20$ and $x/h = 25$ closely overlap indicating that the shear stress profiles have become self-similar by a streamwise location of $x/h = 20$.

The contours of mean x -component of friction velocity, u_τ , and the z -component of friction velocity, w_τ , are studied next. A study of friction velocity is important for the calculation of the friction drag acting on the bottom wall. Further, a qualitative impression of the spanwise spread

This is the author's peer reviewed, accepted manuscript. However, the online version of record will be different from this version once it has been copyedited and typeset.

PLEASE CITE THIS ARTICLE AS DOI: 10.1063/5.0031138

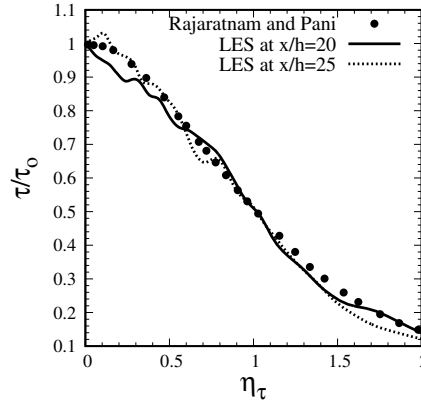


FIG. 20. Normalized profiles of streamwise component of wall shear stress as a function of the normalized spanwise direction.

rate of the jet can be obtained by looking at the contours of u_τ . The $\langle u_\tau \rangle$ and $\langle w_\tau \rangle$ contours on xz -plane are shown in figures 21(a) and 21(b) respectively. In both the figures, friction velocity is non-dimensionalized using the inlet velocity u_o . From figure 21(a) it can be noted that u_τ attains large values close to the nozzle exit and in the potential core region, following which it gradually decreases and also starts to spread in the spanwise direction. Approximately by $x/h = 22$ and beyond, u_τ reaches a constant value of $0.02u_o$ around $z/h = 0$. From the impression of the contours of u_τ the approximate spanwise spread can be quickly calculated. The outer-most contour line that emerges from the nozzle exit, $x = 0$ and $z = 0.5$, can be noted to reach the domain exit at $x = 30$ and $z \approx 7$. Following this contour line, the slope of the same can be calculated to be ≈ 0.217 which is close to the value of $\frac{\Delta z_{1/2}}{\Delta x} = 0.2271$ that was calculated earlier in section III B. This outer-most contour of $\langle u_\tau \rangle$ can also be thought of as the dividing-line between the wet and the dry surfaces on the bottom wall in a time-average sense. The maximum values for $\langle w_\tau \rangle$ can be noted away from the jet centerline in the region where the potential core ends. Unlike the $\langle u_\tau \rangle$ contours which has maximum values close to the nozzle exit, the $\langle w_\tau \rangle$ contours show near zero values in this region and show maximum values in the locations where the jet starts to spread. The peak values reached by $\langle w_\tau \rangle$ are approximately half of those reached by $\langle u_\tau \rangle$. Similarly, in the self-similar region, $x/h \geq 20$, the values attained by $\langle w_\tau \rangle$ are only half as much as those noted for $\langle u_\tau \rangle$. Further, it can be noted that around the jet centerline, in the region defined by $-0.5 \leq z/h \leq 0.5$, $\langle w_\tau \rangle$ shows

This is the author's peer reviewed, accepted manuscript. However, the online version of record will be different from this version once it has been copyedited and typeset.

PLEASE CITE THIS ARTICLE AS DOI: 10.1063/5.0031138

negligible values and this is attributed to the negligible spanwise component of velocity in this region, as can be noted from figures 13(a) and 13(b).

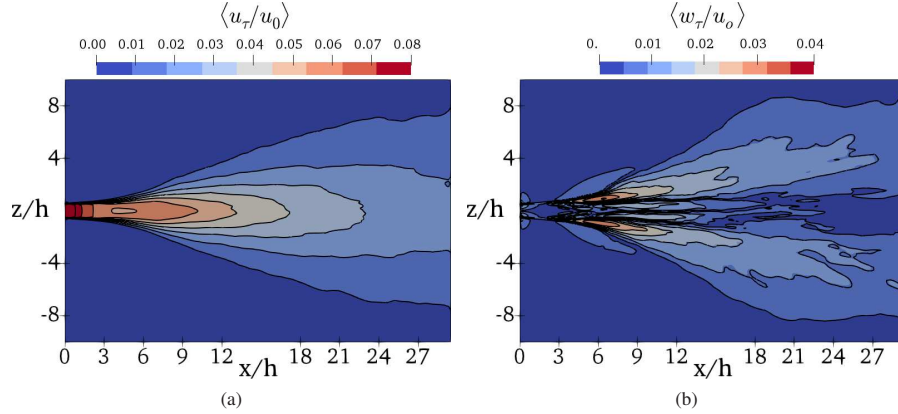


FIG. 21. Contours of mean friction velocity on the xz -plane for (a) normalized streamwise component, $\langle u_\tau \rangle$ (b) normalized spanwise component, $\langle w_\tau \rangle$.

560 E. Mean and second-order statistics of the thermal field

The characteristics of the thermal field using mean and second-order statistics of temperature, evolution of Nusselt number and turbulent heat flux is explored in this section.

1. Temperature characteristics

The temperature characteristics of three-dimensional wall jet are studied in this section. The
565 wall-normal profiles of mean temperature on the jet centerline at different streamwise locations are shown in figure 22(a) for the present simulations and for the planar jet results obtained using DNS by Naqavi, Tyacke, and Tucker²⁸. The profiles at locations $x/h = 15$ and beyond collapse on each other indicating self-similarity. Further, this self-similar profile matches with the planar wall jet profile²⁸.

570 The profiles of root-mean-square (rms) temperature as a function of the wall-normal direction are shown in figure 22(b) for the present results and for the planar wall jet²⁸. It can be noted that similar to mean temperature, the T_{rms} profiles also are qualitatively similar to the planar jet results.

This is the author's peer reviewed, accepted manuscript. However, the online version of record will be different from this version once it has been copyedited and typeset.

PLEASE CITE THIS ARTICLE AS DOI: 10.1063/5.0031138

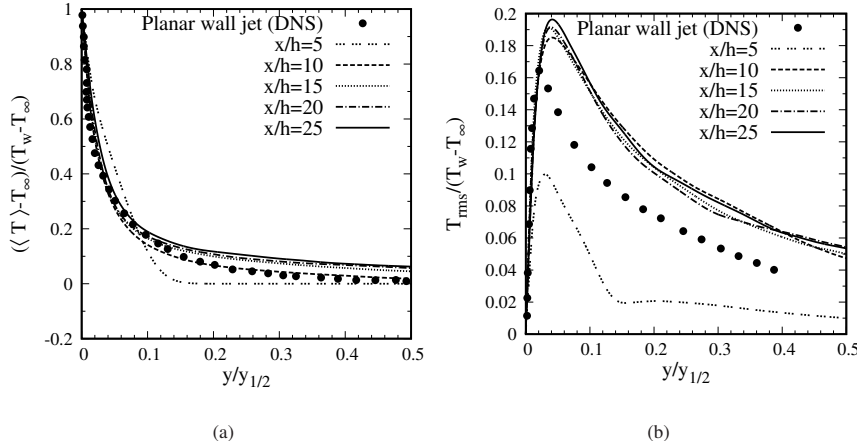


FIG. 22. Profiles in the wall-normal direction on the jet centerline, $z/h = 0$, for the present results and for the planar jet results obtained using DNS²⁹ (a) mean temperature (b) rms temperature.

However, the peak value obtained for three-dimensional wall jet is higher than the planar wall jet. This is consistent with the findings that the turbulent fluctuations are higher in three-dimensional
575 wall jet when compared to the planar wall jet. Further, self-similar profiles for T_{rms} can be noted from $x/h = 15$ and beyond.

The spanwise profiles of mean and rms temperature are analyzed next, to understand the effect of velocity fluctuations on the temperature fluctuations. The mean and rms temperature profiles as a function of the spanwise direction for several streamwise locations are shown in figures 23(a)
580 and 23(b) respectively. These spanwise profiles are plotted at a height y where T_{rms} reaches a maximum value locally. From the mean temperature profile a peak can be observed in the region enclosed by $-1 \leq z/z_{1/2} \leq 1$ for $x/h = 5$. This peak, however, gets dissipated by $x/h = 20$ and a plateau gets formed. In a planar wall jet, owing to homogeneity in the spanwise direction, the entire mean temperature profile in the spanwise direction would be a plateau. The three-dimensional jet,
585 however, mimics this behavior only in a short span around the jet centerline and shows a drop in mean temperature in the regions enclosed by $-4 \leq z/z_{1/2} \leq -1$ and $1 \leq z/z_{1/2} \leq 4$. In the same region where a peak in mean temperature is noted, a dip in T_{rms} can be noted from figure 23(b). Similar to the mean temperature profiles, the T_{rms} profiles show a plateau by $x/h = 15$ and beyond.

To understand the peak in the mean temperature and dip in T_{rms} at $x/h = 5$, contours of T_{rms}

This is the author's peer reviewed, accepted manuscript. However, the online version of record will be different from this version once it has been copyedited and typeset.

PLEASE CITE THIS ARTICLE AS DOI: 10.1063/5.0031138

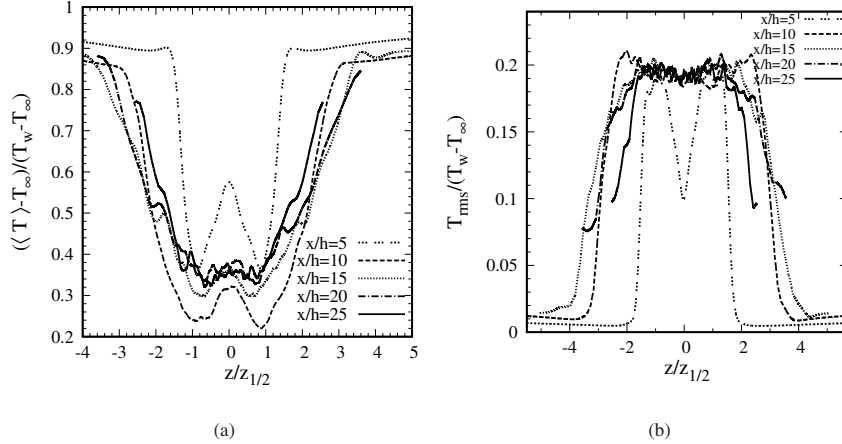


FIG. 23. Profiles in the spanwise direction at a height y where T_{rms} is maximum (a) mean temperature (b) rms temperature.

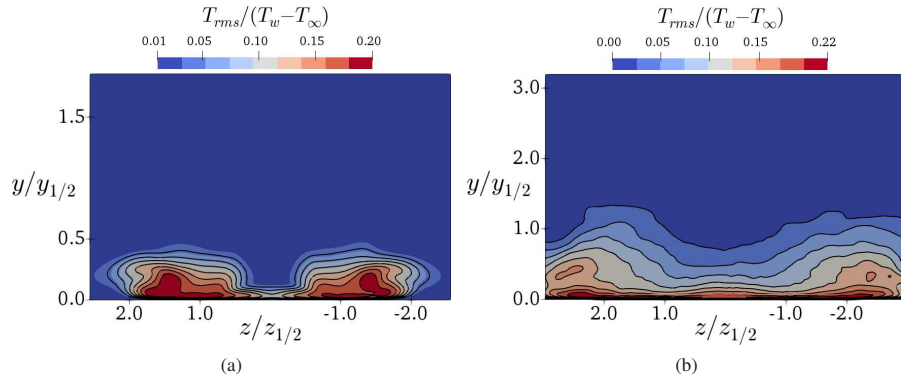


FIG. 24. Contours of rms temperature on yz -plane at streamwise location (a) $x/h = 5$ (b) $x/h = 10$.

and u_{rms} are plotted. The contours of T_{rms} on yz -plane at $x/h = 5$ and $x/h = 10$ are shown in figures 24(a) and 24(b) respectively. Similarly, the contours of u_{rms} on yz -plane at $x/h = 5$ and $x/h = 10$ are shown in figures 25(a) and 25(b). The dip in the T_{rms} profiles and the eventual flat profiles can be noted in the region defined by $-0.5 \leq z/z_{1/2} \leq 0.5$ from figures 24(a) and 24(b) respectively. The reason for this dip in the T_{rms} is attributed to the dip in the u_{rms} profiles in the same regions as can be observed from figures 25(a) and 25(b). At $x/h = 10$ where a plateau was

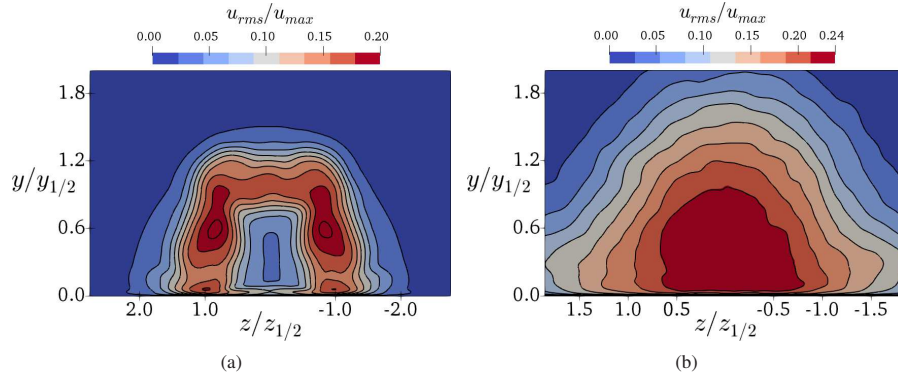


FIG. 25. Contours of rms u -velocity on yz -plane at streamwise location of (a) $x/h = 5$ (b) $x/h = 10$.

observed for T_{rms} , the u_{rms} profiles show locally maximum values.

2. Evolution of Nusselt number

In this section, the evolution of Nusselt number for three-dimensional wall jet is studied. The contours of Nusselt number, suitably normalized using the Reynolds number, on the xz -plane are shown in figure 26(a). A dip in the Nusselt number can be noted in the potential core region, and higher values can be noted around it. This dip in the Nusselt number, and therefore a reduction in heat transfer, is due to reduced velocity fluctuations in this region as observed in figure 25(a). The higher values of Nusselt number that correspond to higher heat transfer, around the potential core region is due to high values of T_{rms} and u_{rms} fluctuations in this region as noted in figures 24(a) and 25(a) respectively. The profiles of Nusselt number as a function of the spanwise direction, extracted at different streamwise locations, are shown in figure 27(a). The dip that was noted in the contour plots of Nusselt number can be noted here at location $x/h = 5$, and as one moves downstream to $x/h = 20$ and beyond a flat profile can be observed. To understand the reason for the flat Nusselt number profile at $x/h = 20$, T_{rms} profiles are plotted. Figure 26(b) shows the normalized contours of T_{rms} in the yz -plane at $x/h = 20$. From this figure T_{rms} values near the wall can be noted to remain constant along the spanwise direction. As both the mean and rms values of temperature are noted to remain nearly constant, the Nusselt number profiles attain a flat profile by $x/h = 20$.

The streamwise evolution of Nusselt number along the jet centerline is shown in figure 27(b). In

This is the author's peer reviewed, accepted manuscript. However, the online version of record will be different from this version once it has been copyedited and typeset.

PLEASE CITE THIS ARTICLE AS DOI: 10.1063/5.0031138

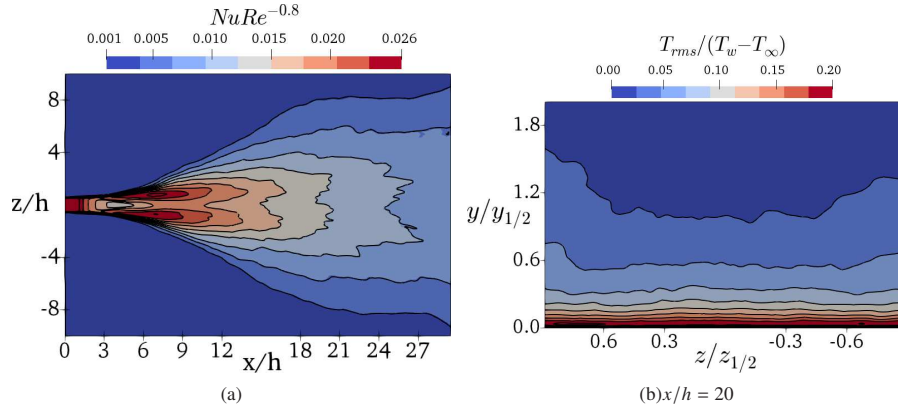


FIG. 26. (a) Contours of Nusselt number on the xz -plane (b) Contours of T_{rms} on the yz -plane at a streamwise location of $x/h = 20$.

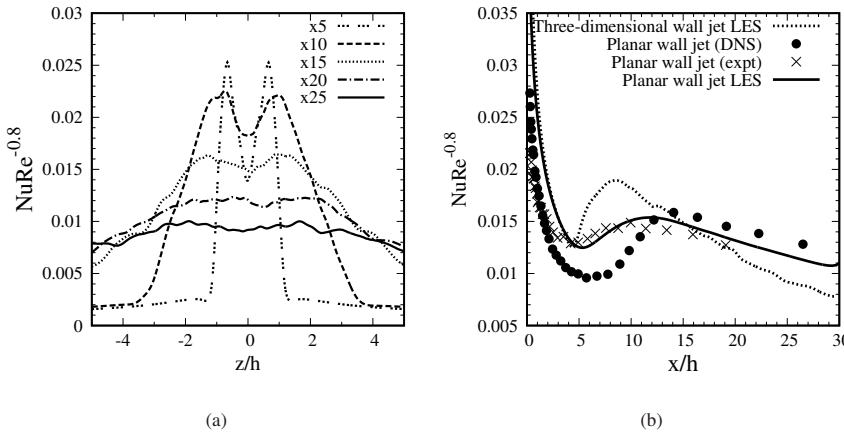


FIG. 27. (a) Spanwise profiles of Nusselt number at indicated streamwise locations (b) Streamwise evolution of Nusselt number for the present simulations, and for the indicated planar jet cases.

615 this figure, together with the results obtained for the present three-dimensional wall jet, the planar wall jet results obtained using DNS by Naqavi, Tyacke, and Tucker²⁹, using LES by Kakka and Anupindi³⁵, and using experiments by AbdulNour *et al.*² are also included. Qualitatively similar streamwise evolution of Nusselt number can be noted between the three-dimensional and planar wall jets. A dip in the Nusselt number can be noted around $x/h = 5$ for both the three-dimensional

This is the author's peer reviewed, accepted manuscript. However, the online version of record will be different from this version once it has been copyedited and typeset.

PLEASE CITE THIS ARTICLE AS DOI: 10.1063/5.0031138

and planar wall jets. However, for the three-dimensional wall jet an increase in heat transfer can be noted corresponding to the peak around $x/h = 8$, which is lower for the planar wall jet. The Nusselt number after the peak at $x/h = 8$ gradually decreases downstream with a steeper gradient than the planar wall jet.

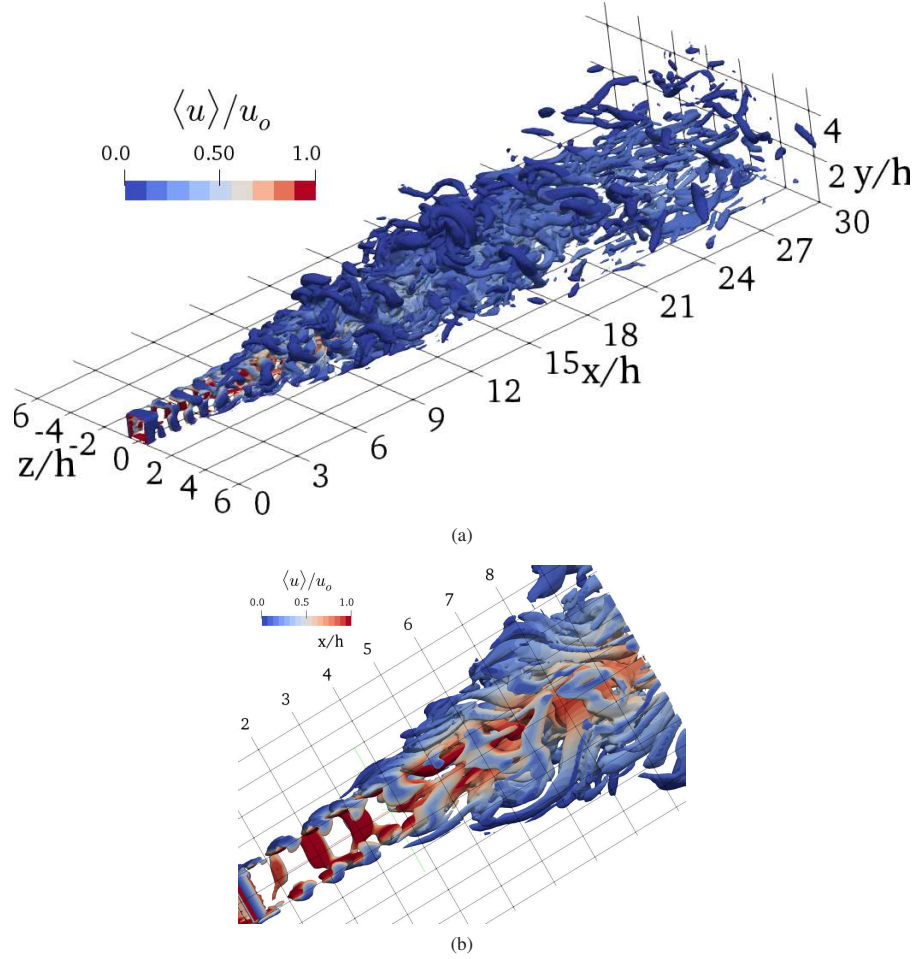


FIG. 28. Iso-surfaces of instantaneous Q -criterion colored by mean u velocity (a) isometric view (b) a view from the bottom wall near the nozzle exit.

To understand the reason for this dip in the Nusselt number, near the nozzle exit in figures 27(b)

This is the author's peer reviewed, accepted manuscript. However, the online version of record will be different from this version once it has been copyedited and typeset.

PLEASE CITE THIS ARTICLE AS DOI: 10.1063/5.0031138

and 27(a), evolution of instantaneous vortical structures is being studied. The instantaneous iso-surfaces of Q -criterion colored by mean u velocity are shown in figures 28(a) and 28(b). The vortical structures are plotted over the entire domain in figure 28(a), whereas a bottom view near the nozzle exit is shown in figure 28(b). From these figures it can be observed that the vortical structures start to interact with the wall beyond $x/h \geq 4$ and this leads to an increase in the heat transfer. Further downstream, the vortical structures emanating from the edges of the jet merge at the jet centerline and make the Nusselt number reach a peak around $x/h = 8$ as observed in figure 27(b). As these eddies convect downstream, they heat up due to their interaction with the heated isothermal wall and further mixing of the flow leads to a lower near wall temperature gradient. This reduction in near wall temperature gradient downstream is the reason for the reduction in heat transfer. The salient features that are noted for heat transfer for three-dimensional wall jet are a dip near the nozzle exit and in the potential core region, a peak near $x/h = 8$, and gradual decrease as one moves downstream. These features may be helpful in the design and analysis of film-cooled devices that use three-dimensional wall jets.

3. Turbulent heat flux characteristics

Finally, in this section, turbulent heat flux characteristics for three-dimensional wall jets are presented. The contours of $\langle u'T' \rangle$ on xz and xy -planes are shown in figures 29(a) and 29(b) respectively. The contours of $\langle u'T' \rangle$ on xz -plane are plotted at a height y for which T_{rms} attains a maximum value at a given location of $x/h = 20$. From figure 29(a), negative values for $\langle u'T' \rangle$ can be noted beyond $x/h = 10$. Negative turbulent heat flux values indicate that heat is being transported in the opposite direction of local u' . Although $\langle u'T' \rangle$ is negative for most of the domain, a small region with positive values can be observed near the trailing portion of the potential core. From figure 29(b), negative values can be noted for $\langle u'T' \rangle$ near the wall throughout all the streamwise locations. However, positive values can be noted away from wall in the region defined by $x/h \geq 12$.

The reason for positive $\langle u'T' \rangle$ in three-dimensional wall jets is because the Reynolds shear stress term, $\langle u'v' \rangle$, is positive in this region as shown in figures 30(a) and 30(b). Particularly, the small region of positive heat-flux observed in figure 29(a) is explained using positive values of $\langle u'v' \rangle$ around the potential core region in the region defined by $-1 \leq z/z_{1/2} \leq 1$ as shown in figure 30(a). This positive values of $\langle u'v' \rangle$ coupled with strong negative wall-normal temperature gradients makes the production term $P_{\langle u'T' \rangle} \sim -\langle u'v' \rangle \frac{\partial \langle T \rangle}{\partial y}$ for the streamwise turbulent heat flux

This is the author's peer reviewed, accepted manuscript. However, the online version of record will be different from this version once it has been copyedited and typeset.

PLEASE CITE THIS ARTICLE AS DOI: 10.1063/5.0031138

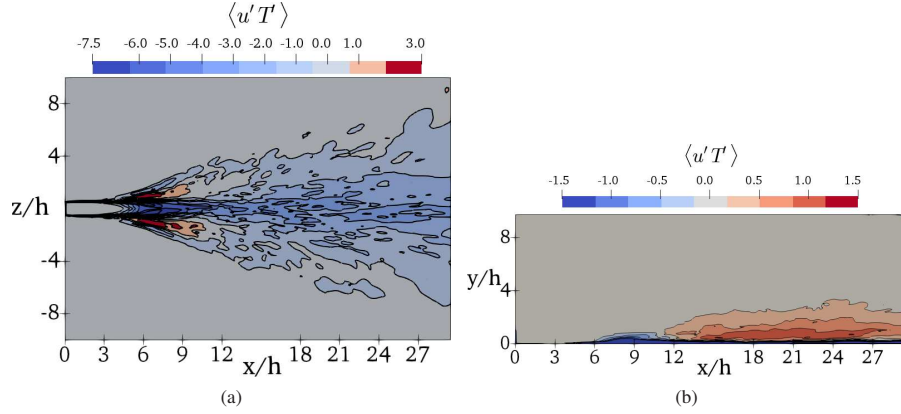


FIG. 29. Contours of $\langle u' T' \rangle$ on (a) xz -plane at a height y for which T_{rms} is noted to be maximum (b) on xy -plane on the jet centerline.

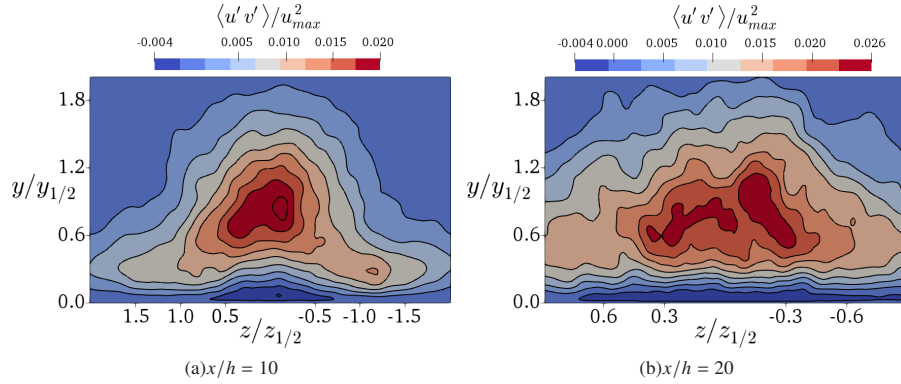


FIG. 30. Contours of Reynolds shear stress, $\langle u' v' \rangle$, on yz -plane at streamwise locations (a) $x/h = 10$ (b) $x/h = 20$.

positive. Due to a strong temperature gradient near the wall, the magnitude of positive streamwise heat flux is less than that of the near wall negative heat flux, as shown in figure 29(b). This change of direction in turbulent heat transfer in the streamwise direction at different heights of the three-dimensional wall jets might play an important role in the film-cooling mechanism where the jet prevents the hot-stream of gas over it to interact with the surface of the wall over which it flows.

The other two components of turbulent heat flux namely, $\langle v' T' \rangle$ and $\langle w' T' \rangle$ are analyzed next. The contours of $\langle v' T' \rangle$ are plotted on xz and xy -planes in figures 31(a) and 31(b) respectively.

This is the author's peer reviewed, accepted manuscript. However, the online version of record will be different from this version once it has been copyedited and typeset.

PLEASE CITE THIS ARTICLE AS DOI: 10.1063/5.0031138

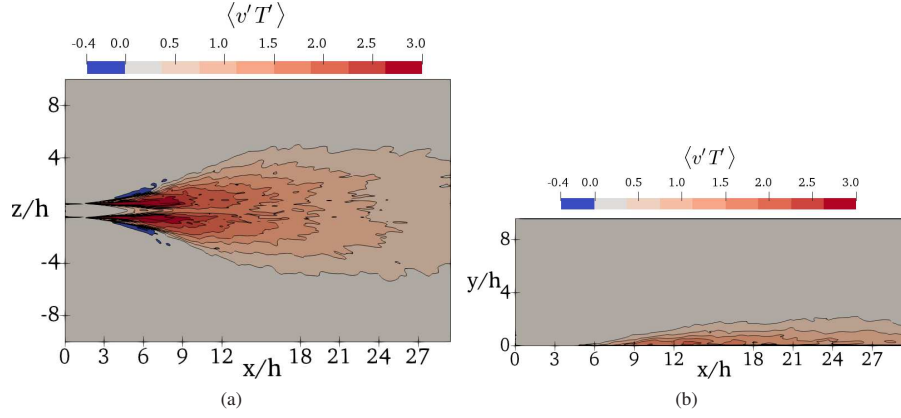


FIG. 31. Contours of $\langle v' T' \rangle$ (a) on xz -plane at a height y for which T_{rms} is maximum (b) on xy -plane on the jet centerline.

From figures 31(a) and 31(b) it can be noted that the wall-normal heat-flux is positive in most of the regions, as the heat is carried away from the wall due to high negative wall-normal temperature gradient. The reason for this is the same as found in planar wall jets²⁹, where the temperature gradient in the wall-normal direction is negative and $\langle v' v' \rangle$ being a positive quantity leading to dominant positive production term $P_{\langle v' T' \rangle} \sim -\langle v' v' \rangle \frac{\partial \langle T \rangle}{\partial y}$.

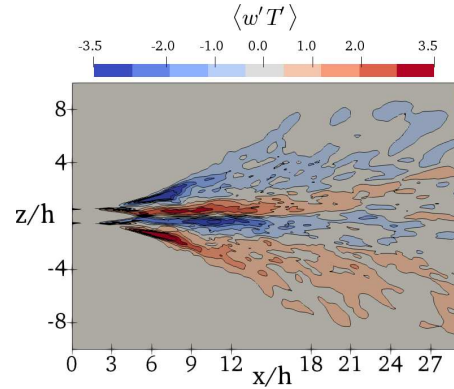


FIG. 32. Contours of $\langle w' T' \rangle$ on xz -plane at a height y for which T_{rms} is maximum.

The contours of $\langle w' T' \rangle$ on xz -plane are shown in figure 32. An interesting observation about the directionality of turbulent heat transport can be made for $\langle w' T' \rangle$. For the three-dimensional wall

This is the author's peer reviewed, accepted manuscript. However, the online version of record will be different from this version once it has been copyedited and typeset.

PLEASE CITE THIS ARTICLE AS DOI: 10.1063/5.0031138

jets, the spanwise heat-flux $\langle w'T' \rangle$ is positive near the centerline in the positive z -axis at $z/h = 0$,
and thus, the heat is carried away from the center of the z -axis as shown in figure 32, whereas
 $\langle w'T' \rangle$ is negative in the region around the outer edge of the jet of the positive z -axis, and thus the
heat is transported towards the jet center. This opposing spanwise component of turbulent heat flux
in both halves of the domain may be important in the analysis involving multiple slots of parallel
three-dimensional wall jets for film-cooling applications.

675 **IV. CONCLUSIONS AND FUTURE WORK**

In the present work, the flow and thermal characteristics of three-dimensional turbulent wall
jet are studied using LES. The mesh used in all the simulations is first established to be sufficient
using a grid sensitivity test. Further, the flow solver used is validated for mean and second-order
statistics of the flow field using reference experiments. The spanwise spread of the jet is analyzed
680 using the mean streamwise VTE and using contours of vorticity and vorticity budgets. Further, the
heat transfer characteristics are studied using the mean and rms temperature profiles, evolution of
Nusselt number and distribution of turbulent heat flux. The following conclusions can be drawn
from the present study:

1. The constant coefficient Smagorinsky model with van-Driest damping used in the present
685 simulations has accurately captured the centerline velocity decay, spread rate of the jet in
the wall-normal and spanwise directions, the mean and second-order statistics of the flow.
Therefore the Smagorinsky model is recommended for turbulent wall jet simulations.
2. Two pairs of oppositely rotating $\langle \Omega_x \rangle$ vortices are observed around the potential core region.
The direction of these vortices is such that the spanwise spread of the flow is promoted
690 causing strong entrainment. Further downstream, these mean vortices show reduction in
magnitude.
3. The magnitude of contours of $\langle \Omega_y \rangle$ are comparable to that of $\langle \Omega_x \rangle$. The direction of rotation
of the $\langle \Omega_y \rangle$ vortices is such that they further aid in the secondary flow in the spanwise
direction leading to enhancing spanwise spread. Therefore, it is suggested that together
695 with $\langle \Omega_x \rangle$ vortices, the $\langle \Omega_y \rangle$ vortices also help in increasing in the spanwise spread of
three-dimensional wall jets.

This is the author's peer reviewed, accepted manuscript. However, the online version of record will be different from this version once it has been copyedited and typeset.

PLEASE CITE THIS ARTICLE AS DOI: 10.1063/5.0031138

- 700
4. The significance of mean streamwise and wall-normal vorticity in the lateral spread of three-dimensional wall jets can be verified by comparing them to the vortices of planar wall jets. The streamwise and wall-normal vortices have significantly larger magnitude in three-dimensional wall jets when compared to planar wall jets that have no secondary flow. Moreover, it is observed that the spanwise vorticity, which aids in the wall-normal growth of the jet, is higher in the planar wall jet, and therefore the planar wall jets have larger wall-normal spread rate than three-dimensional jets.

705

 5. All the terms occurring in the mean streamwise VTE, eq. 1, are analyzed. The obtained profiles are verified for correctness by comparing the sum of all the terms on the right-hand-side of the equation with those balancing them. It is observed that the vortex line bending term, term-C, plays a significant role near the nozzle exit, however its dominance decreases relatively as one moves downstream.

710

 6. The diffusion term, term-F, in the mean streamwise VTE has a larger magnitude near the wall due to larger values of second derivatives of $\langle \Omega_x \rangle$ in this region. The effect of vorticity diffusion diminishes swiftly as one moves away from the wall.

715

 7. The Reynolds stress terms are the dominant source in the mean streamwise VTE and thus can be considered as significant contributors towards the streamwise vorticity leading to large spanwise spread. The term with the gradients of Reynolds normal stress, term-D, shows higher magnitude and is out of phase with the gradients of Reynolds shear stress term, term-E.

720

 8. Two dominant Reynolds stress terms, term-D and term-E in the mean streamwise VTE are further split into two parts each, term-D2 and term-E2 are responsible for the higher magnitude for term-D and term-E respectively. Moreover, term-D2 and term-E2 are out of phase with each other in most of the regions and the summation of these terms act as sources for the streamwise vorticity to be large.

725

 9. Profile of wall shear stress as a function of the spanwise direction, appropriately non-dimensionalized, is plotted and it was noted that the wall shear stress profiles become self-similar beyond $x/h = 20$. The spanwise component of friction velocity is noted to be about half as large as the streamwise component of the friction velocity.

This is the author's peer reviewed, accepted manuscript. However, the online version of record will be different from this version once it has been copyedited and typeset.

PLEASE CITE THIS ARTICLE AS DOI: 10.1063/5.0031138

10. The profiles of mean and rms temperature as a function of the wall-normal direction are noted to be similar between the three-dimensional and planar wall jets in the self-similar region. The three-dimensional wall jet, however, shows a larger peak for rms temperature when compared to planar wall jet.
730
11. A dip in the rms temperature is observed, owing to lower rms u velocity, in the potential core region. The reduction in rms temperature leads to a reduction in heat transfer. This drop in heat transfer is also assisted by reduced interaction of eddies near the nozzle exit region. This dip in heat transfer near the potential core region may be considered as a design criterion while designing three-dimensional wall jets used in film-cooled components.
735
12. It is observed that the peak in the Nusselt number at the jet centerline for three-dimensional wall jets is higher than that of the planar wall jets, but further downstream, the Nusselt number in the three-dimensional wall jet falls sharply as compared to the planar wall jets.
740
13. The nature of heat transport is studied by plotting turbulent heat flux contours. A positive streamwise heat flux above the wall tends to transport heat along the positive streamwise direction, whereas the negative heat flux near the wall transports the heat in the negative streamwise direction. This change in the direction of heat transport might play a vital role in the analysis of three-dimensional wall jet which protect the components from the hot stream of gas above it.
745
14. The wall-normal component of turbulent heat flux, $\langle v'T' \rangle$, in the three-dimensional wall jet is positive in the domain, and thus heat is transported away from the wall.
750
15. The spanwise component of turbulent heat flux, $\langle w'T' \rangle$, in the three-dimensional wall jet has a sign change as one moves away from the jet centerline. This change of sign means that heat is transported away from the centerline while heat from the outer edge of the jet is transported towards the centerline. The phenomenon might be useful in the analysis of the heat transfer interaction among multiple parallel slot jets in film-cooled applications.
755

To conclude, three-dimensional wall jet can be accurately simulated using LES and with the constant coefficient Smagorinsky model with van-Driest near wall damping. The large spanwise spread of the wall jet is attributed to the mean streamwise component of vorticity and a potential contribution from the mean wall-normal component of vorticity. The gradients of Reynolds

This is the author's peer reviewed, accepted manuscript. However, the online version of record will be different from this version once it has been copyedited and typeset.

PLEASE CITE THIS ARTICLE AS DOI: 10.1063/5.0031138

⁷⁵⁵ normal stresses have the highest contribution to streamwise component of vorticity transport and, therefore, the spread of the three-dimensional wall jets. The turbulent heat flux characteristics and heat transfer plots show peculiar characteristics, which can impact the design of the film-cooled components. Therefore, the present work can be extended to study the heat transfer involved due to the interaction of hot free stream with multiple parallel three-dimensional wall jets to replicate film-
⁷⁶⁰ cooling in turbine blades. Further, numerical simulations can be carried out to study turbulence and heat flux budgets involved in the flow to enhance our understanding of turbulence in the wall jets. The data from energy budgets can also help in improving turbulence models for the simulation of wall jets.

V. ACKNOWLEDGEMENTS

⁷⁶⁵ The authors are grateful for the computational resources provided by P.G. Senapathy Center for Computer Resources on the VIRGO computing cluster at Indian Institute of Technology (IIT) Madras. The second author would like to acknowledge the funding received through the new-faculty initiation-grant, MEE1617852NFIGKAME, given by IIT Madras.

VI. DATA AVAILABILITY

⁷⁷⁰ The data that support the findings of this study are available from the corresponding author upon reasonable request.

REFERENCES

- ¹C. Fu, M. Uddin, and A. Curley, "Insights derived from CFD studies on the evolution of planar wall jets," *Engineering Applications of Computational Fluid Mechanics* **10**, 44–56 (2016).
- ⁷⁷⁵ ²R. AbdulNour, K. Willenborg, J. McGrath, J. Foss, and B. AbdulNour, "Measurements of the convection heat transfer coefficient for a planar wall jet: uniform temperature and uniform heat flux boundary conditions," *Experimental Thermal and Fluid Science* **22**, 123–131 (2000).
- ³I. Z. Naqavi, P. G. Tucker, and Y. Liu, "Large-eddy simulation of the interaction of wall jets with external stream," *International Journal of Heat and Fluid Flow* **50**, 431–444 (2014).
- ⁷⁸⁰ ⁴E. Curd, "Possible applications of wall jets in controlling air contaminants," *The Annals of Occupational Hygiene* **24**, 133–146 (1981).

This is the author's peer reviewed, accepted manuscript. However, the online version of record will be different from this version once it has been copyedited and typeset.

PLEASE CITE THIS ARTICLE AS DOI: 10.1063/5.0031138

- ⁵T. Guo, M. J. Rau, P. P. Vlachos, and S. V. Garimella, "Axisymmetric wall jet development in confined jet impingement," *Physics of Fluids* **29**, 025102 (2017).
- ⁶S. Sharma, V. Jesudhas, R. Balachandar, and R. Barron, "Turbulence structure of a counter-flowing wall jet," *Physics of Fluids* **31**, 025110 (2019).
- ⁷S. Dey, G. Ravi Kishore, O. Castro-Orgaz, and S. Z. Ali, "Hydrodynamics of submerged turbulent plane offset jets," *Physics of Fluids* **29**, 065112 (2017).
- ⁸P. M. Sforza and G. Herbst, "A study of three-dimensional, incompressible, turbulent wall jets," *AIAA Journal* **8**, 276–283 (1970).
- ⁹B. Newman, R. Patel, S. Savage, and H. Tjio, "Three-dimensional wall jet originating from a circular orifice," *The Aeronautical Quarterly* **23**, 188–200 (1972).
- ¹⁰N. Rajaratnam and B. S. Pani, "Three-dimensional turbulent wall jets," *Journal of the Hydraulics Division* **100**, 69–83 (1974).
- ¹¹H. Sun and D. Ewing, "Effect of initial and boundary conditions on development of three-dimensional wall jets," in *40th AIAA Aerospace Sciences Meeting & Exhibit* (2002) p. 733.
- ¹²J. W. Hall and D. Ewing, "Three-dimensional turbulent wall jets issuing from moderate-aspect-ratio rectangular channels," *AIAA Journal* **45**, 1177–1186 (2007).
- ¹³M. Agelin-Chaab and M. Tachie, "Characteristics of turbulent three-dimensional wall jets," *Journal of Fluids Engineering* **133** (2011).
- ¹⁴G. Padmanabham and B. H. Lakshmana Gowda, "Mean and Turbulence Characteristics of a Class of Three-Dimensional Wall Jets – Part 2: Turbulence Characteristics," *Journal of Fluids Engineering* **113**, 629–634 (1991).
- ¹⁵H. Abrahamsson, B. Johansson, and L. Löfdahl, "An investigation of the turbulence field in a three-dimensional wall jet," in *Advances in Turbulence VI* (Springer, 1996) pp. 417–420.
- ¹⁶A. W.-K. Law and Herlina, "An experimental study on turbulent circular wall jets," *Journal of Hydraulic Engineering* **128**, 161–174 (2002).
- ¹⁷A. W.-K. Law *et al.*, "Measurements of turbulent mass transport of a circular wall jet," *International Journal of Heat and Mass Transfer* **45**, 4899–4905 (2002).
- ¹⁸J. J. Ai, S. Yu, A. W.-K. Law, and L. Chua, "Vortex dynamics in starting square water jets," *Physics of Fluids* **17**, 014106 (2005).
- ¹⁹S. C. Godi, A. Pattamatta, and C. Balaji, "Effect of the inlet geometry on the flow and heat transfer characteristics of three-dimensional wall jets," *Journal of Heat Transfer* **141** (2019).

This is the author's peer reviewed, accepted manuscript. However, the online version of record will be different from this version once it has been copyedited and typeset.

PLEASE CITE THIS ARTICLE AS DOI: 10.1063/5.0031138

- ²⁰S. C. Godi, A. Pattamatta, and C. Balaji, "Heat transfer from a single and row of three dimensional wall jets-a combined experimental and numerical study," *International Journal of Heat and Mass Transfer* **159**, 119801 (2020).
- ⁸¹⁵²¹B. Launder and W. Rodi, "The turbulent wall jet," *Progress in Aerospace Sciences* **19**, 81–128 (1979).
- ²²B. Launder and W. Rodi, "The turbulent wall jet measurements and modeling," *Annual Review of Fluid Mechanics* **15**, 429–459 (1983).
- ⁸²⁰²³T. Craft and B. Launder, "On the spreading mechanism of the three-dimensional turbulent wall jet," *Journal of Fluid Mechanics* **435**, 305–326 (2001).
- ²⁴L. Namgyal and J. W. Hall, "Coherent streamwise vortex structures in the near-field of the three-dimensional wall jet," *Journal of Fluids Engineering* **135** (2013).
- ⁸²⁵²⁵L. Namgyal and J. Hall, "Reynolds stress distribution and turbulence generated secondary flow in the turbulent three-dimensional wall jet," *Journal of Fluid Mechanics* **800**, 613–644 (2016).
- ²⁶T. Panidis, R. Schwab, and A. Pollard, "The role of vorticity in the near field development of sharp-edged, rectangular, wall jets," *International Journal of Heat and Fluid Flow* **67**, 3–22 (2017).
- ⁸³⁰²⁷A. P. Vouros, T. Panidis, A. Pollard, and R. R. Schwab, "Near field vorticity distributions from a sharp-edged rectangular jet," *International Journal of Heat and Fluid Flow* **51**, 383–394 (2015).
- ²⁸I. Z. Naqavi, J. C. Tyacke, and P. G. Tucker, "Direct numerical simulation of a wall jet: flow physics," *Journal of Fluid Mechanics* **852**, 507–542 (2018).
- ⁸³⁵²⁹I. Z. Naqavi, J. C. Tyacke, and P. G. Tucker, "A numerical study of a plane wall jet with heat transfer," *International Journal of Heat and Fluid Flow* **63**, 99–107 (2017).
- ³⁰N. Rostamy, D. Bergstrom, D. Sumner, and J. Bugg, "The effect of surface roughness on the turbulence structure of a plane wall jet," *Physics of Fluids* **23**, 085103 (2011).
- ³¹D. Ahlman, G. Brethouwer, and A. V. Johansson, "Direct numerical simulation of a plane turbulent wall-jet including scalar mixing," *Physics of fluids* **19**, 065102 (2007).
- ⁸⁴⁰³²D. Ahlman, G. Velter, G. Brethouwer, and A. V. Johansson, "Direct numerical simulation of nonisothermal turbulent wall jets," *Physics of fluids* **21**, 035101 (2009).
- ³³Z. Pouransari, G. Brethouwer, and A. V. Johansson, "Direct numerical simulation of an isothermal reacting turbulent wall-jet," *Physics of fluids* **23**, 085104 (2011).
- ³⁴A. Dejoan and M. A. Leschziner, "Large eddy simulation of a plane turbulent wall jet," *Physics of Fluids* **17**, 025102 (2005).

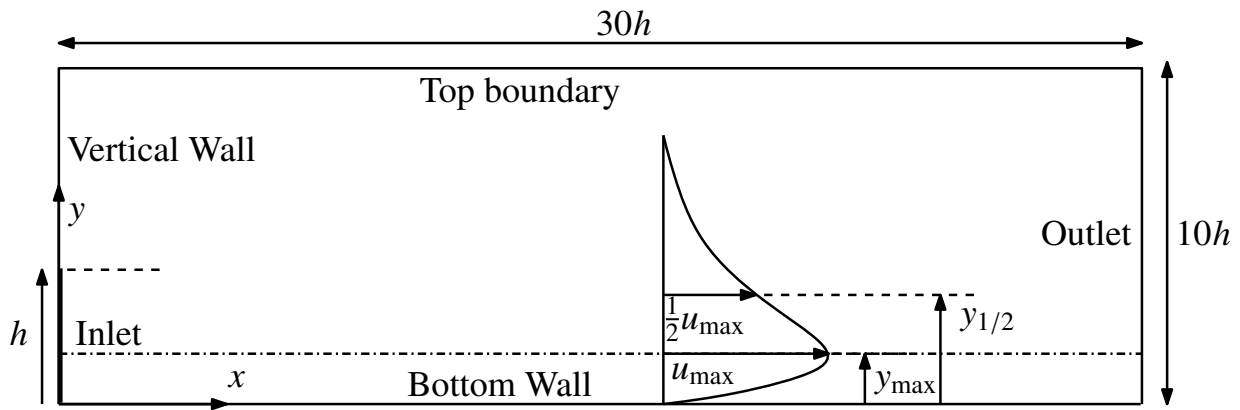
This is the author's peer reviewed, accepted manuscript. However, the online version of record will be different from this version once it has been copyedited and typeset.

PLEASE CITE THIS ARTICLE AS DOI: 10.1063/5.0031138

- ⁸⁴⁵ ³⁵P. Kakka and K. Anupindi, "Assessment of subgrid-scale models for large-eddy simulation of a planar turbulent wall-jet with heat transfer," International Journal of Heat and Mass Transfer **153**, 119593 (2020).
- ³⁶S. Zhang, A. W.-K. Law, and B. Zhao, "Large eddy simulations of turbulent circular wall jets," International Journal of Heat and Mass Transfer **80**, 72–84 (2015).
- ⁸⁵⁰ ³⁷S. B. Pope, "Turbulent flows," (2001).
- ³⁸H. G. Weller, G. Tabor, H. Jasak, and C. Fureby, "A tensorial approach to computational continuum mechanics using object-oriented techniques," Computers in Physics **12**, 620–631 (1998).
- ³⁹"OpenFOAM documentation, <http://www.openfoam.org/>," (Version 5.0).
- ⁸⁵⁵ ⁴⁰U. Ayachit, "The paraview guide: A parallel visualization application," (2015).
- ⁴¹T. Williams, C. Kelley, and many others, "Gnuplot 4.4: an interactive plotting program," <http://gnuplot.sourceforge.net/> (2010).
- ⁴²I. Celik, M. Klein, and J. Janicka, "Assessment measures for engineering les applications," Journal of Fluids Engineering **131**, 031102 (2009).

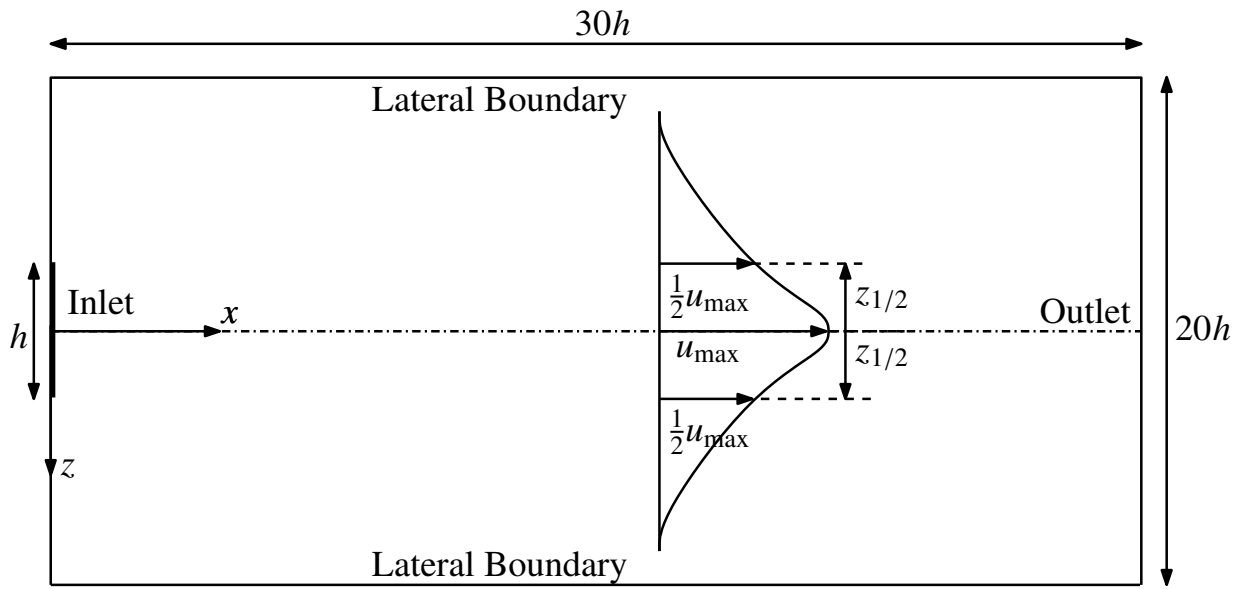
This is the author's peer reviewed, accepted manuscript. However, the online version of record will be different from this version once it has been copyedited and typeset.

PLEASE CITE THIS ARTICLE AS DOI: 10.1063/5.0031138



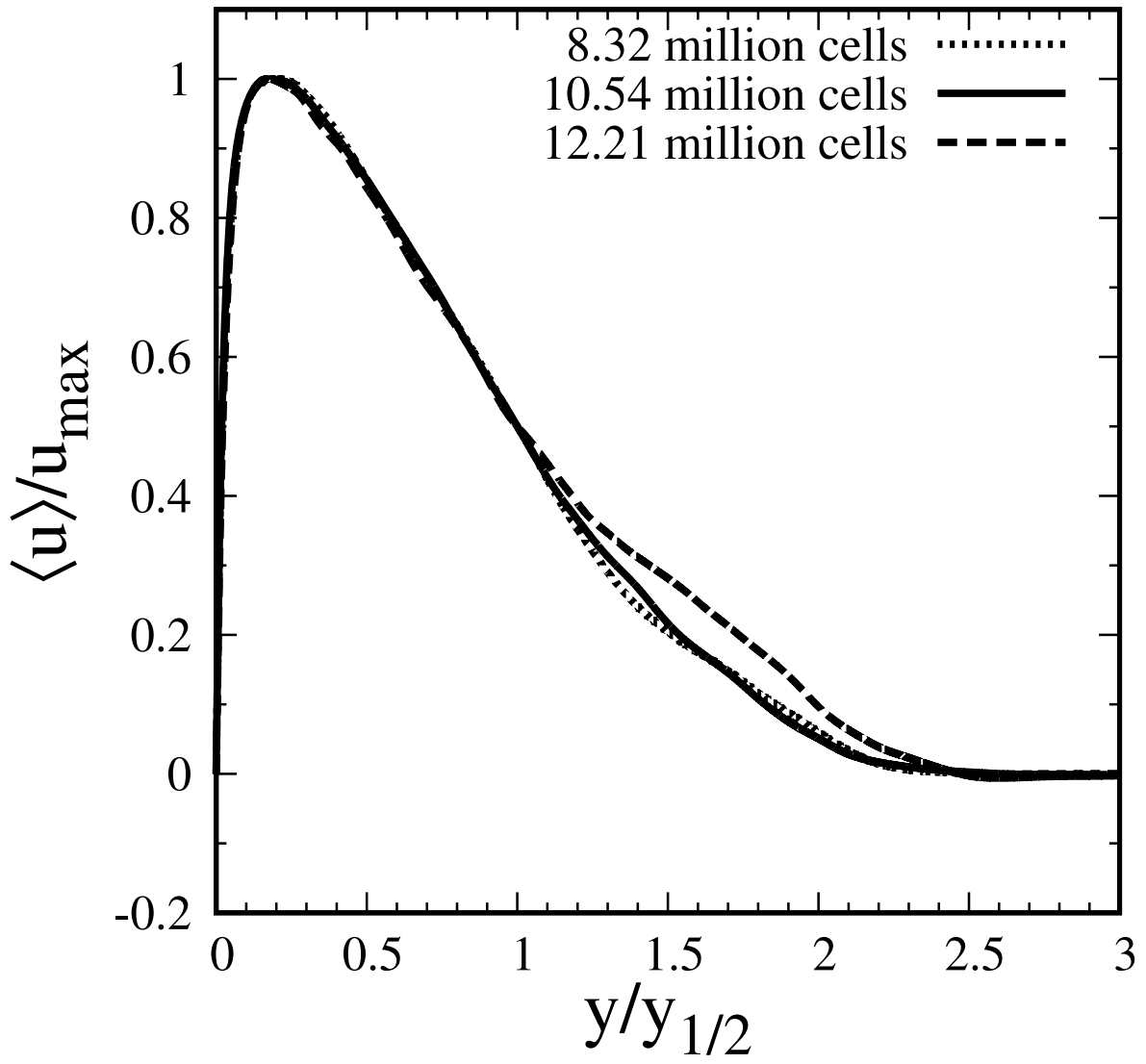
This is the author's peer reviewed, accepted manuscript. However, the online version of record will be different from this version once it has been copyedited and typeset.

PLEASE CITE THIS ARTICLE AS DOI: 10.1063/5.0031138



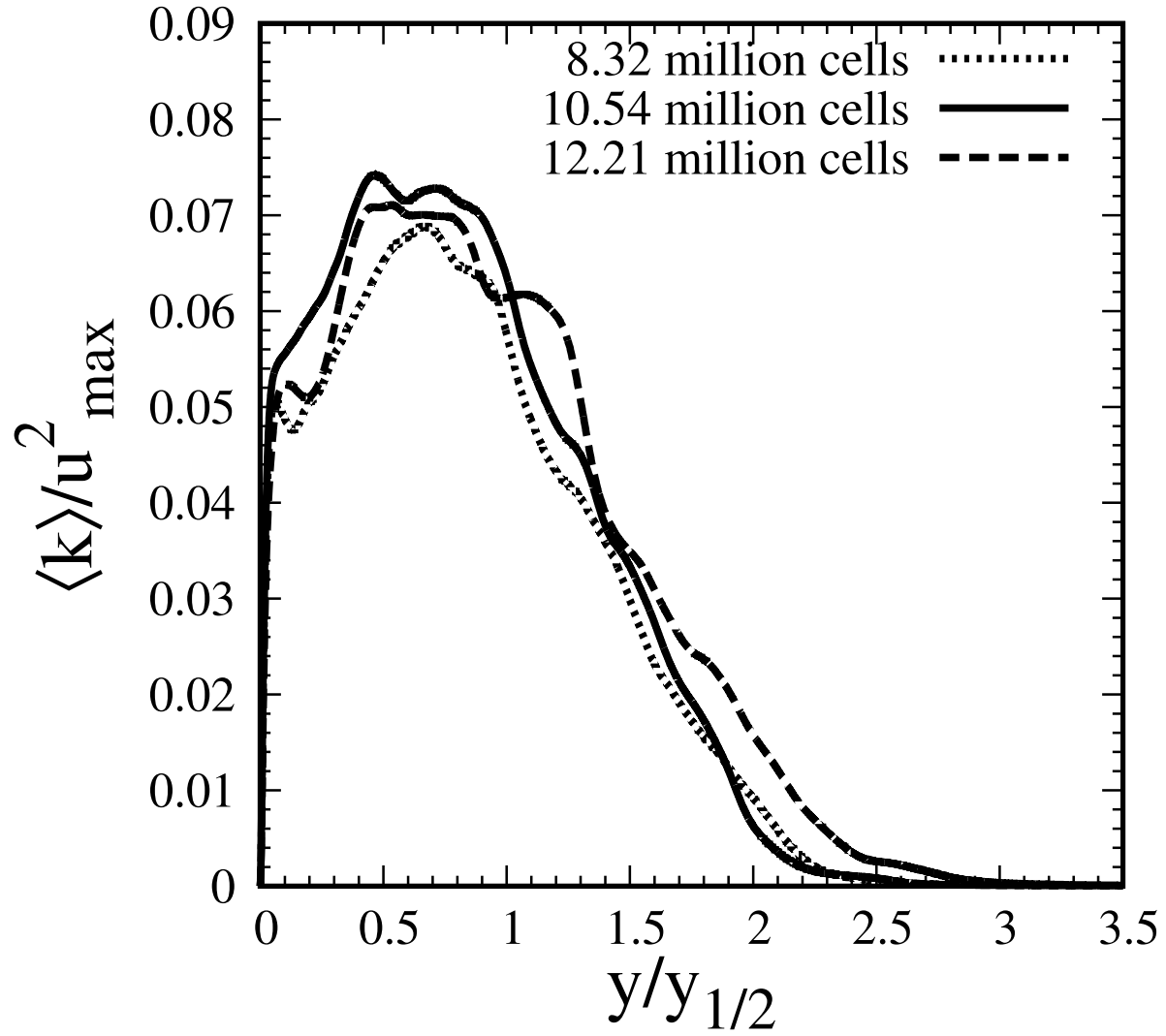
This is the author's peer reviewed, accepted manuscript. However, the online version of record will be different from this version once it has been copyedited and typeset.

PLEASE CITE THIS ARTICLE AS DOI: 10.1063/5.0031138



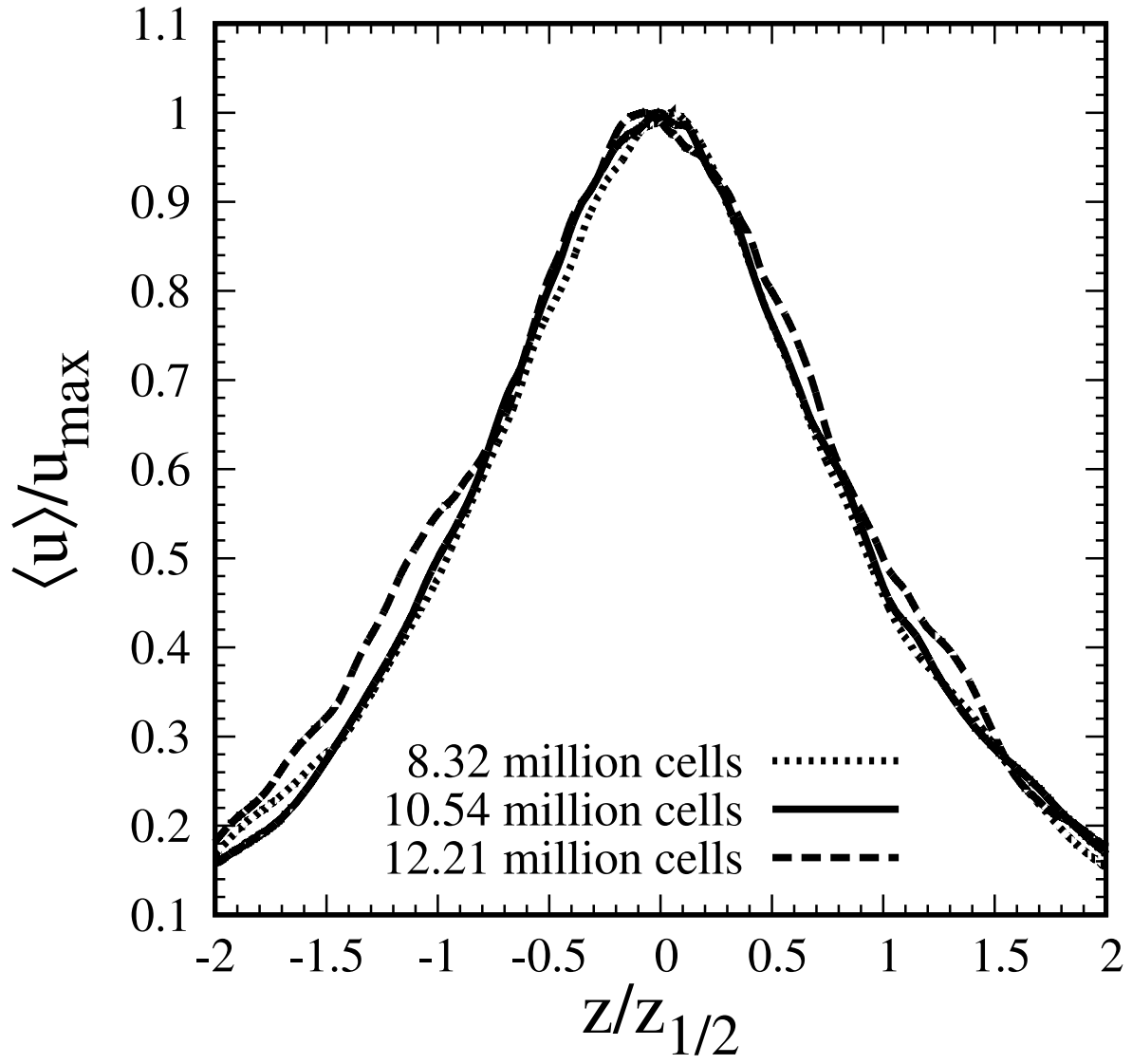
This is the author's peer reviewed, accepted manuscript. However, the online version of record will be different from this version once it has been copyedited and typeset.

PLEASE CITE THIS ARTICLE AS DOI: 10.1063/5.0031138



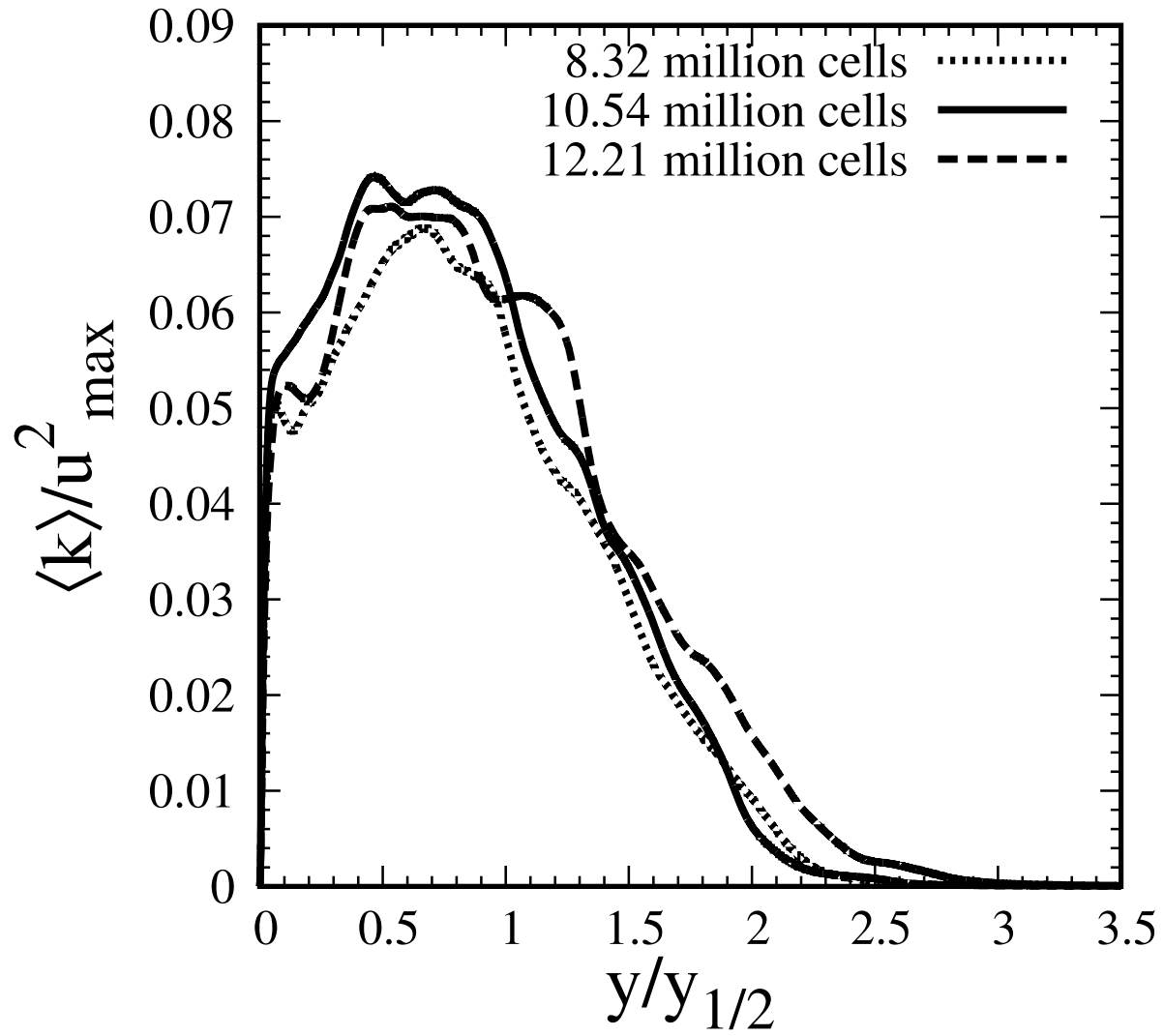
This is the author's peer reviewed, accepted manuscript. However, the online version of record will be different from this version once it has been copyedited and typeset.

PLEASE CITE THIS ARTICLE AS DOI: 10.1063/5.0031138



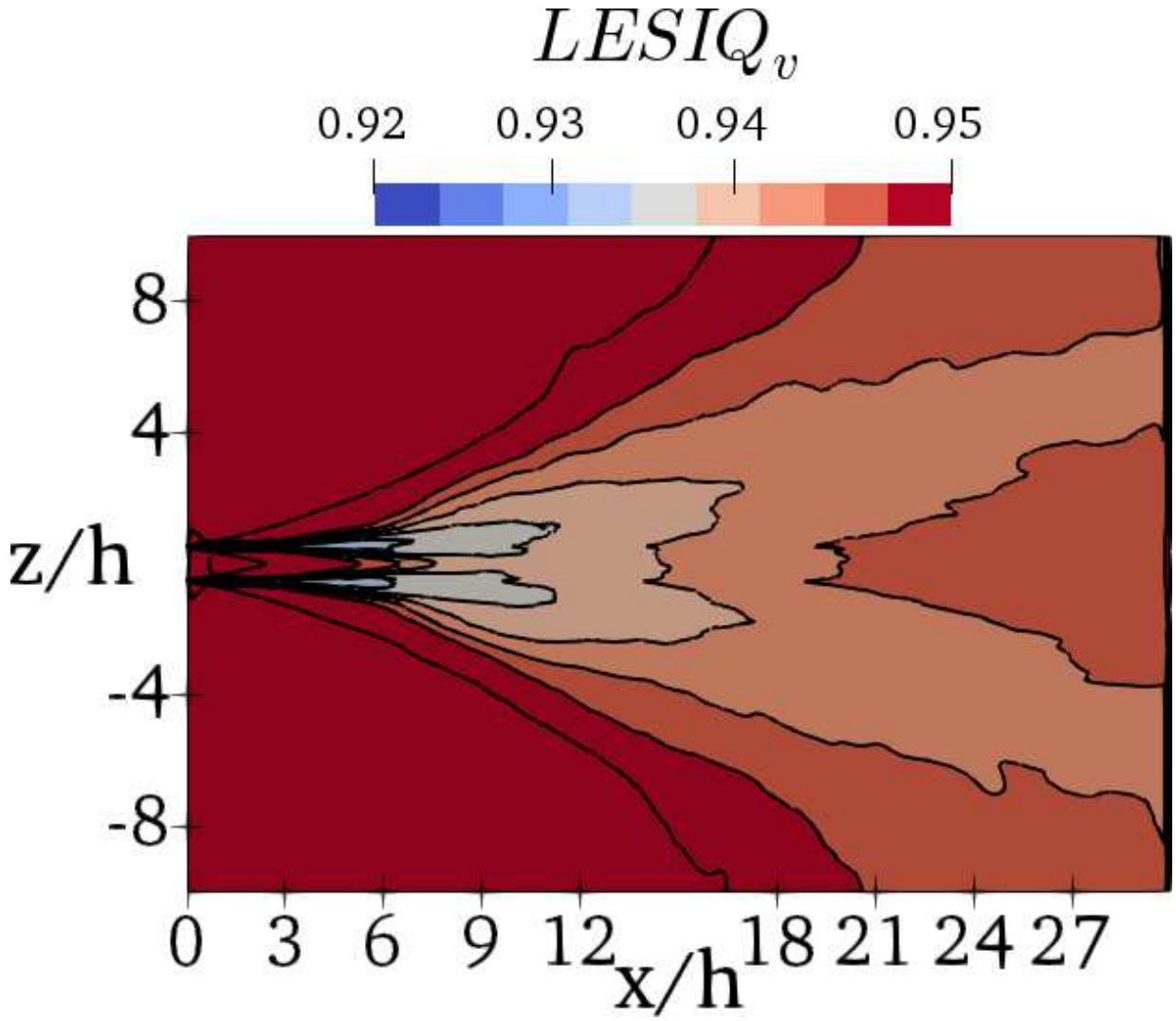
This is the author's peer reviewed, accepted manuscript. However, the online version of record will be different from this version once it has been copyedited and typeset.

PLEASE CITE THIS ARTICLE AS DOI: 10.1063/5.0031138



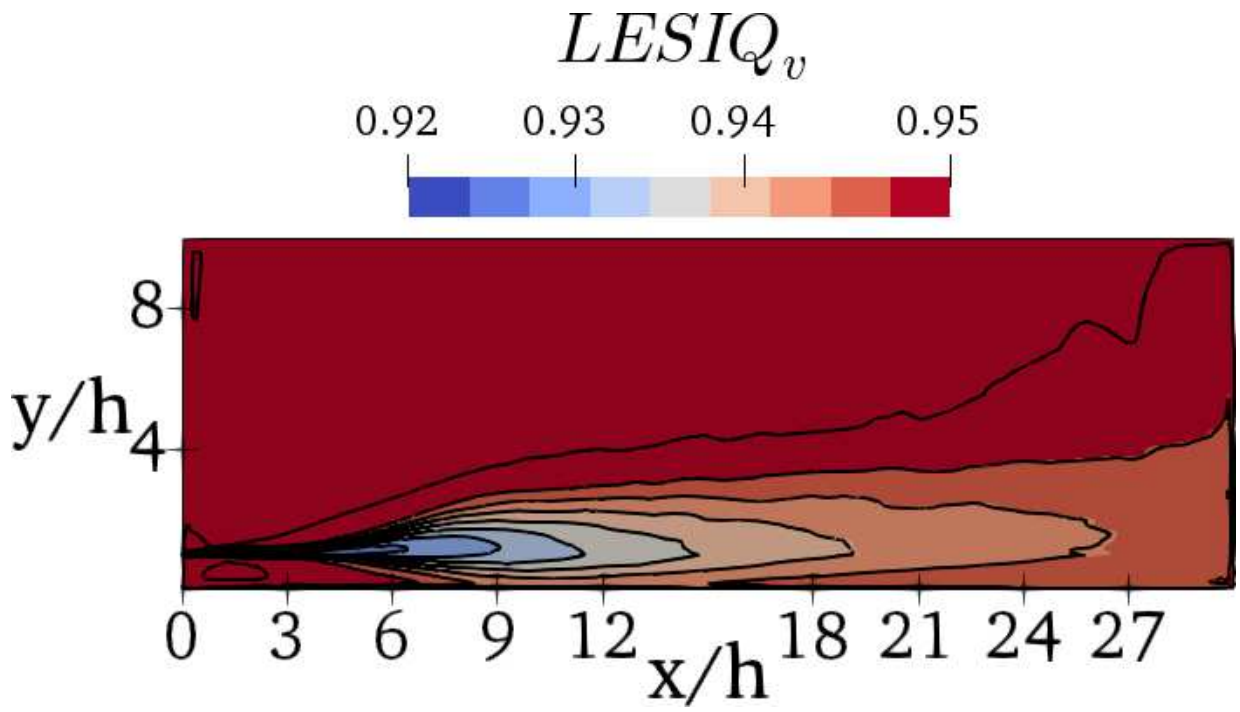
This is the author's peer reviewed, accepted manuscript. However, the online version of record will be different from this version once it has been copyedited and typeset.

PLEASE CITE THIS ARTICLE AS DOI: 10.1063/5.0031138



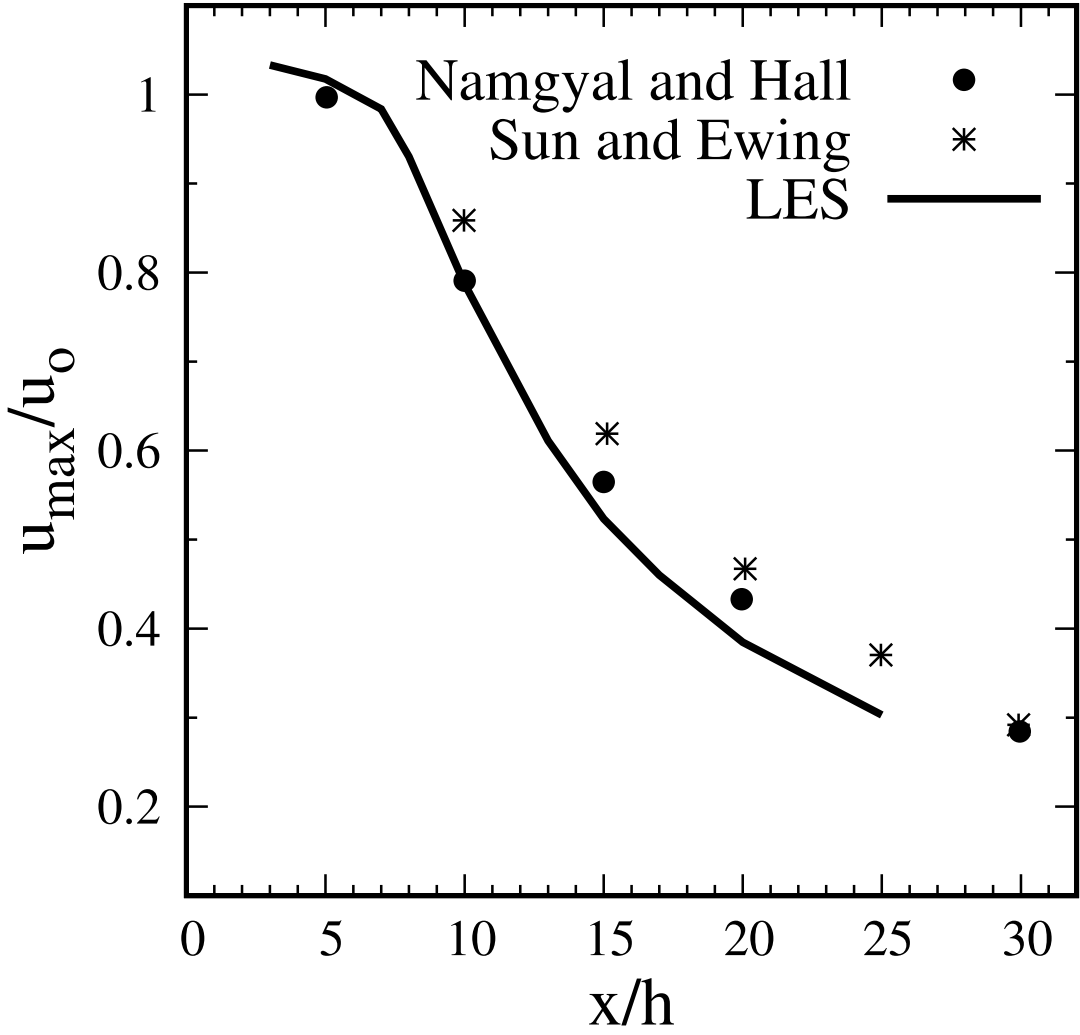
This is the author's peer reviewed, accepted manuscript. However, the online version of record will be different from this version once it has been copyedited and typeset.

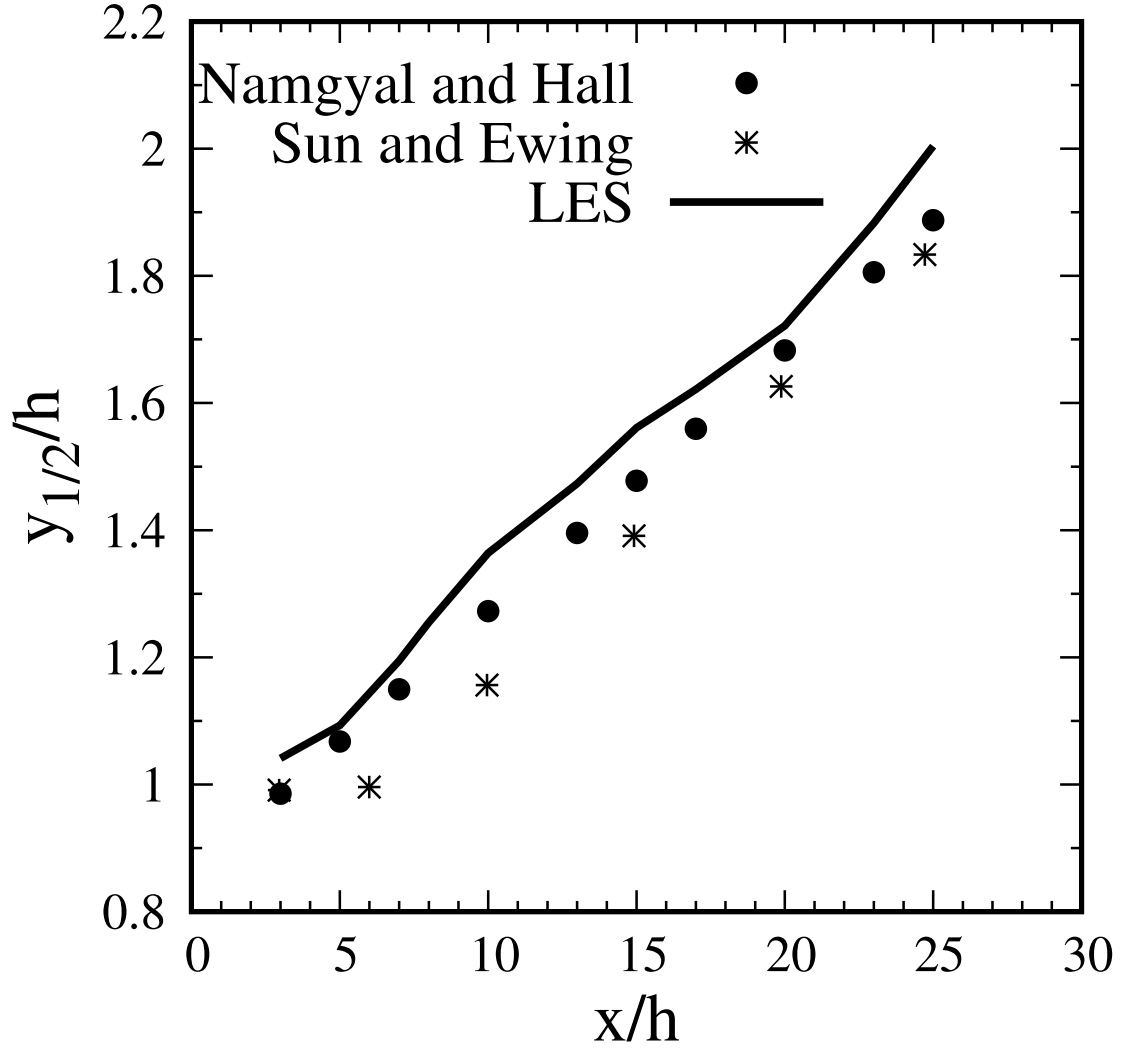
PLEASE CITE THIS ARTICLE AS DOI: 10.1063/5.0031138

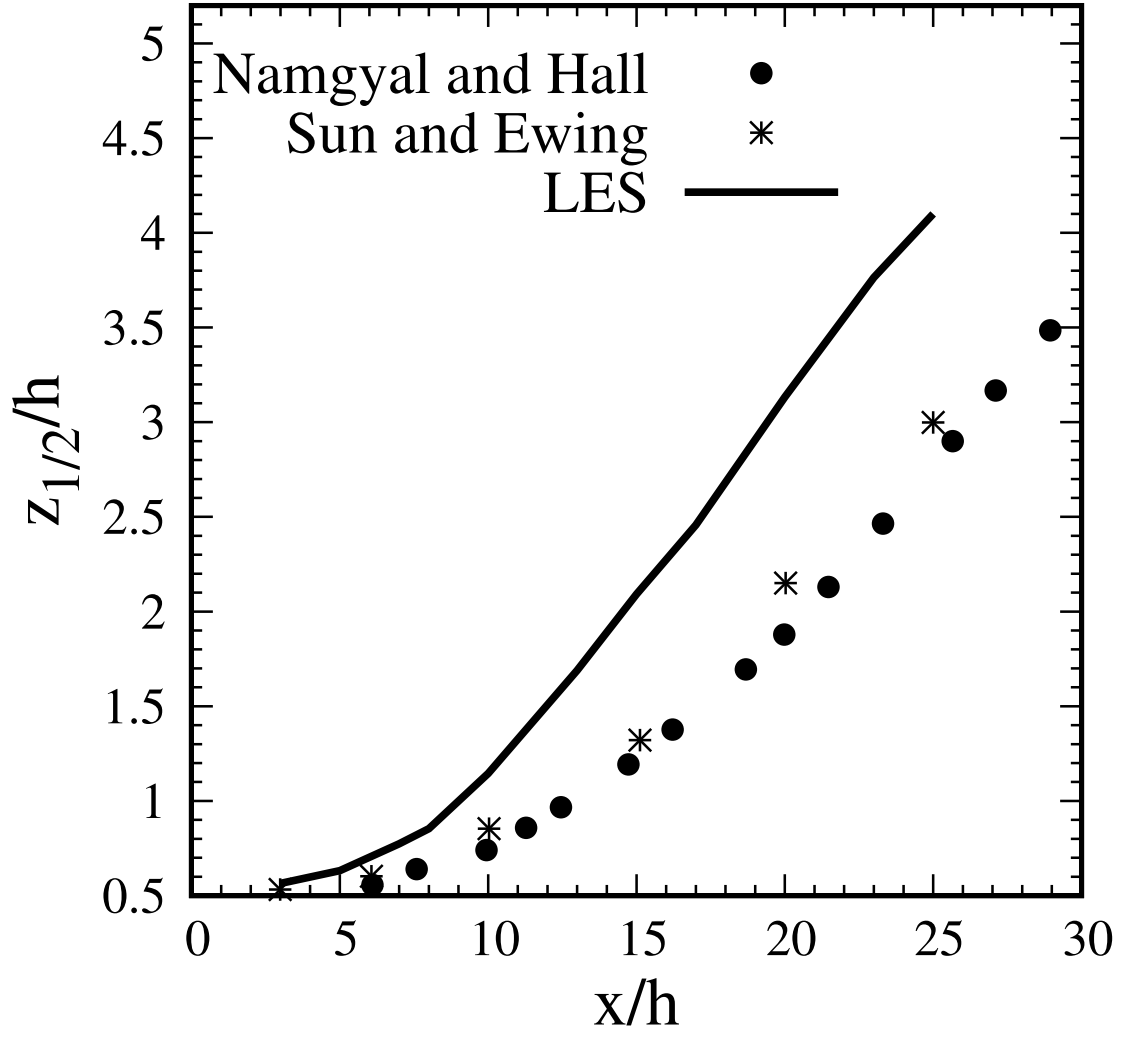


This is the author's peer reviewed, accepted manuscript. However, the online version of record will be different from this version once it has been copyedited and typeset.

PLEASE CITE THIS ARTICLE AS DOI: 10.1063/5.0031138

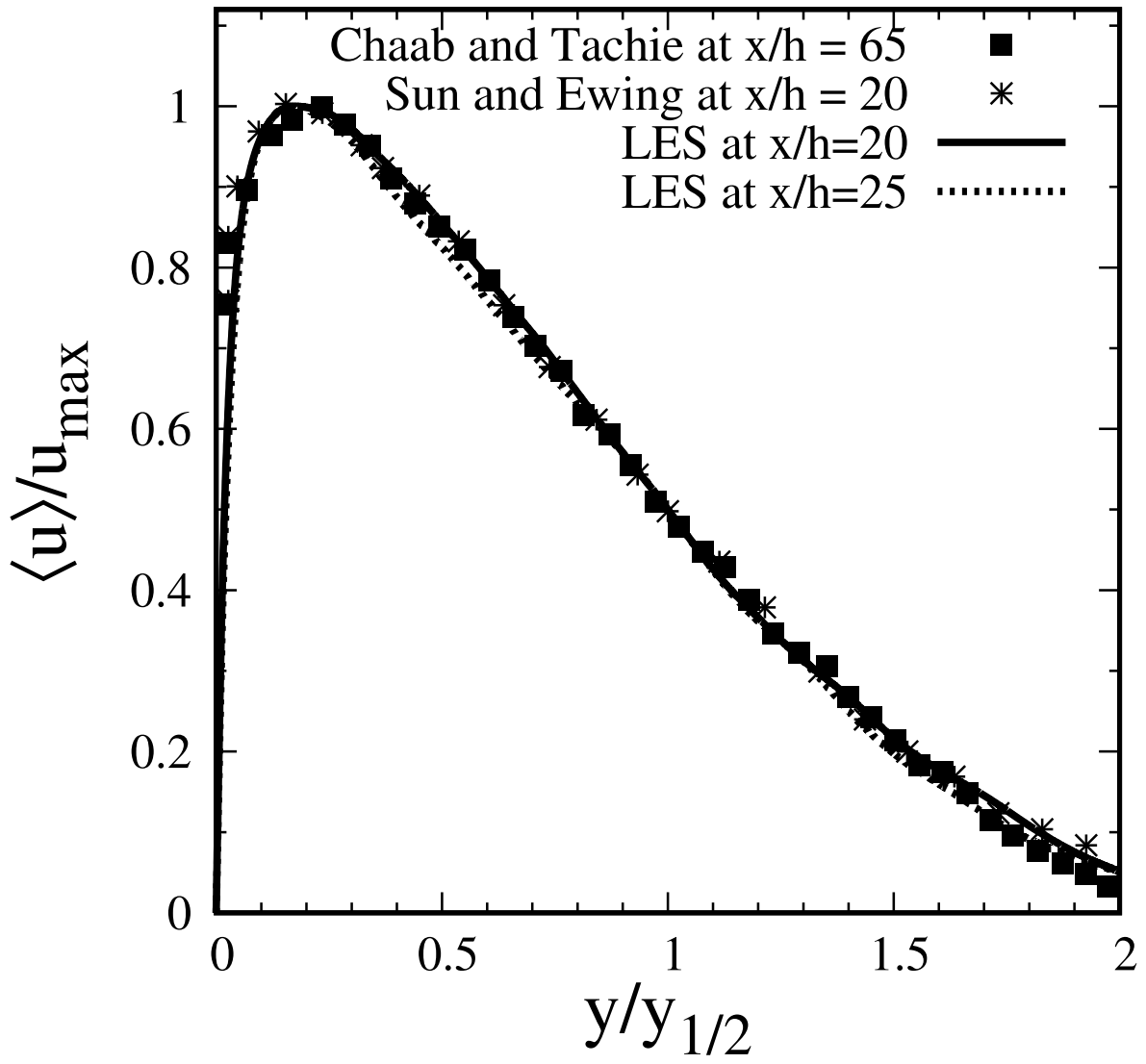






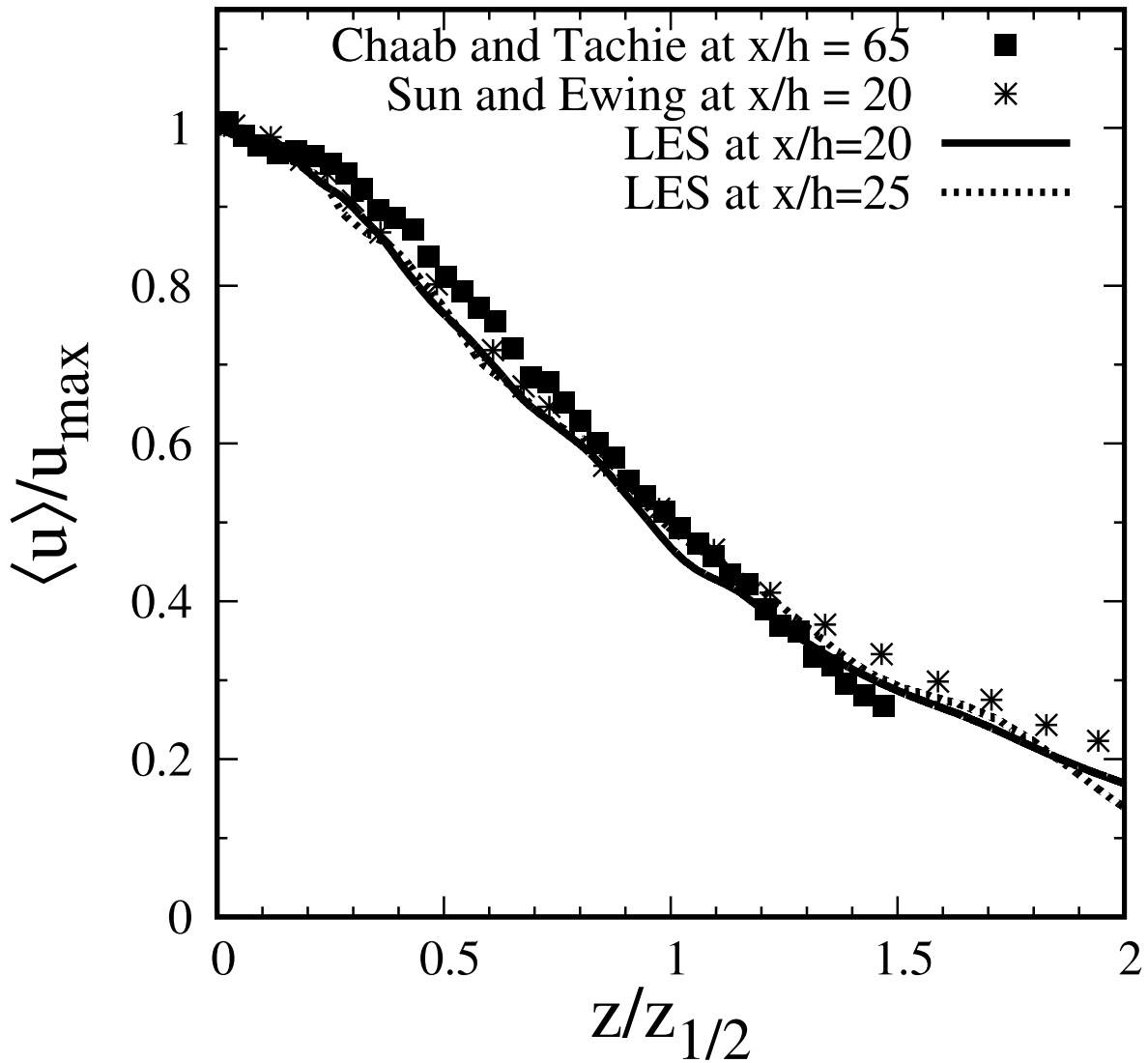
This is the author's peer reviewed, accepted manuscript. However, the online version of record will be different from this version once it has been copyedited and typeset.

PLEASE CITE THIS ARTICLE AS DOI: 10.1063/5.0031138



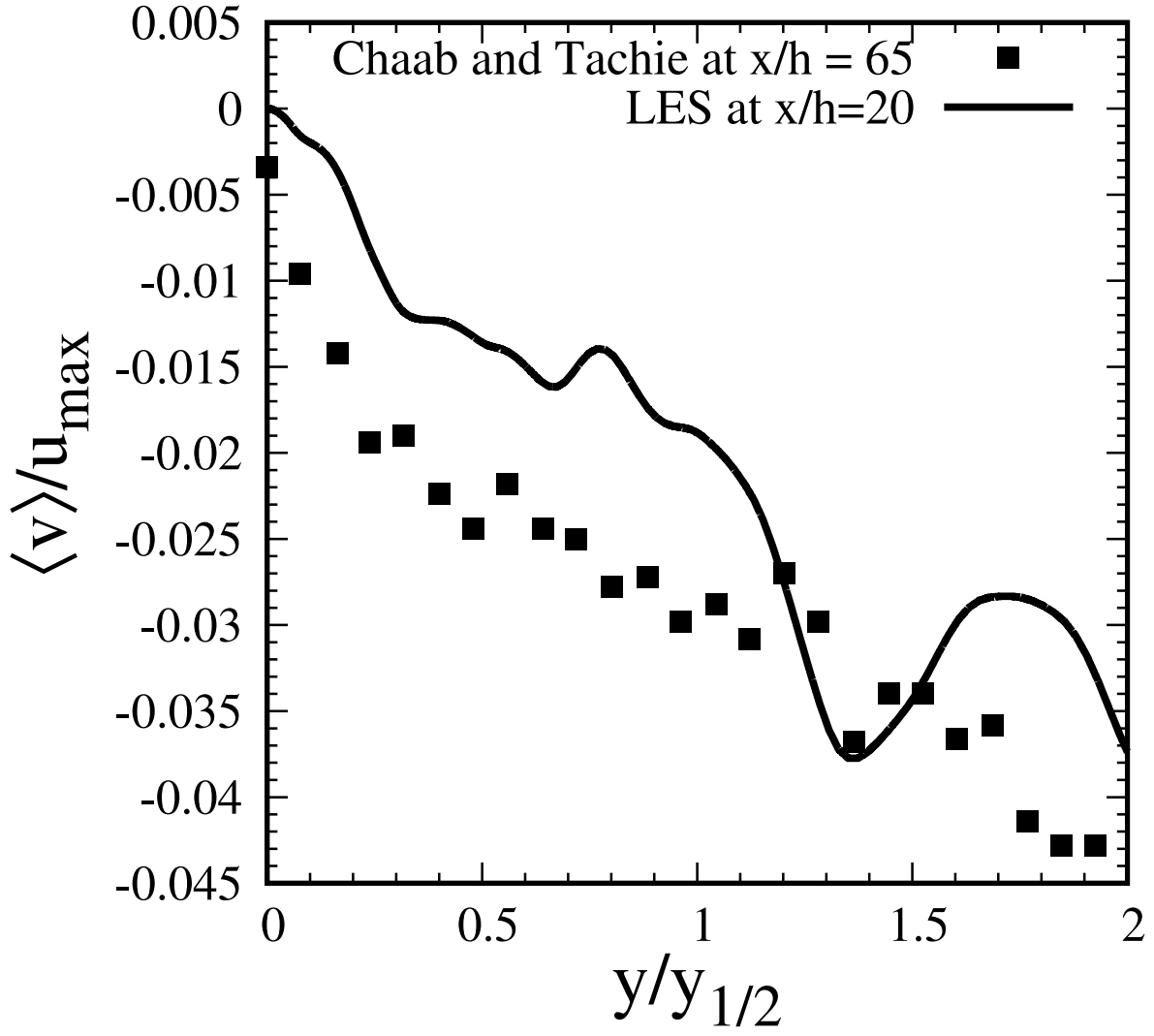
This is the author's peer reviewed, accepted manuscript. However, the online version of record will be different from this version once it has been copyedited and typeset.

PLEASE CITE THIS ARTICLE AS DOI: 10.1063/5.0031138



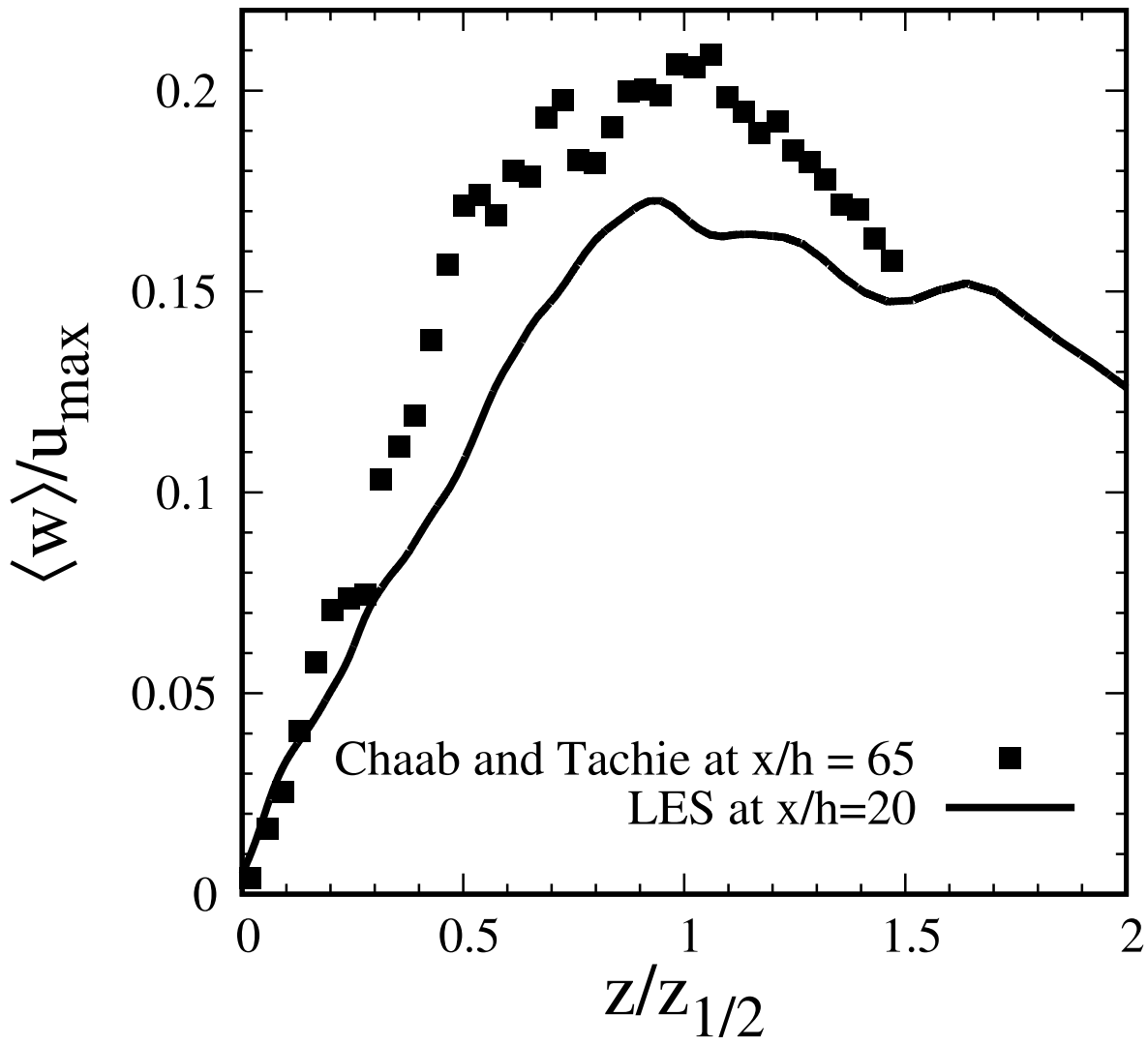
This is the author's peer reviewed, accepted manuscript. However, the online version of record will be different from this version once it has been copyedited and typeset.

PLEASE CITE THIS ARTICLE AS DOI: 10.1063/5.0031138



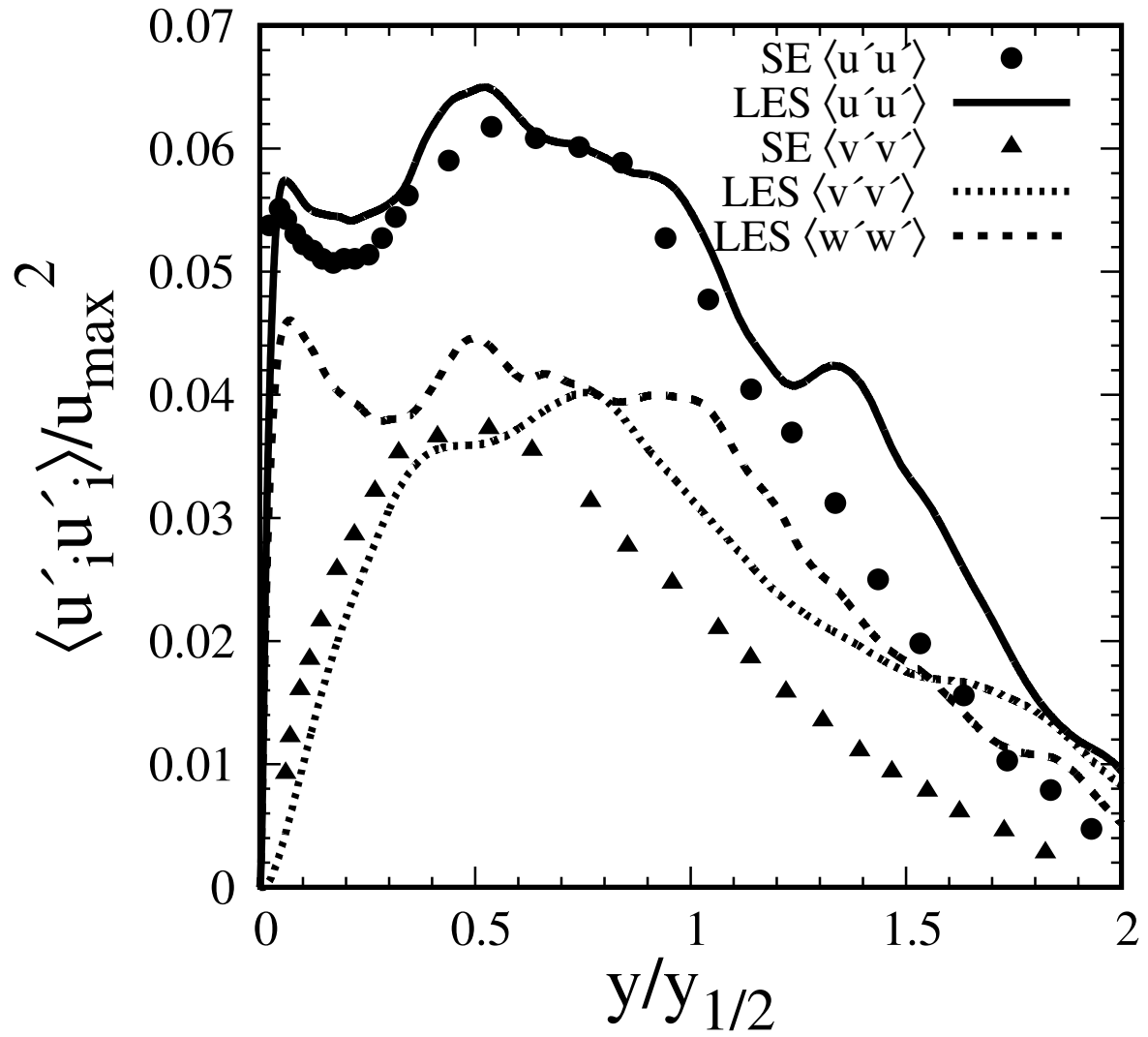
This is the author's peer reviewed, accepted manuscript. However, the online version of record will be different from this version once it has been copyedited and typeset.

PLEASE CITE THIS ARTICLE AS DOI: 10.1063/5.0031138



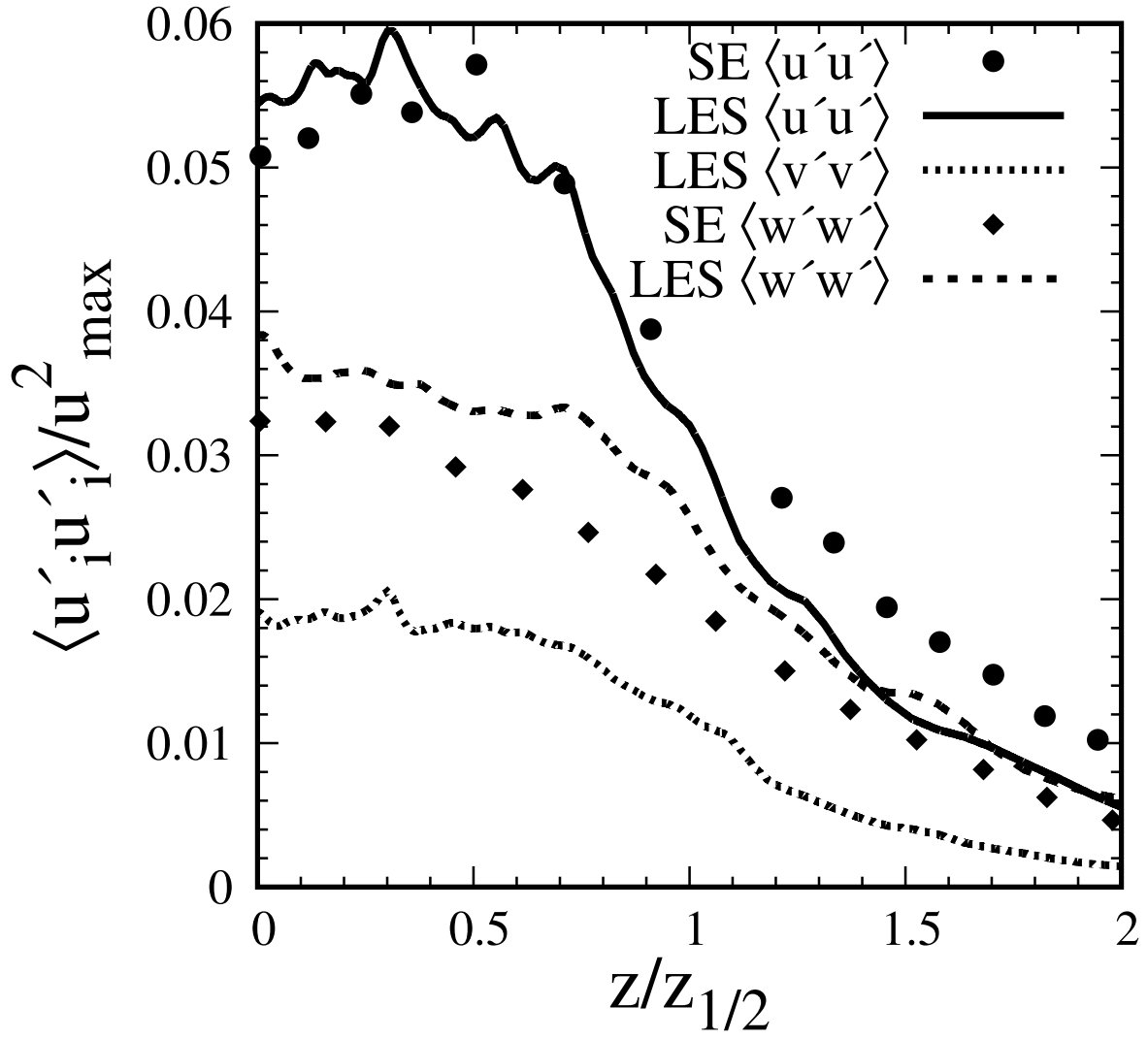
This is the author's peer reviewed, accepted manuscript. However, the online version of record will be different from this version once it has been copyedited and typeset.

PLEASE CITE THIS ARTICLE AS DOI: 10.1063/5.0031138

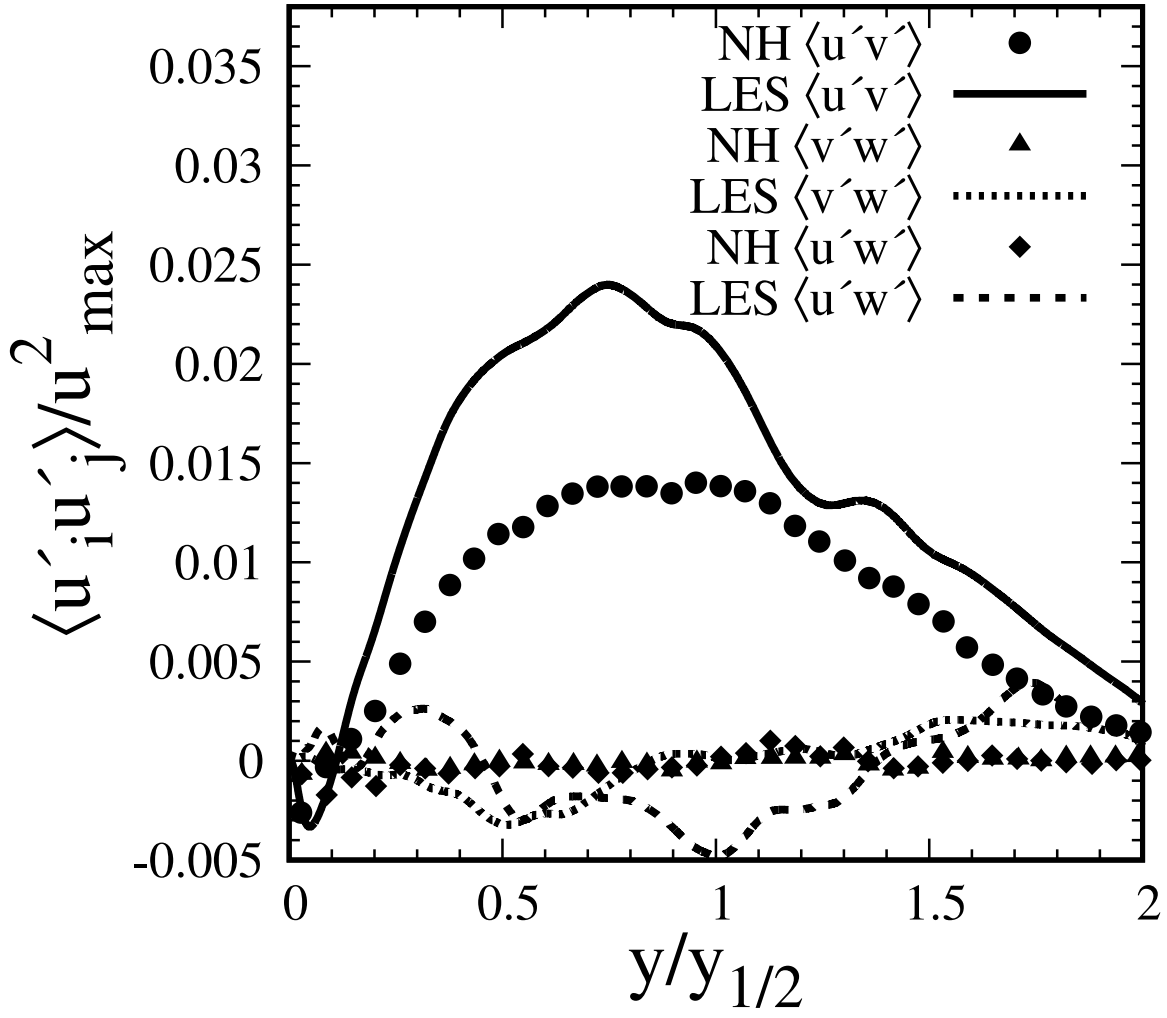


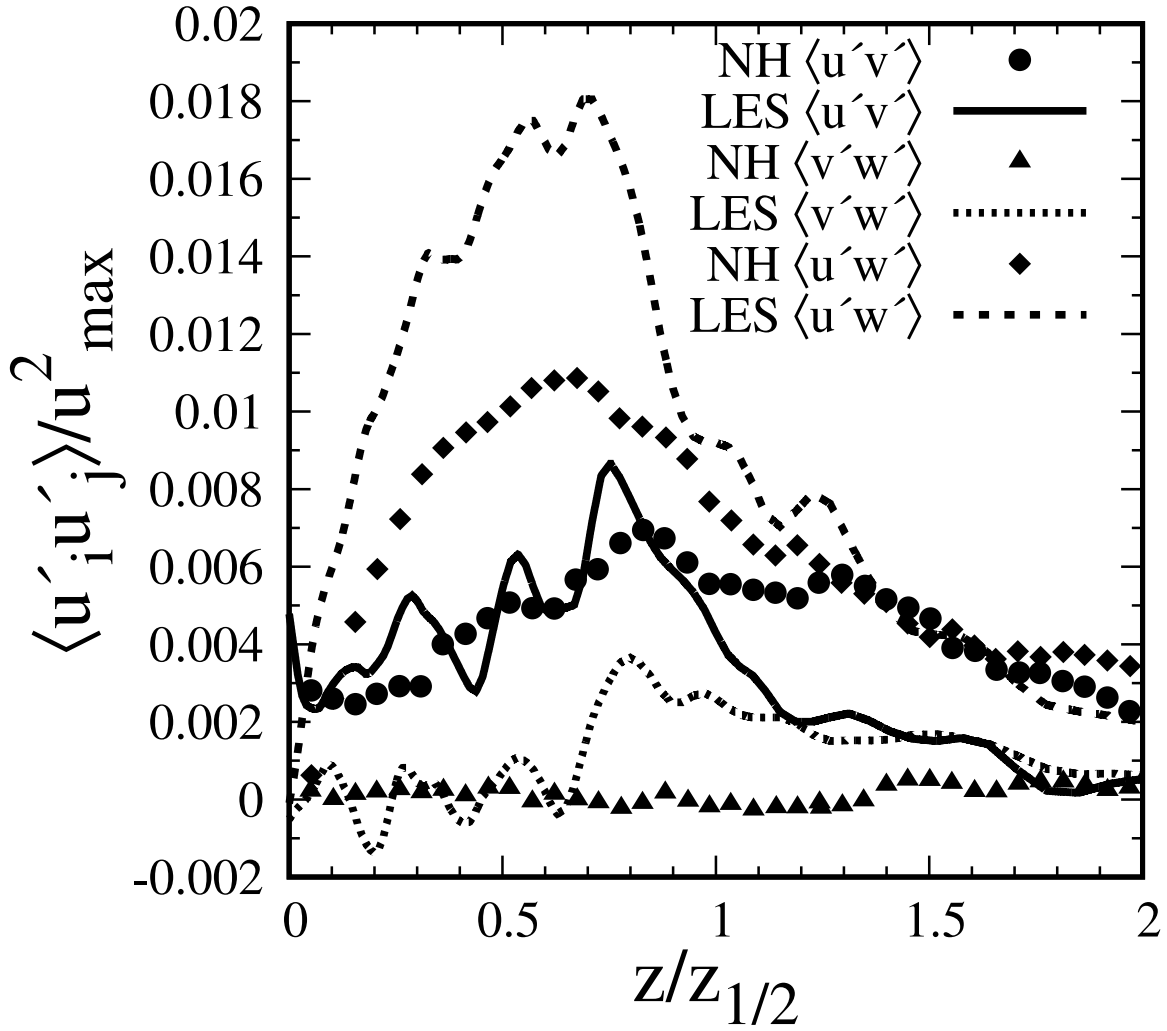
This is the author's peer reviewed, accepted manuscript. However, the online version of record will be different from this version once it has been copyedited and typeset.

PLEASE CITE THIS ARTICLE AS DOI: 10.1063/5.0031138



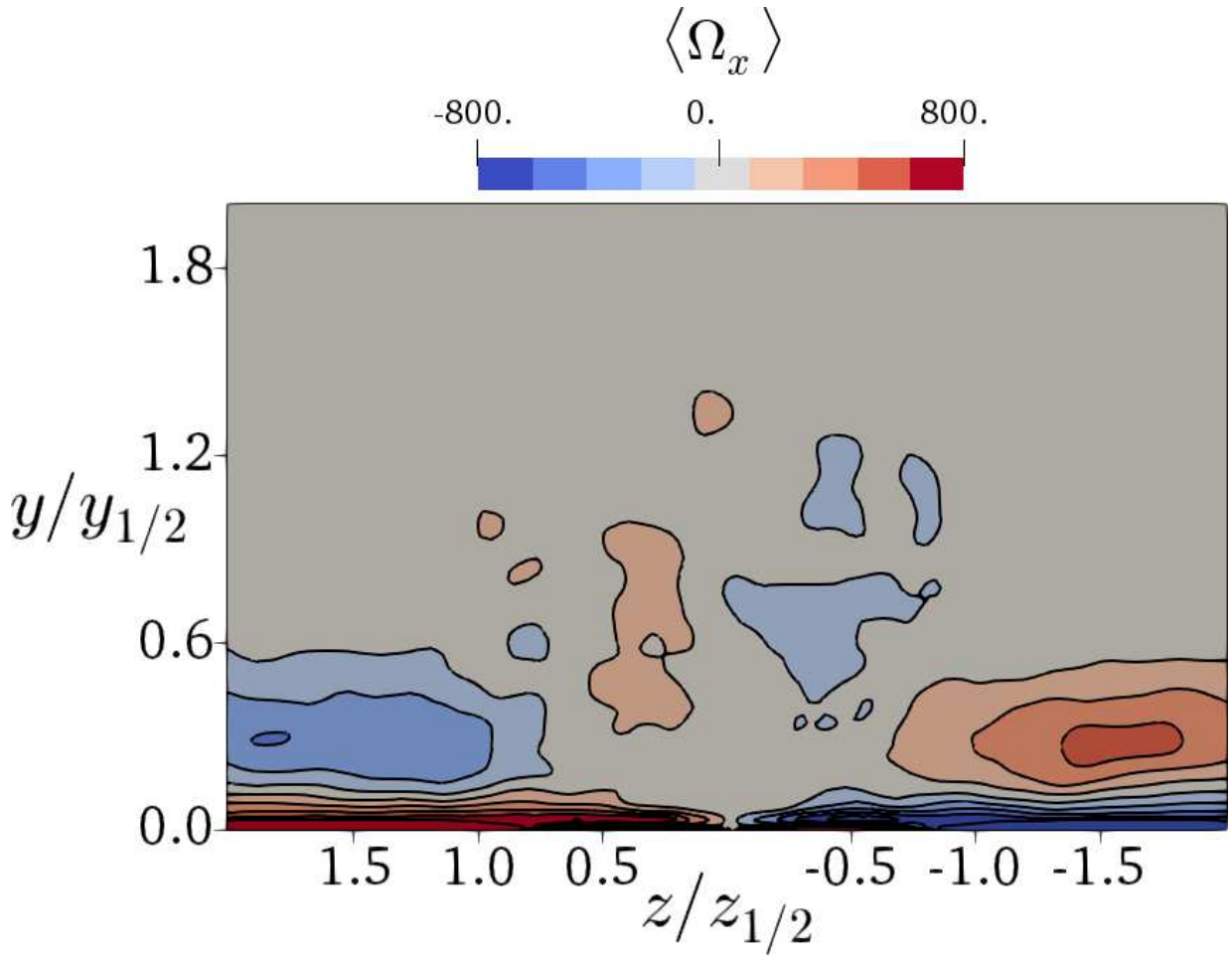
This is the author's peer reviewed, accepted manuscript. However, the online version of record will be different from this version once it has been copyedited and typeset.
PLEASE CITE THIS ARTICLE AS DOI: 10.1063/5.0031138





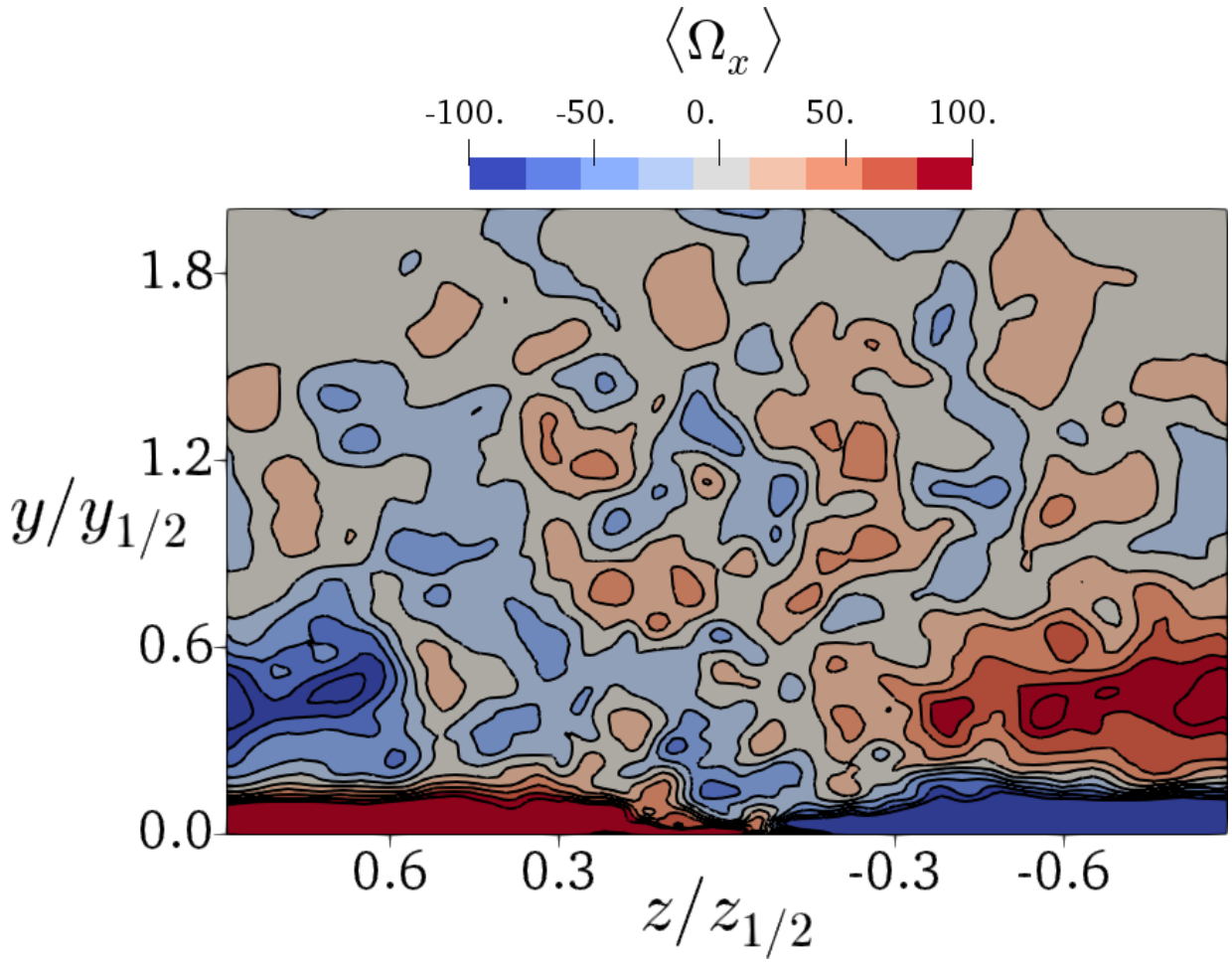
This is the author's peer reviewed, accepted manuscript. However, the online version of record will be different from this version once it has been copyedited and typeset.

PLEASE CITE THIS ARTICLE AS DOI: 10.1063/5.0031138



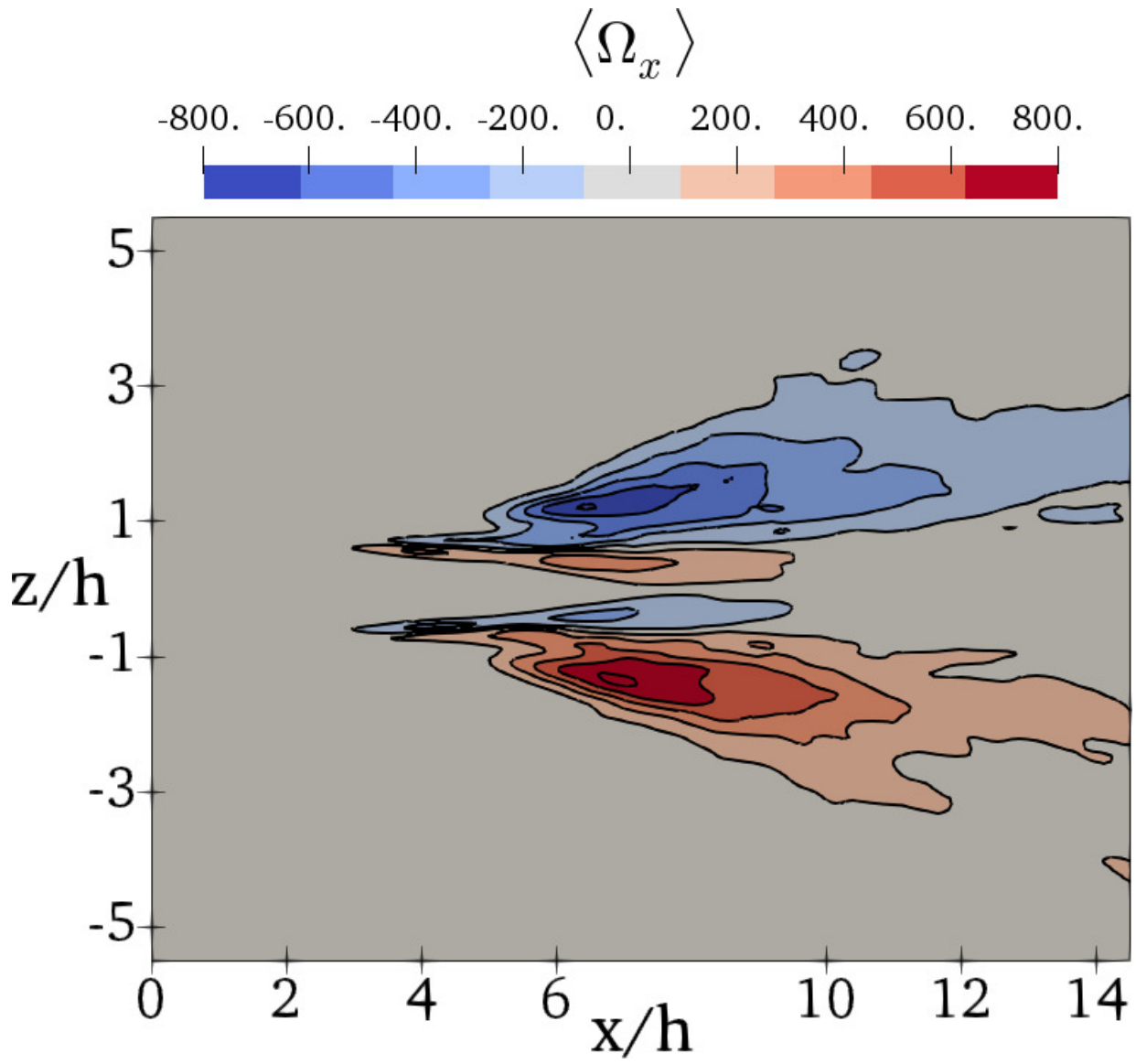
This is the author's peer reviewed, accepted manuscript. However, the online version of record will be different from this version once it has been copyedited and typeset.

PLEASE CITE THIS ARTICLE AS DOI: 10.1063/5.0031138



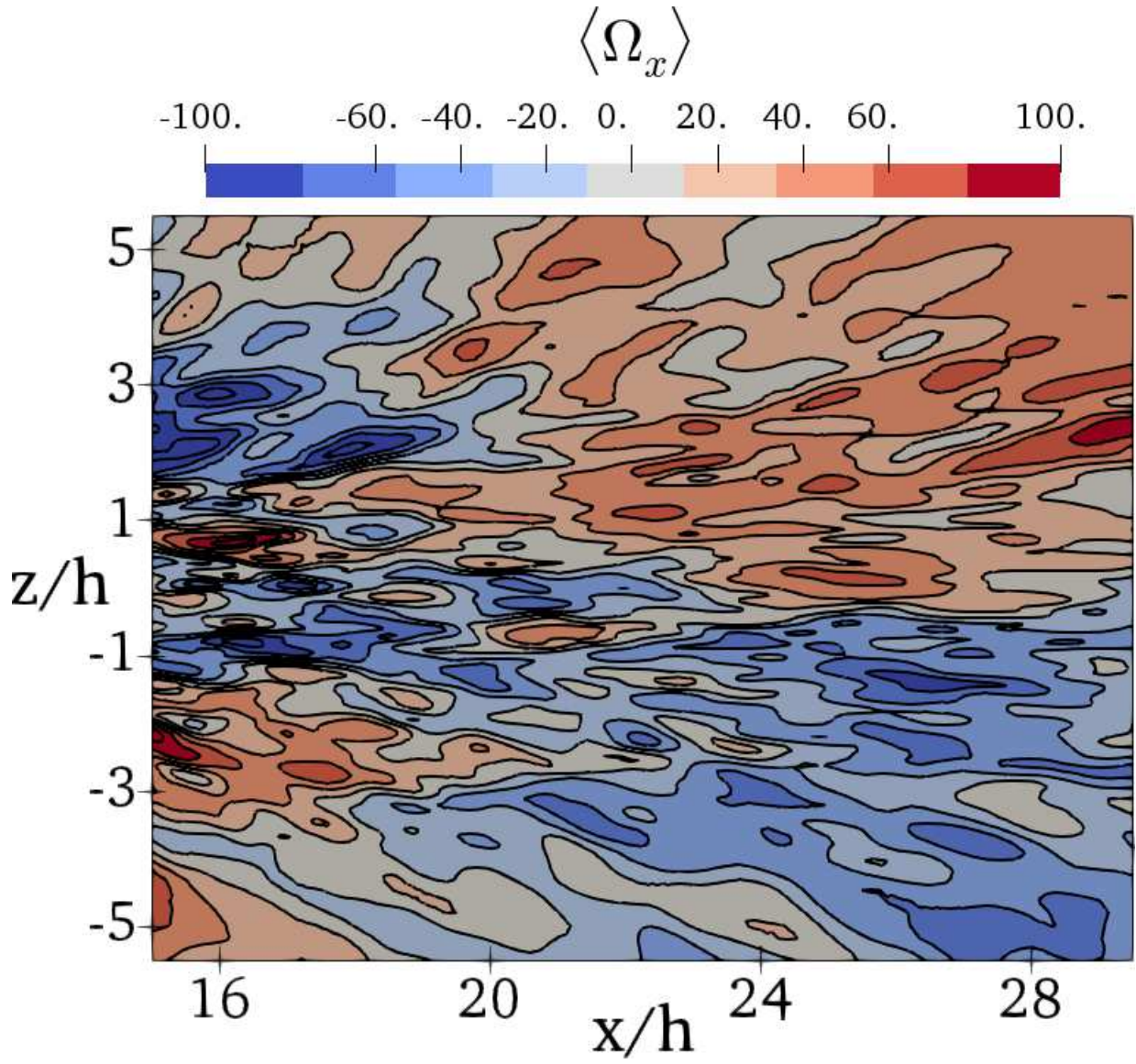
This is the author's peer reviewed, accepted manuscript. However, the online version of record will be different from this version once it has been copyedited and typeset.

PLEASE CITE THIS ARTICLE AS DOI: 10.1063/5.0031138



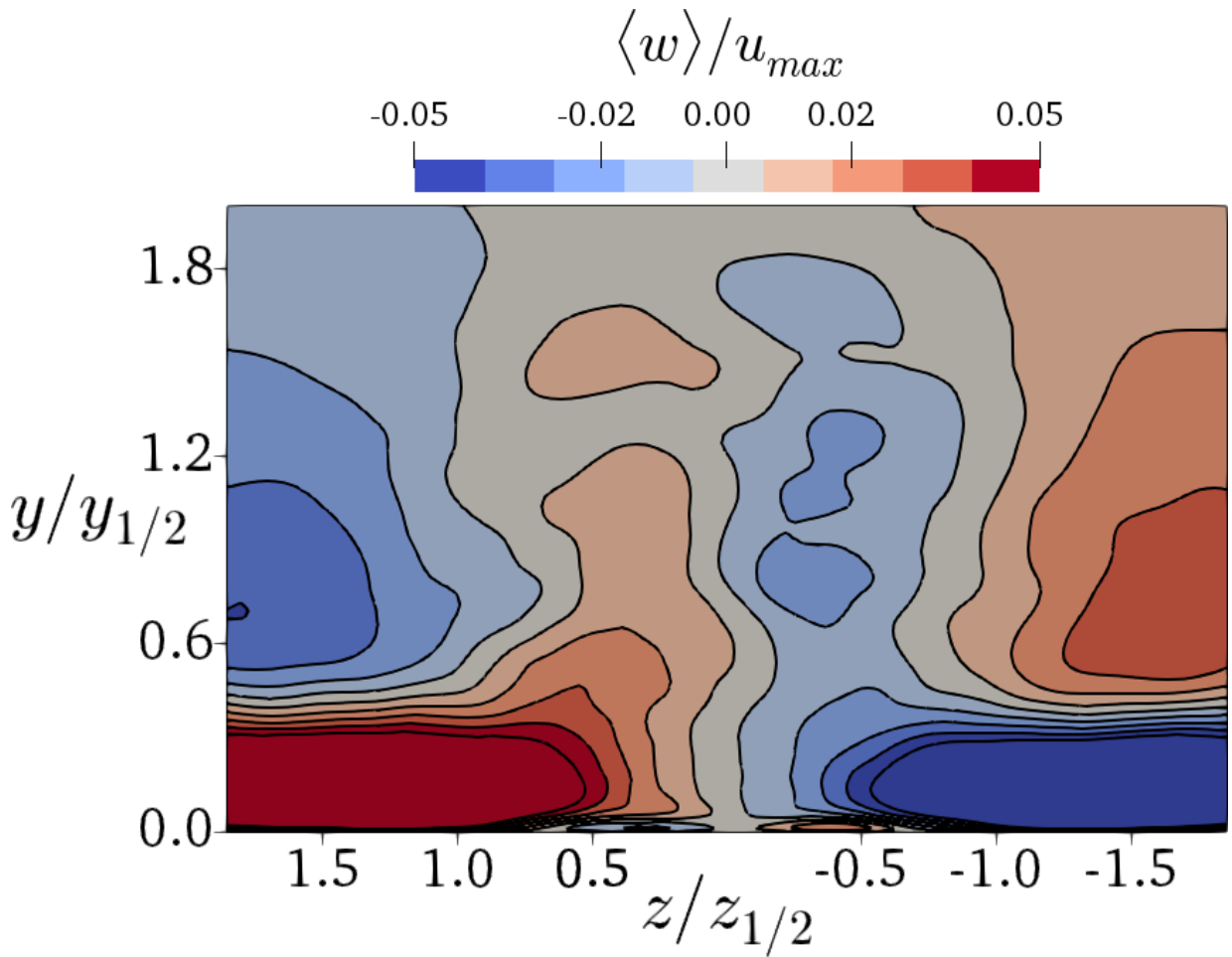
This is the author's peer reviewed, accepted manuscript. However, the online version of record will be different from this version once it has been copyedited and typeset.

PLEASE CITE THIS ARTICLE AS DOI: 10.1063/5.0031138



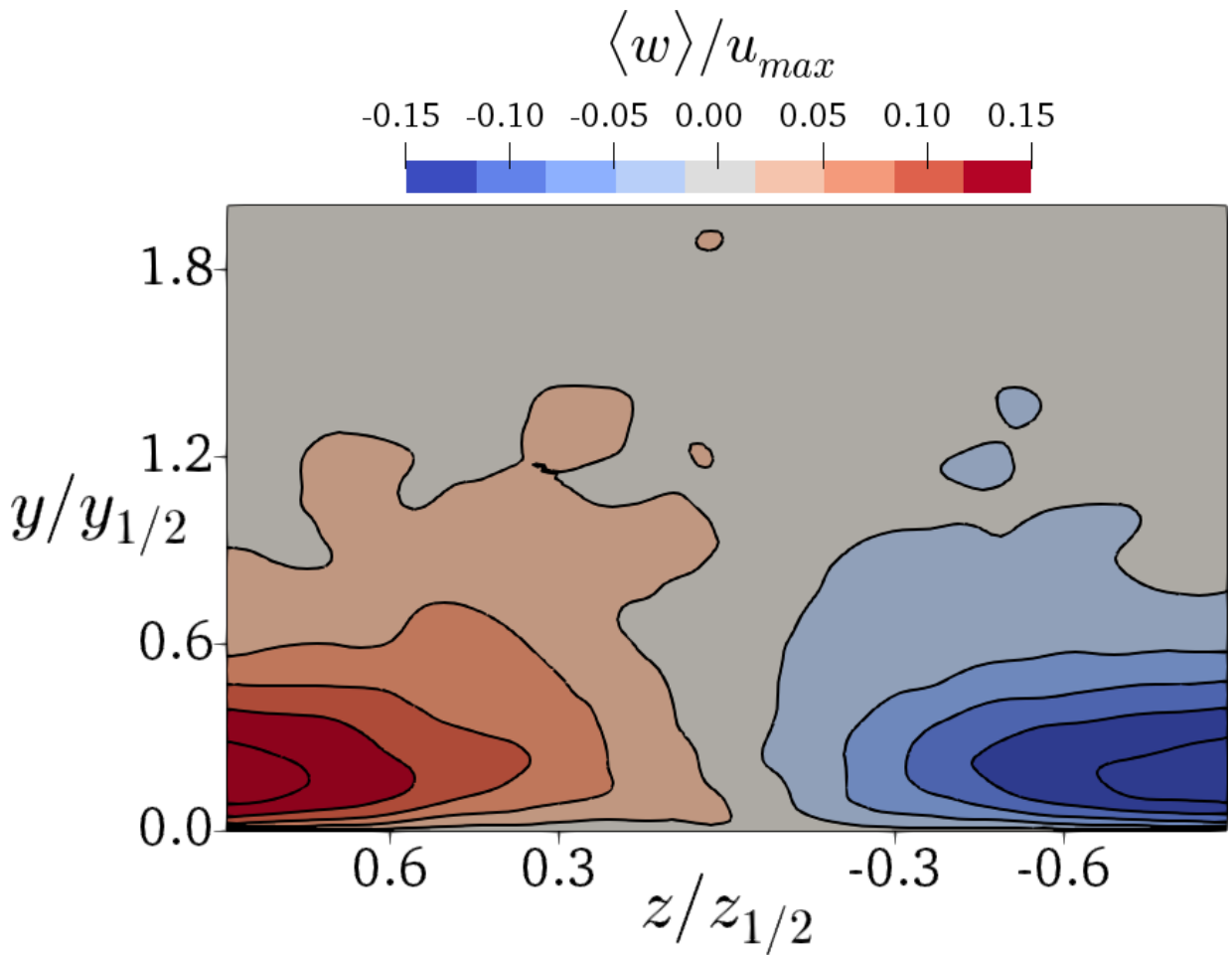
This is the author's peer reviewed, accepted manuscript. However, the online version of record will be different from this version once it has been copyedited and typeset.

PLEASE CITE THIS ARTICLE AS DOI: 10.1063/5.0031138



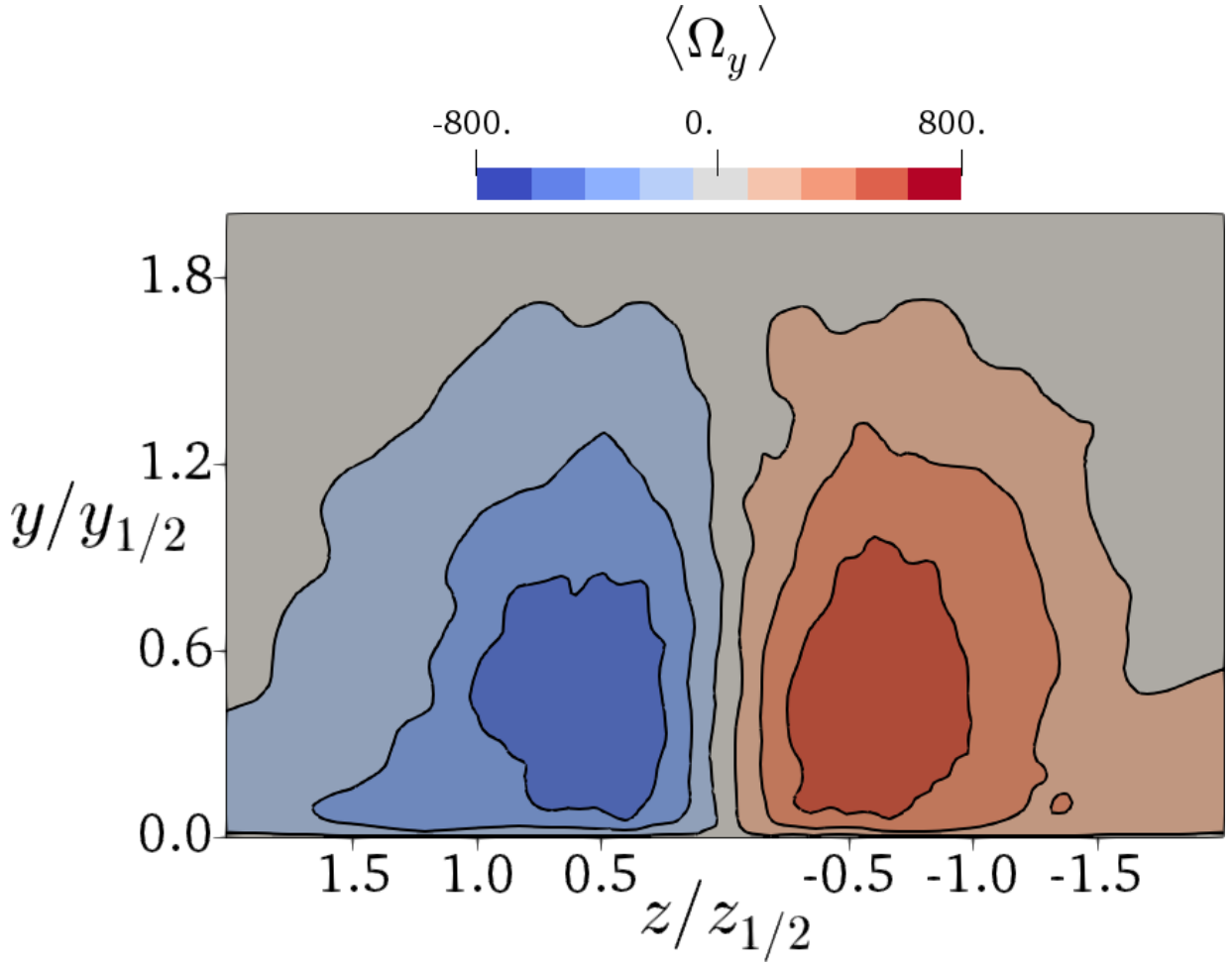
This is the author's peer reviewed, accepted manuscript. However, the online version of record will be different from this version once it has been copyedited and typeset.

PLEASE CITE THIS ARTICLE AS DOI: 10.1063/5.0031138



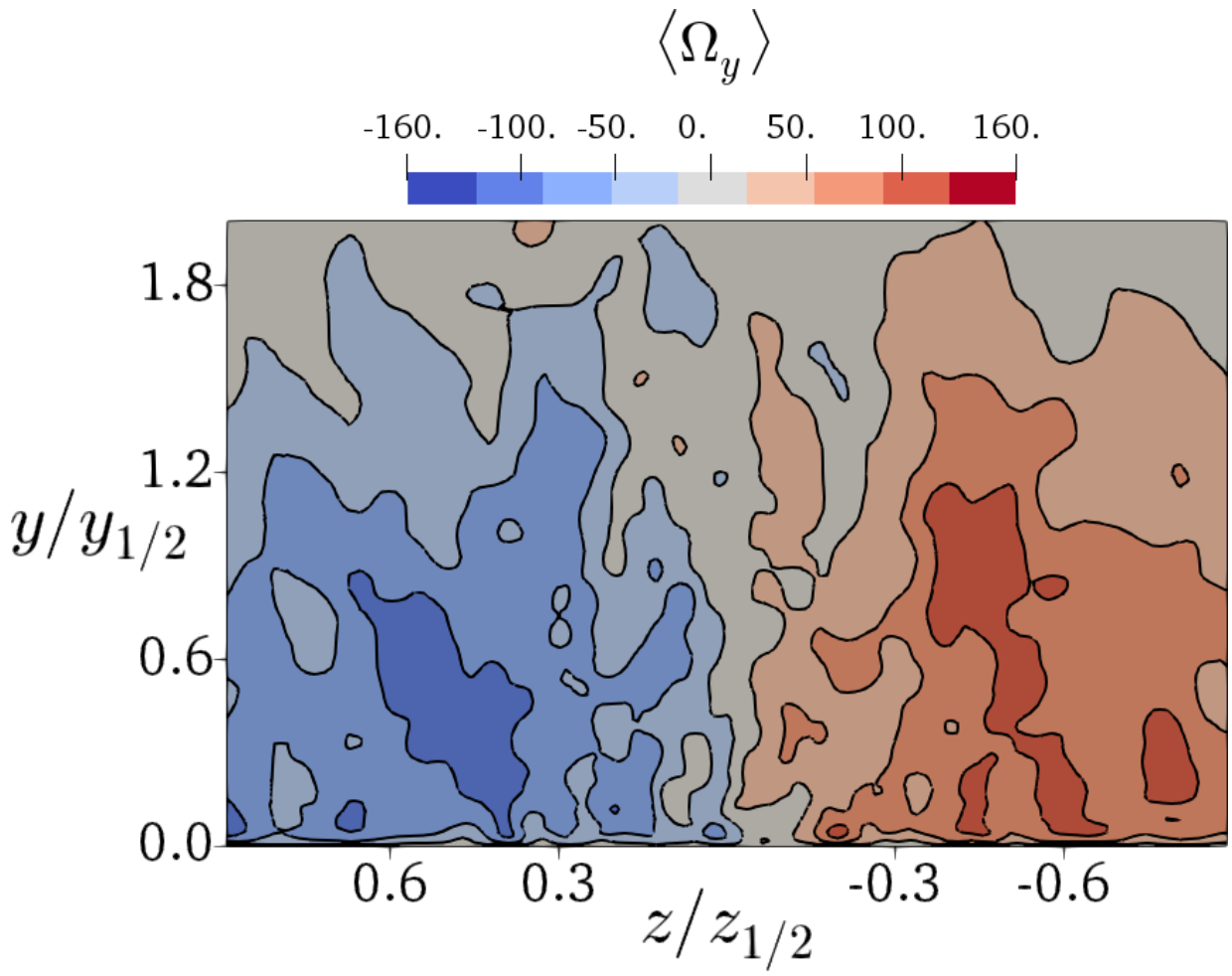
This is the author's peer reviewed, accepted manuscript. However, the online version of record will be different from this version once it has been copyedited and typeset.

PLEASE CITE THIS ARTICLE AS DOI: 10.1063/5.0031138



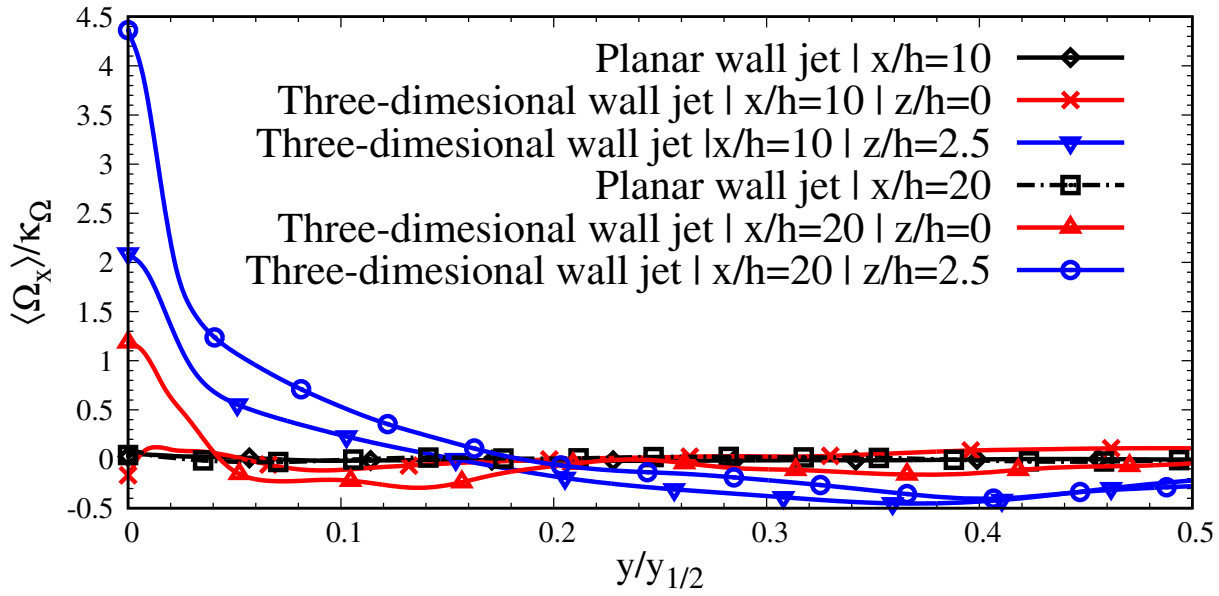
This is the author's peer reviewed, accepted manuscript. However, the online version of record will be different from this version once it has been copyedited and typeset.

PLEASE CITE THIS ARTICLE AS DOI: 10.1063/5.0031138



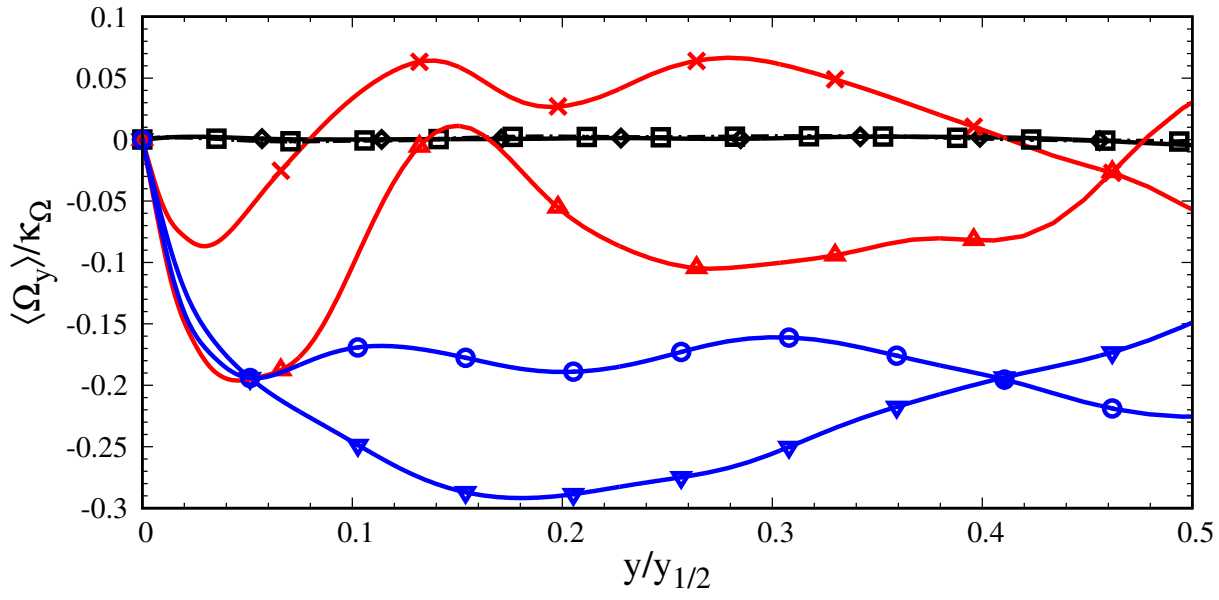
This is the author's peer reviewed, accepted manuscript. However, the online version of record will be different from this version once it has been copyedited and typeset.

PLEASE CITE THIS ARTICLE AS DOI: 10.1063/5.0031138



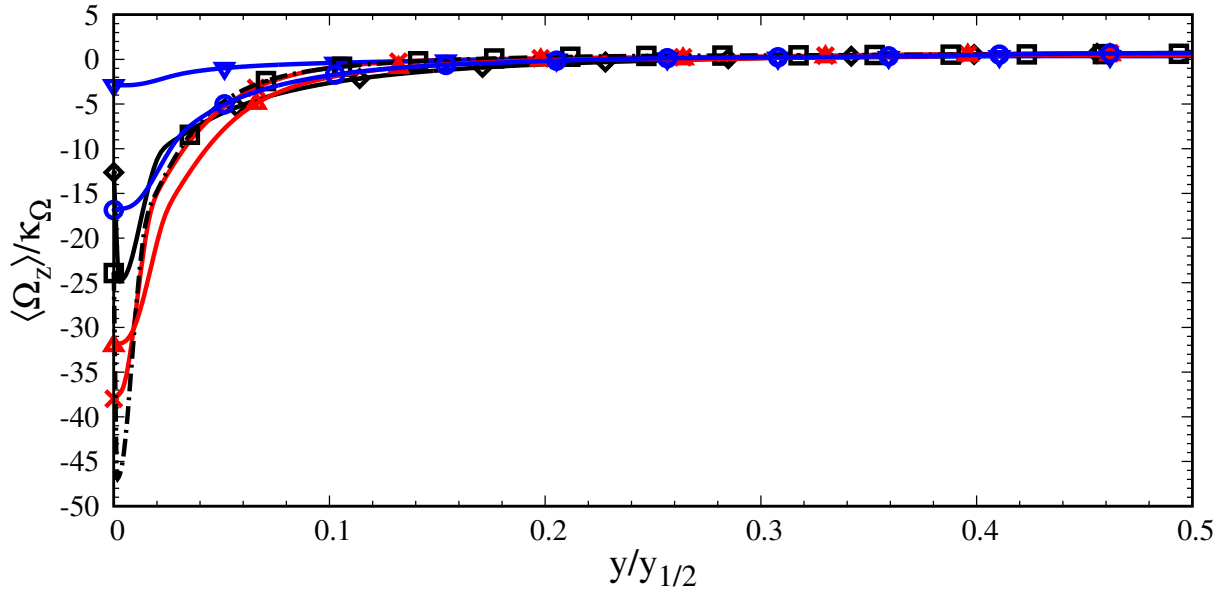
This is the author's peer reviewed, accepted manuscript. However, the online version of record will be different from this version once it has been copyedited and typeset.

PLEASE CITE THIS ARTICLE AS DOI: 10.1063/5.0031138



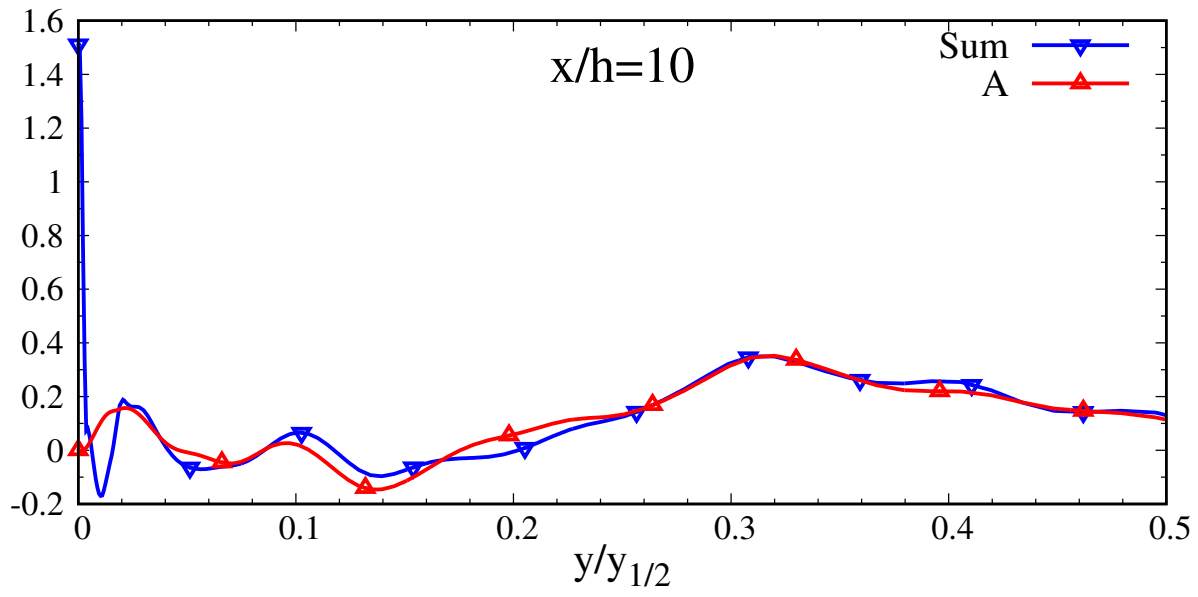
This is the author's peer reviewed, accepted manuscript. However, the online version of record will be different from this version once it has been copyedited and typeset.

PLEASE CITE THIS ARTICLE AS DOI: 10.1063/5.0031138



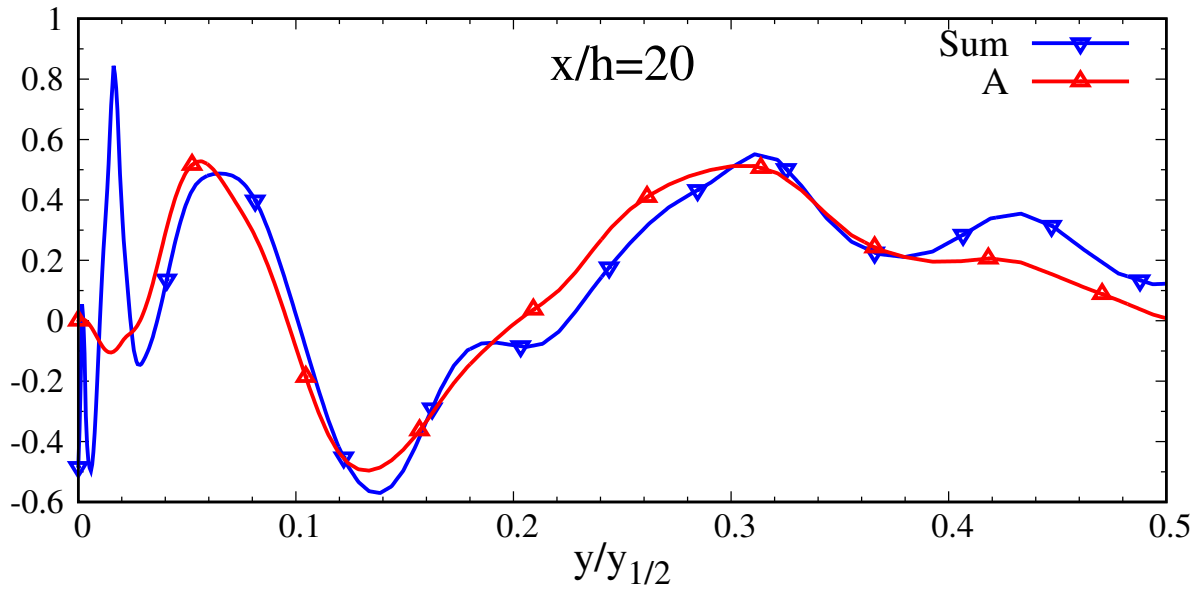
This is the author's peer reviewed, accepted manuscript. However, the online version of record will be different from this version once it has been copyedited and typeset.

PLEASE CITE THIS ARTICLE AS DOI: 10.1063/5.0031138



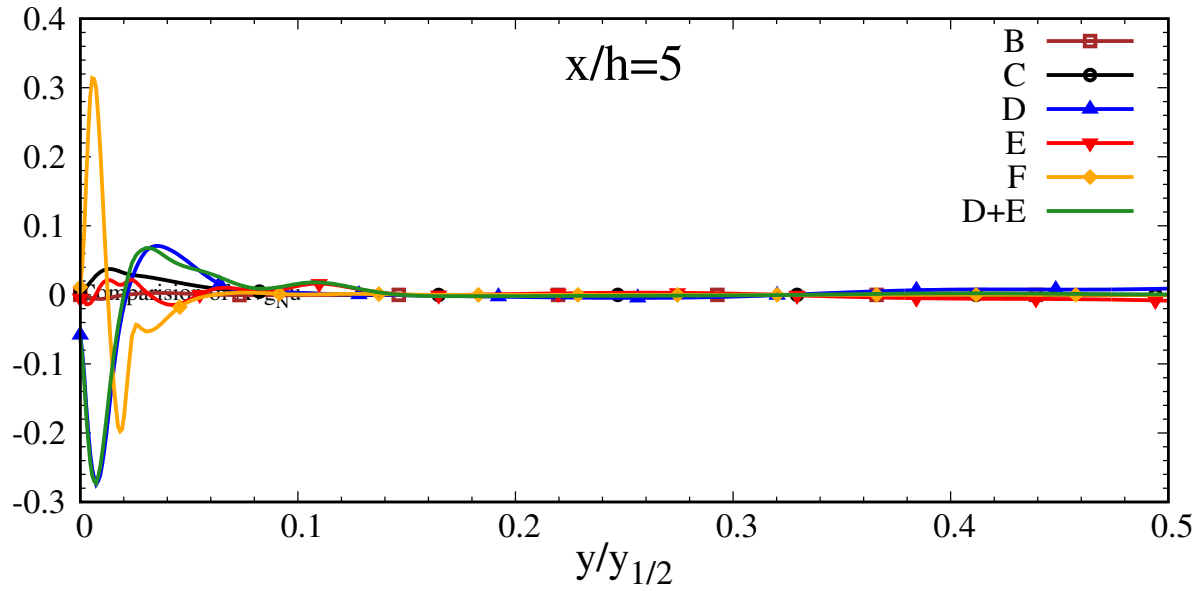
This is the author's peer reviewed, accepted manuscript. However, the online version of record will be different from this version once it has been copyedited and typeset.

PLEASE CITE THIS ARTICLE AS DOI: 10.1063/5.0031138



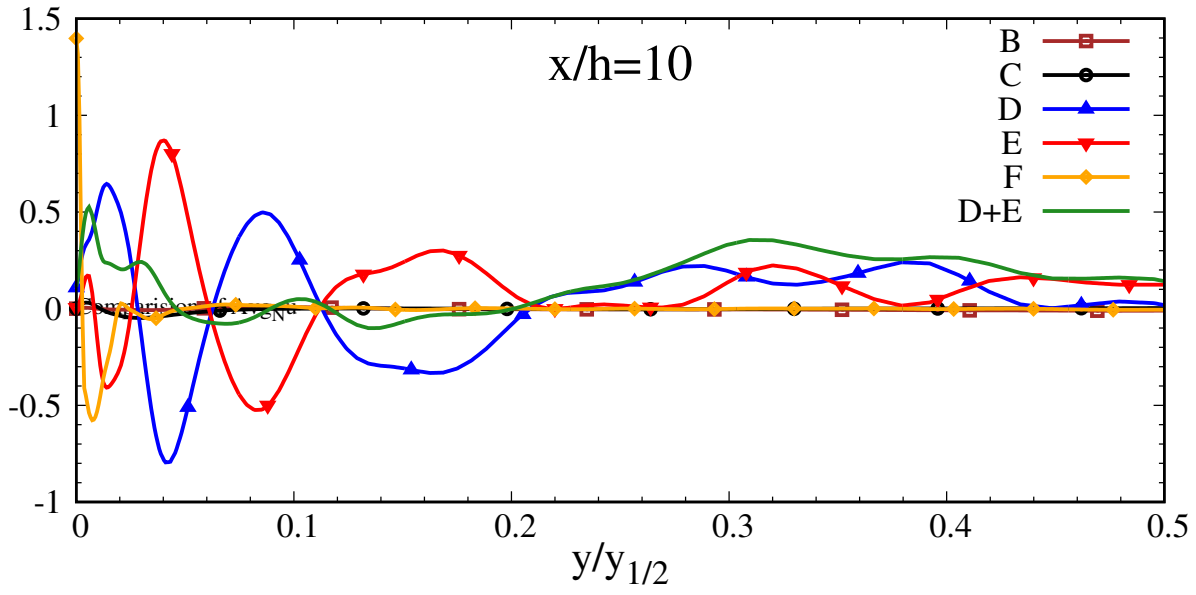
This is the author's peer reviewed, accepted manuscript. However, the online version of record will be different from this version once it has been copyedited and typeset.

PLEASE CITE THIS ARTICLE AS DOI: 10.1063/5.0031138



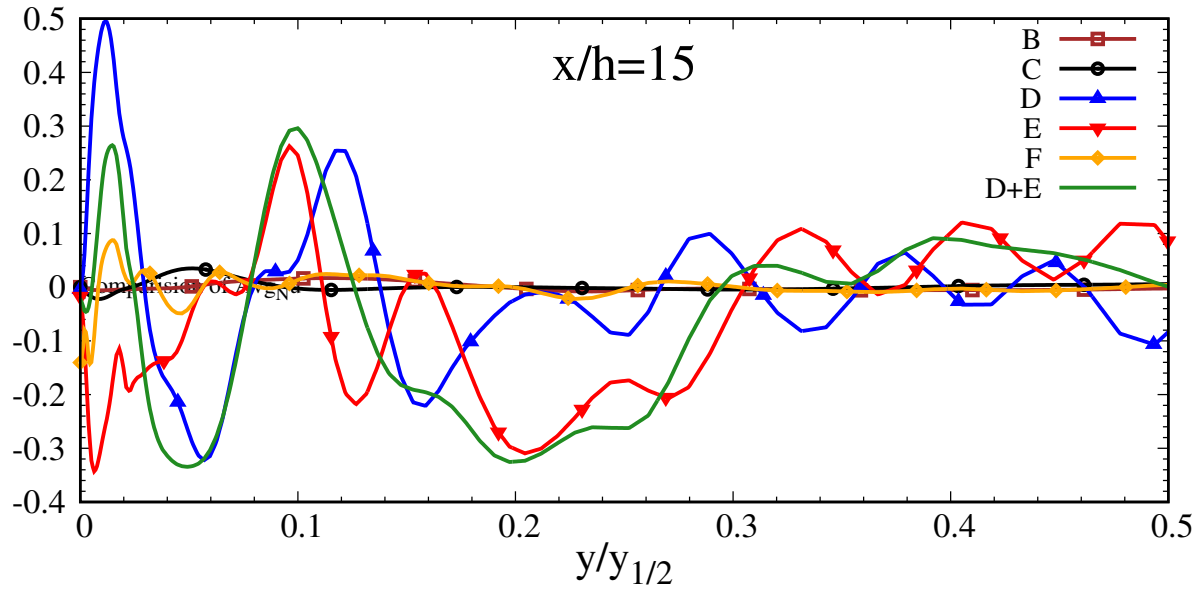
This is the author's peer reviewed, accepted manuscript. However, the online version of record will be different from this version once it has been copyedited and typeset.

PLEASE CITE THIS ARTICLE AS DOI: 10.1063/5.0031138



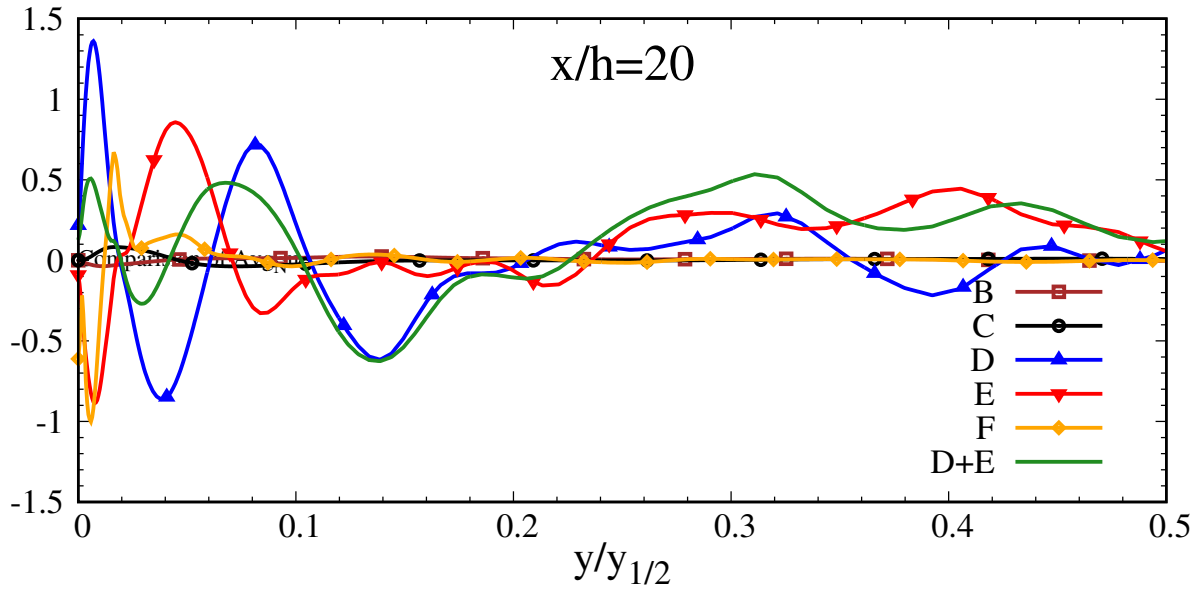
This is the author's peer reviewed, accepted manuscript. However, the online version of record will be different from this version once it has been copyedited and typeset.

PLEASE CITE THIS ARTICLE AS DOI: 10.1063/5.0031138



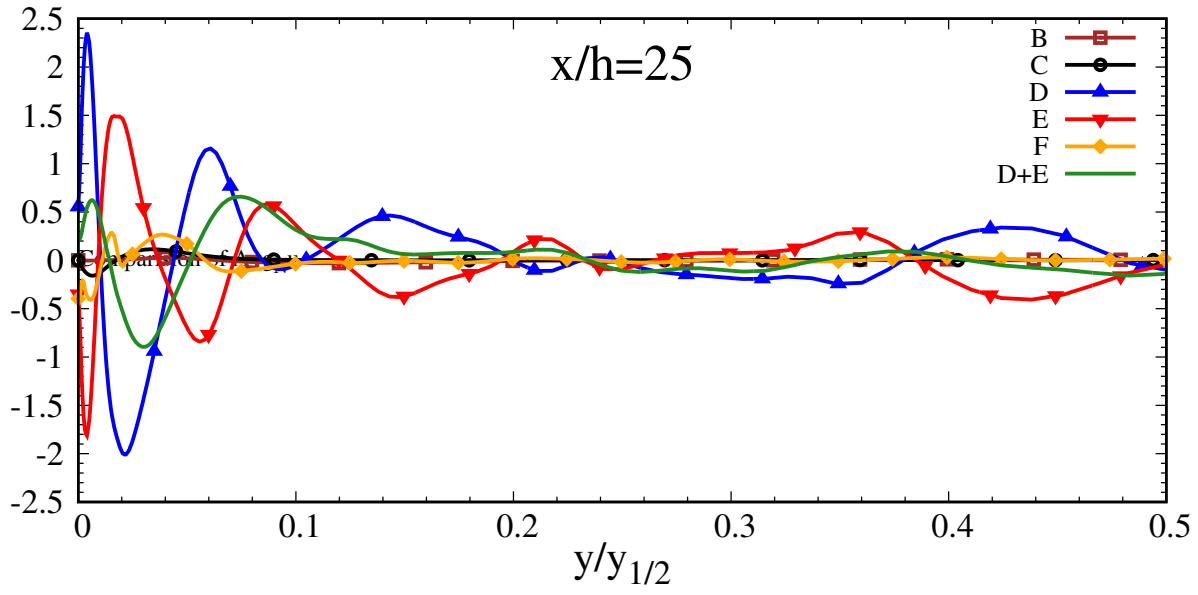
This is the author's peer reviewed, accepted manuscript. However, the online version of record will be different from this version once it has been copyedited and typeset.

PLEASE CITE THIS ARTICLE AS DOI: 10.1063/5.0031138



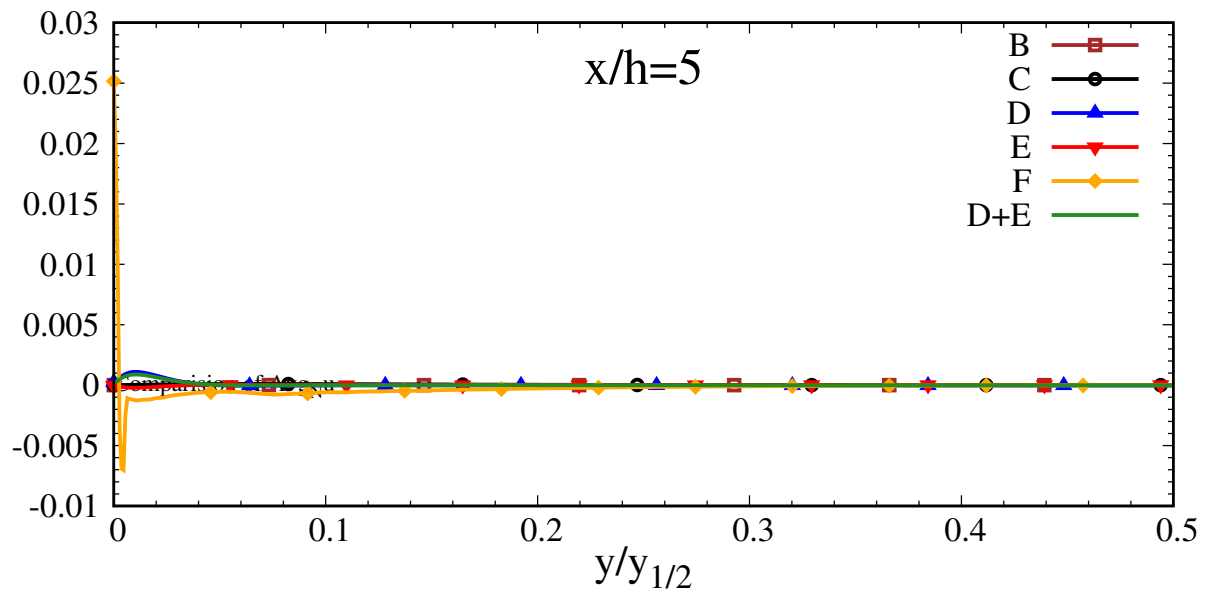
This is the author's peer reviewed, accepted manuscript. However, the online version of record will be different from this version once it has been copyedited and typeset.

PLEASE CITE THIS ARTICLE AS DOI: 10.1063/5.0031138



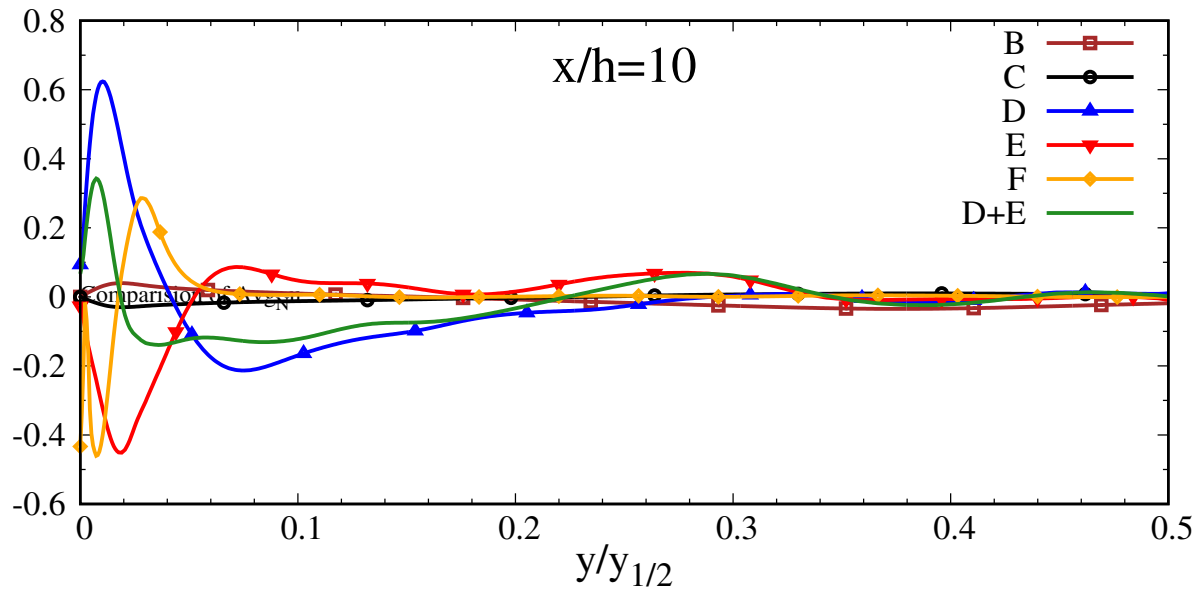
This is the author's peer reviewed, accepted manuscript. However, the online version of record will be different from this version once it has been copyedited and typeset.

PLEASE CITE THIS ARTICLE AS DOI: 10.1063/5.0031138



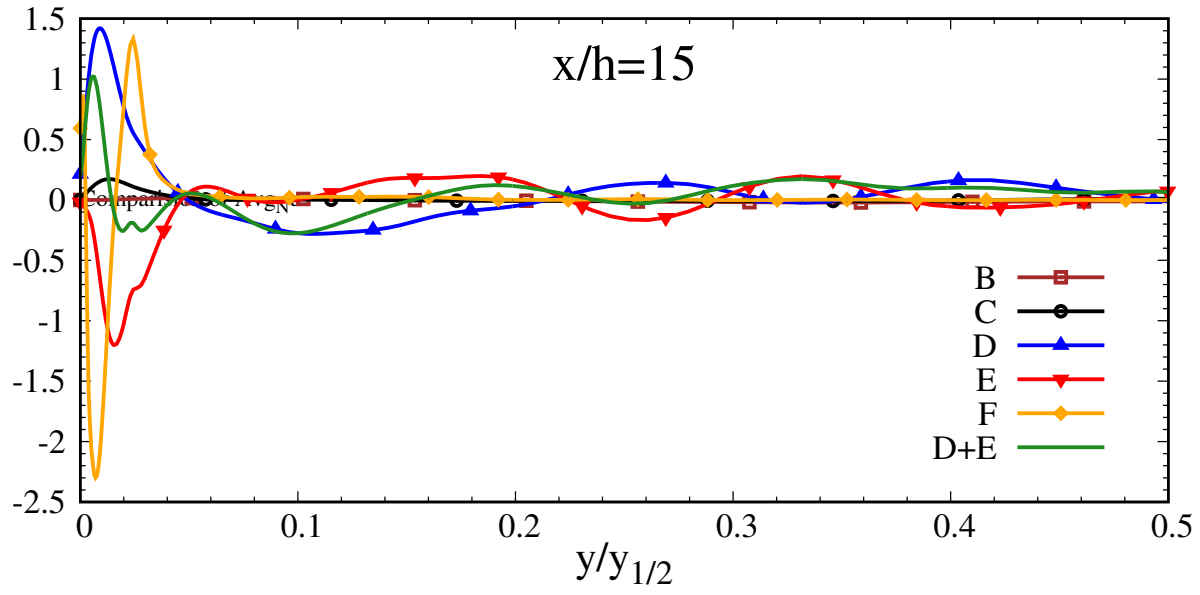
This is the author's peer reviewed, accepted manuscript. However, the online version of record will be different from this version once it has been copyedited and typeset.

PLEASE CITE THIS ARTICLE AS DOI: 10.1063/5.0031138



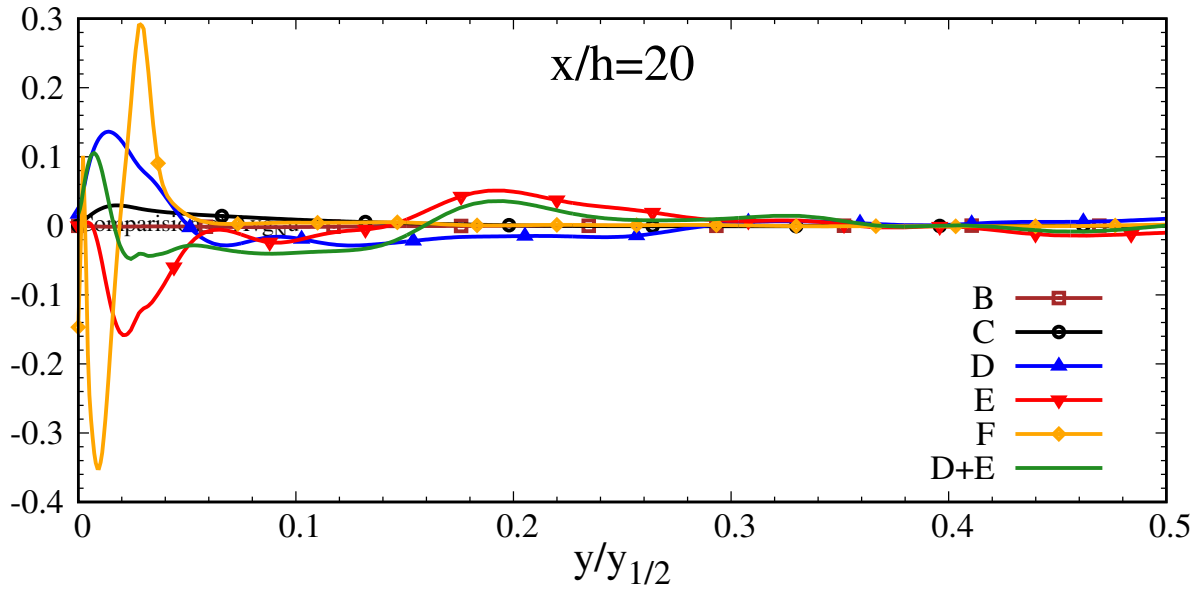
This is the author's peer reviewed, accepted manuscript. However, the online version of record will be different from this version once it has been copyedited and typeset.

PLEASE CITE THIS ARTICLE AS DOI: 10.1063/5.0031138



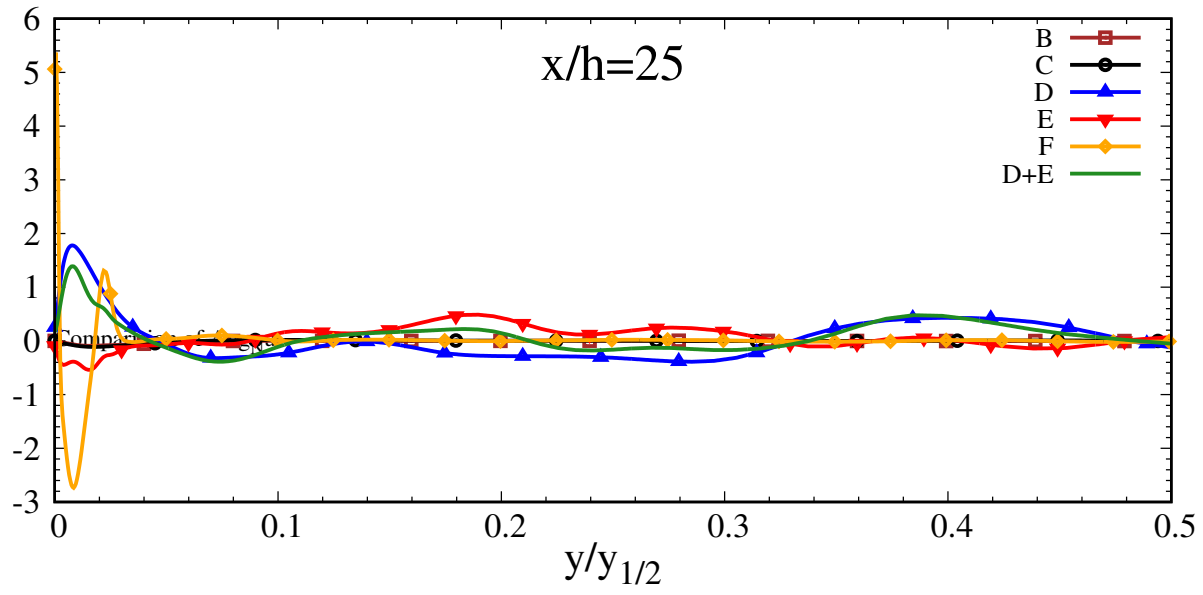
This is the author's peer reviewed, accepted manuscript. However, the online version of record will be different from this version once it has been copyedited and typeset.

PLEASE CITE THIS ARTICLE AS DOI: 10.1063/5.0031138



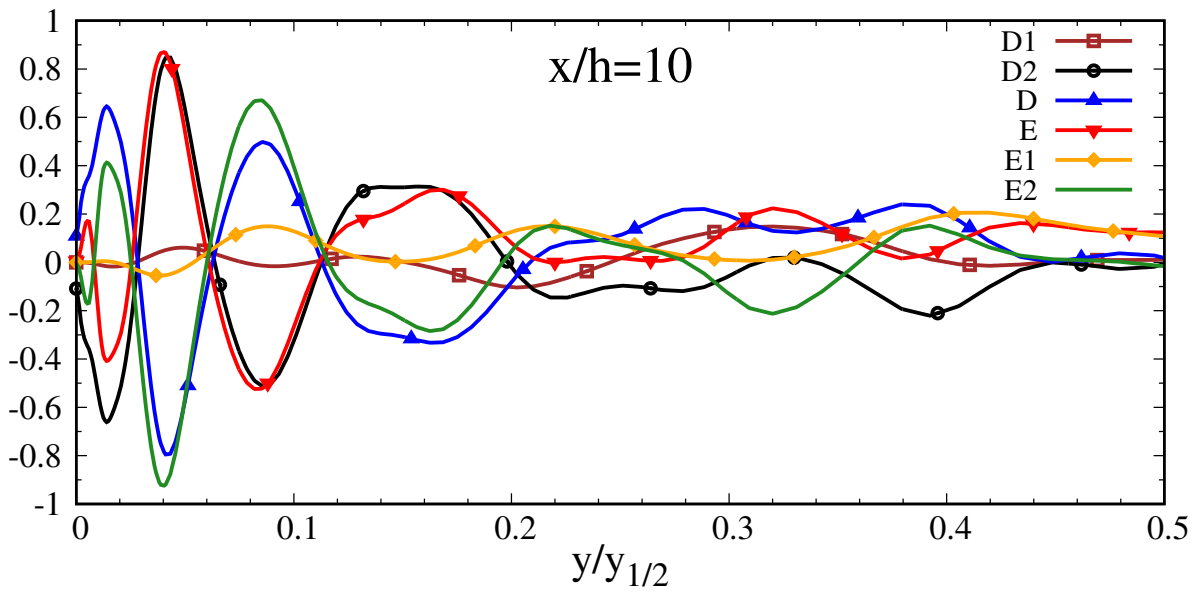
This is the author's peer reviewed, accepted manuscript. However, the online version of record will be different from this version once it has been copyedited and typeset.

PLEASE CITE THIS ARTICLE AS DOI: 10.1063/5.0031138



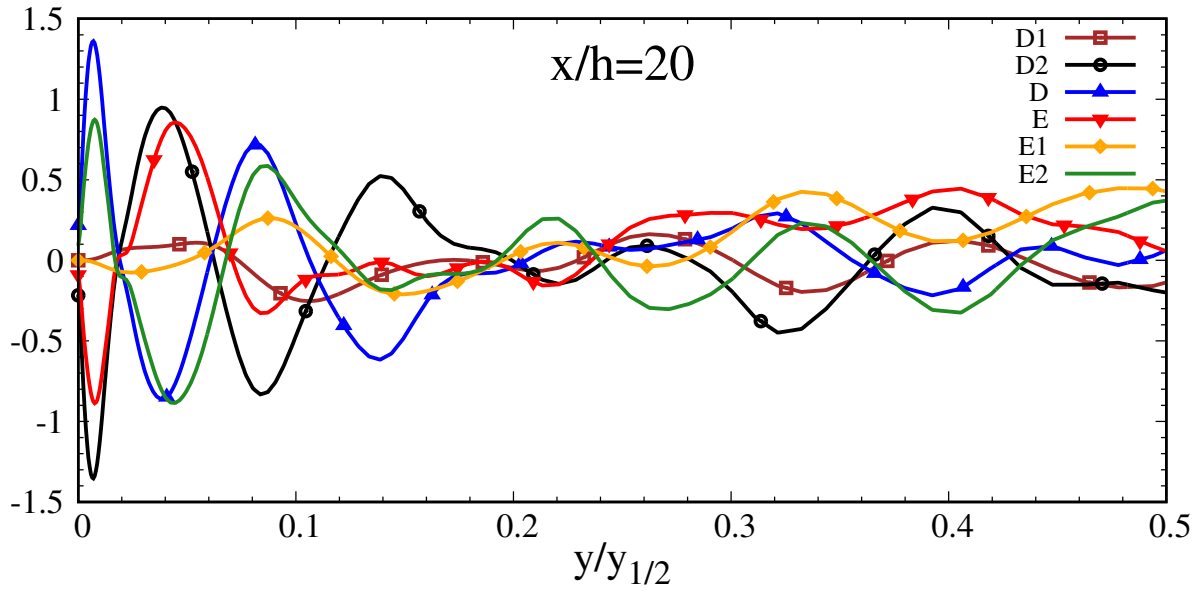
This is the author's peer reviewed, accepted manuscript. However, the online version of record will be different from this version once it has been copyedited and typeset.

PLEASE CITE THIS ARTICLE AS DOI: 10.1063/5.0031138



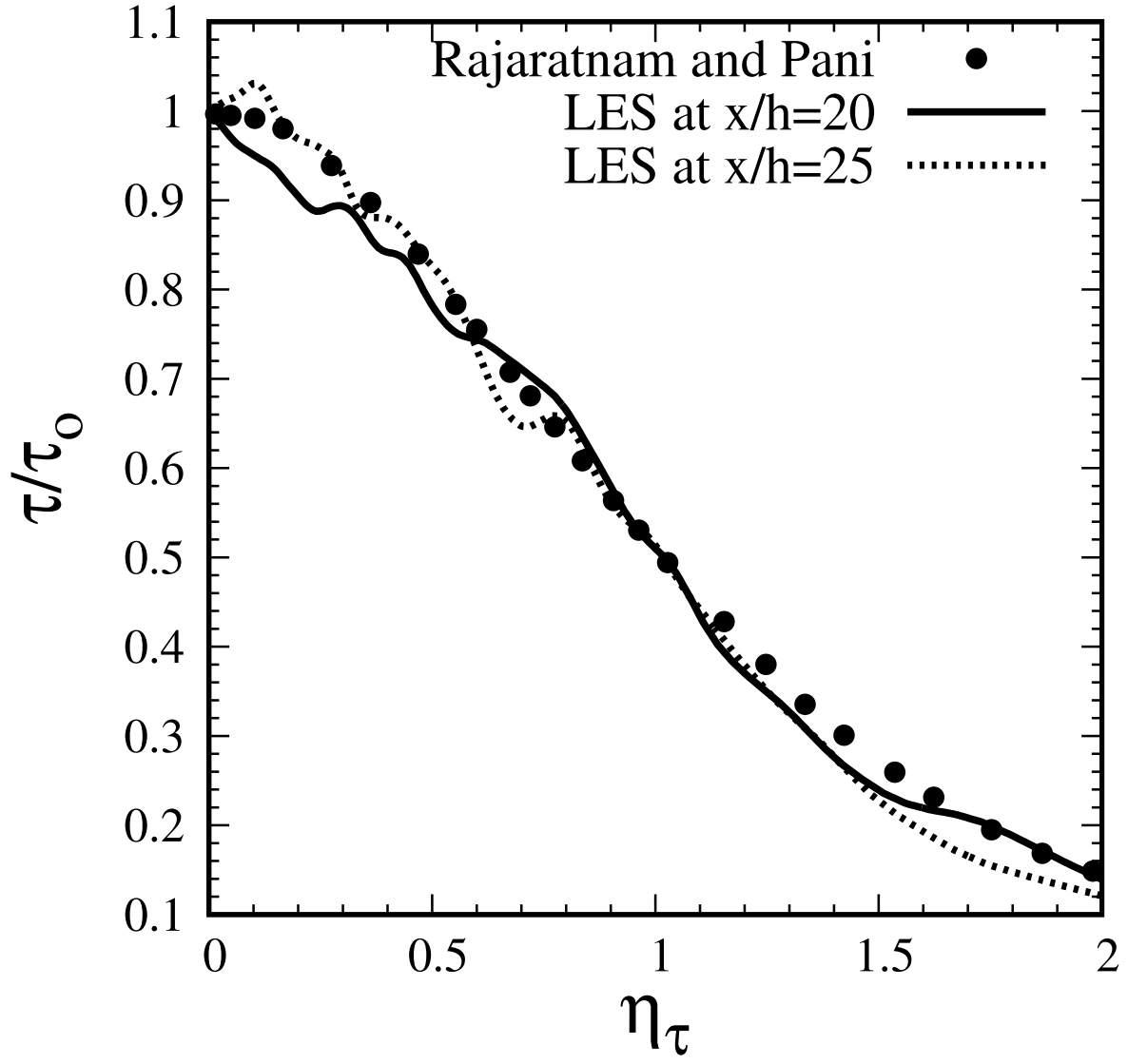
This is the author's peer reviewed, accepted manuscript. However, the online version of record will be different from this version once it has been copyedited and typeset.

PLEASE CITE THIS ARTICLE AS DOI: 10.1063/5.0031138



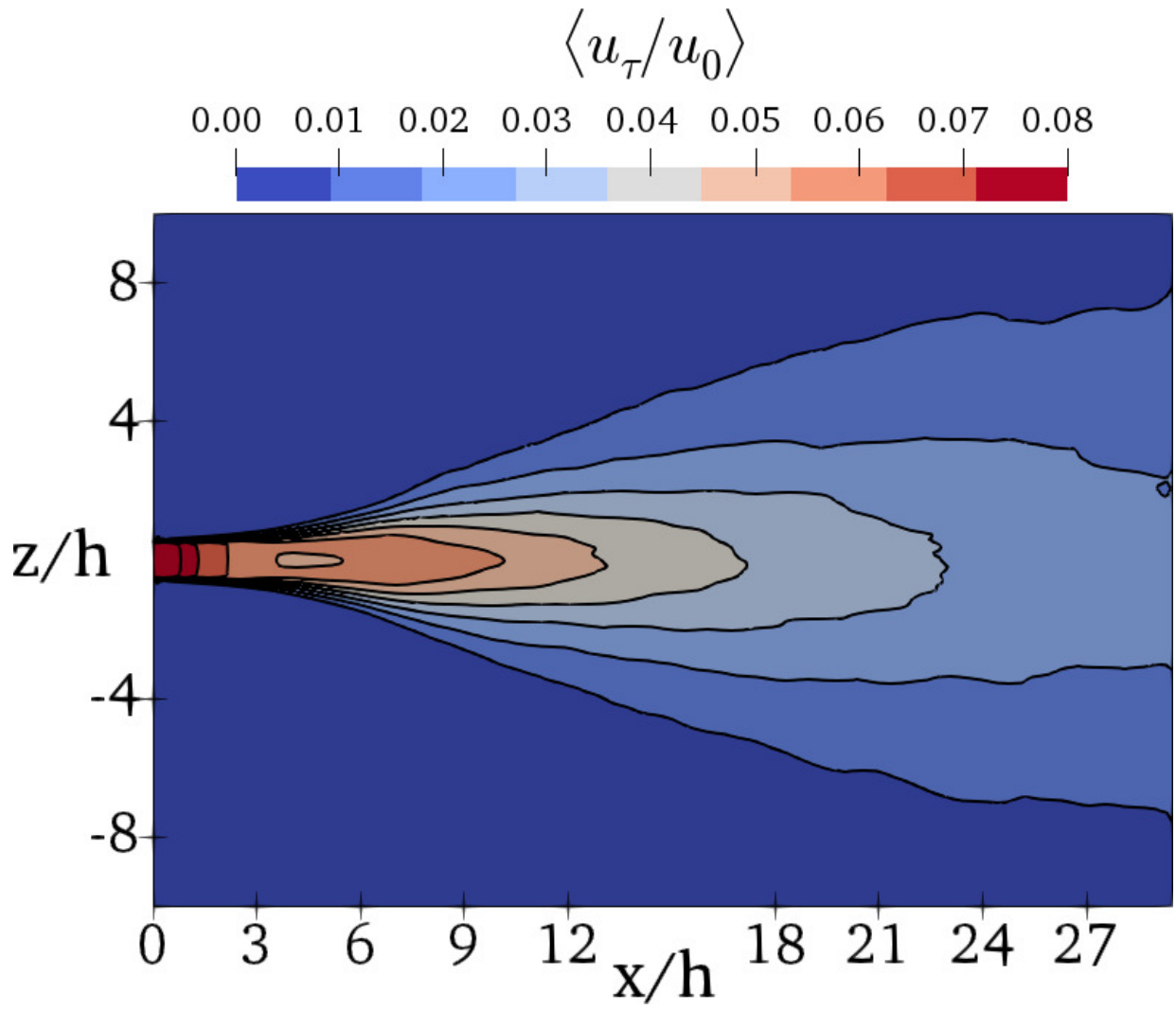
This is the author's peer reviewed, accepted manuscript. However, the online version of record will be different from this version once it has been copyedited and typeset.

PLEASE CITE THIS ARTICLE AS DOI: 10.1063/5.0031138



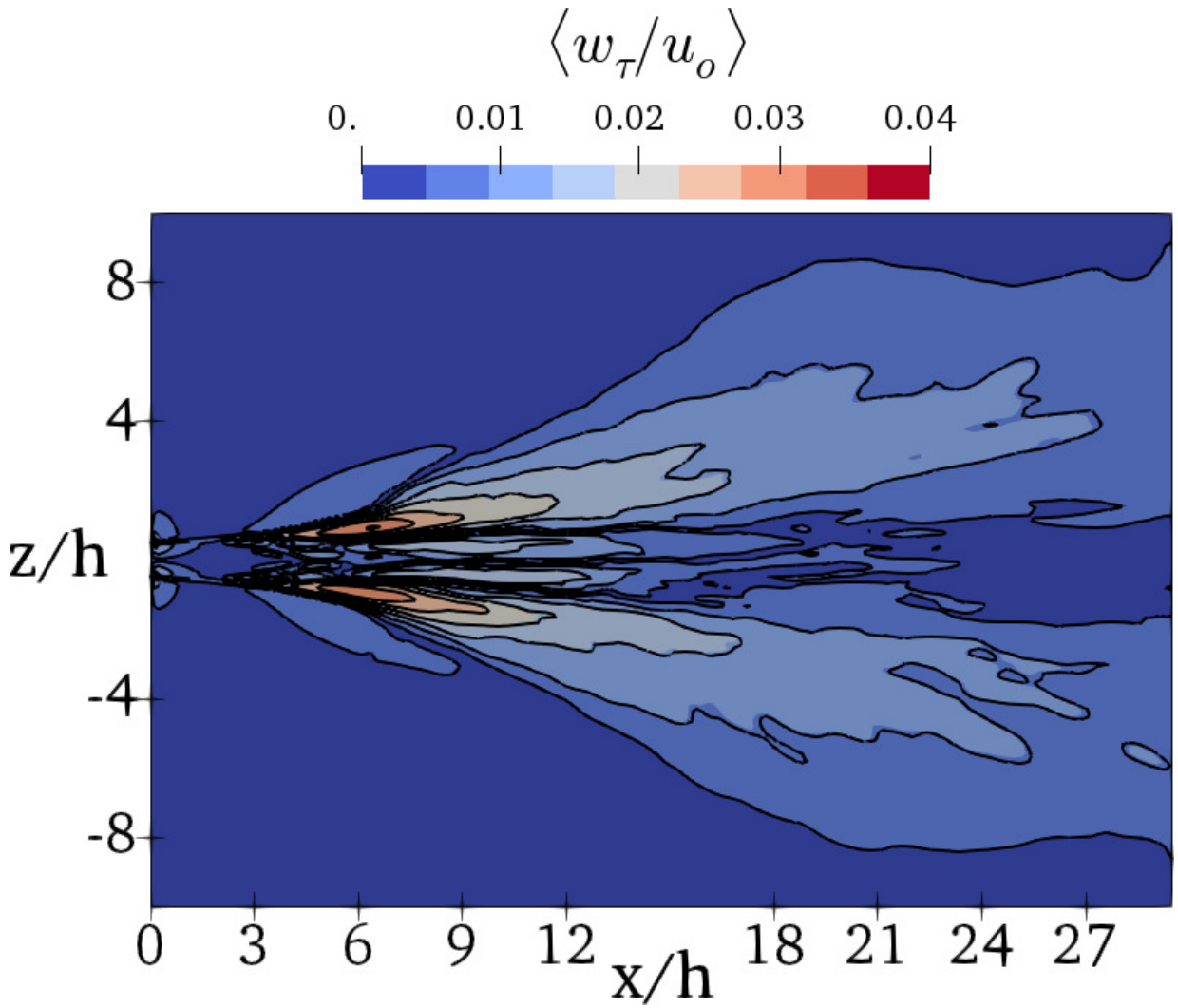
This is the author's peer reviewed, accepted manuscript. However, the online version of record will be different from this version once it has been copyedited and typeset.

PLEASE CITE THIS ARTICLE AS DOI: 10.1063/5.0031138



This is the author's peer reviewed, accepted manuscript. However, the online version of record will be different from this version once it has been copyedited and typeset.

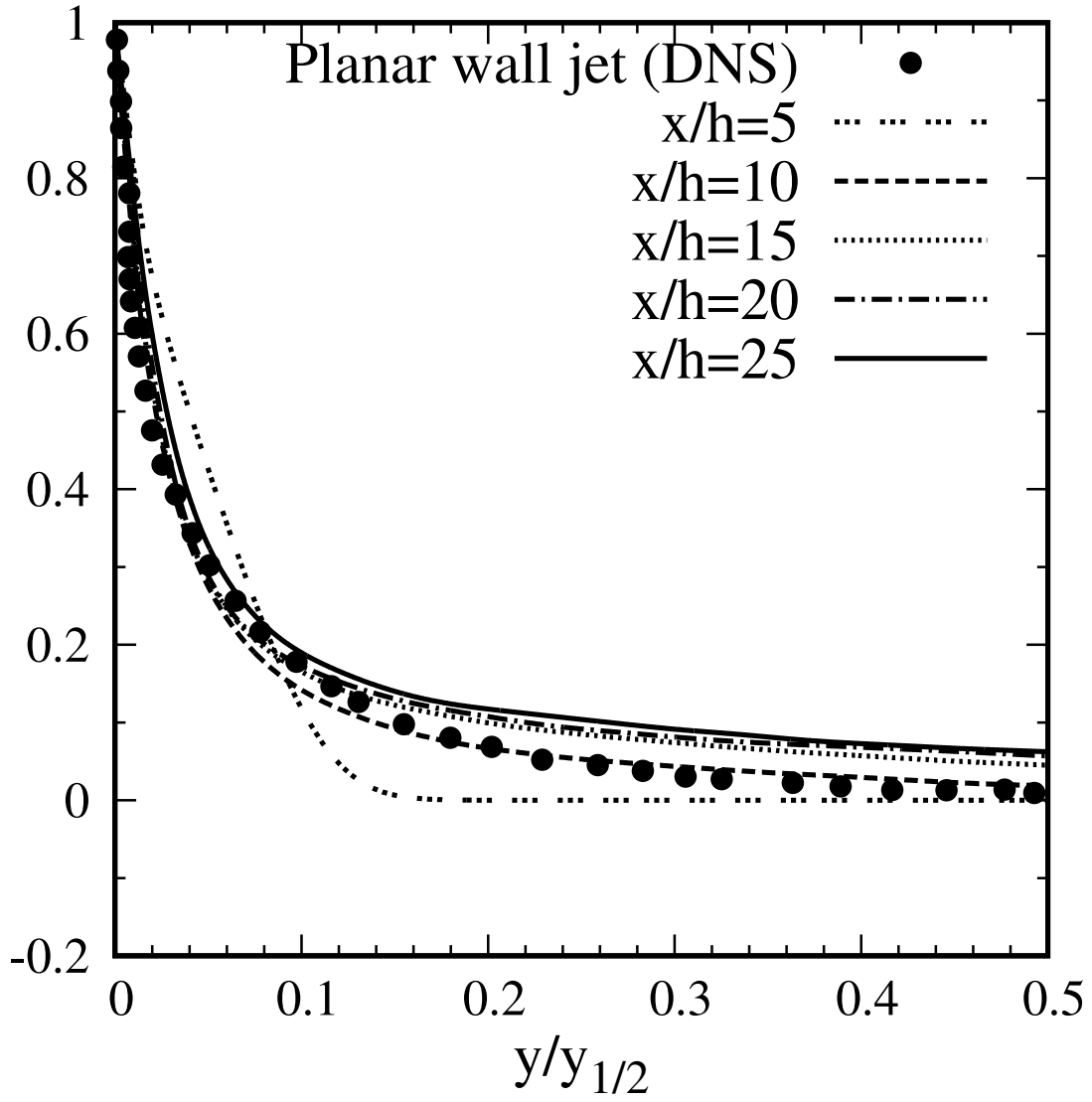
PLEASE CITE THIS ARTICLE AS DOI: 10.1063/5.0031138

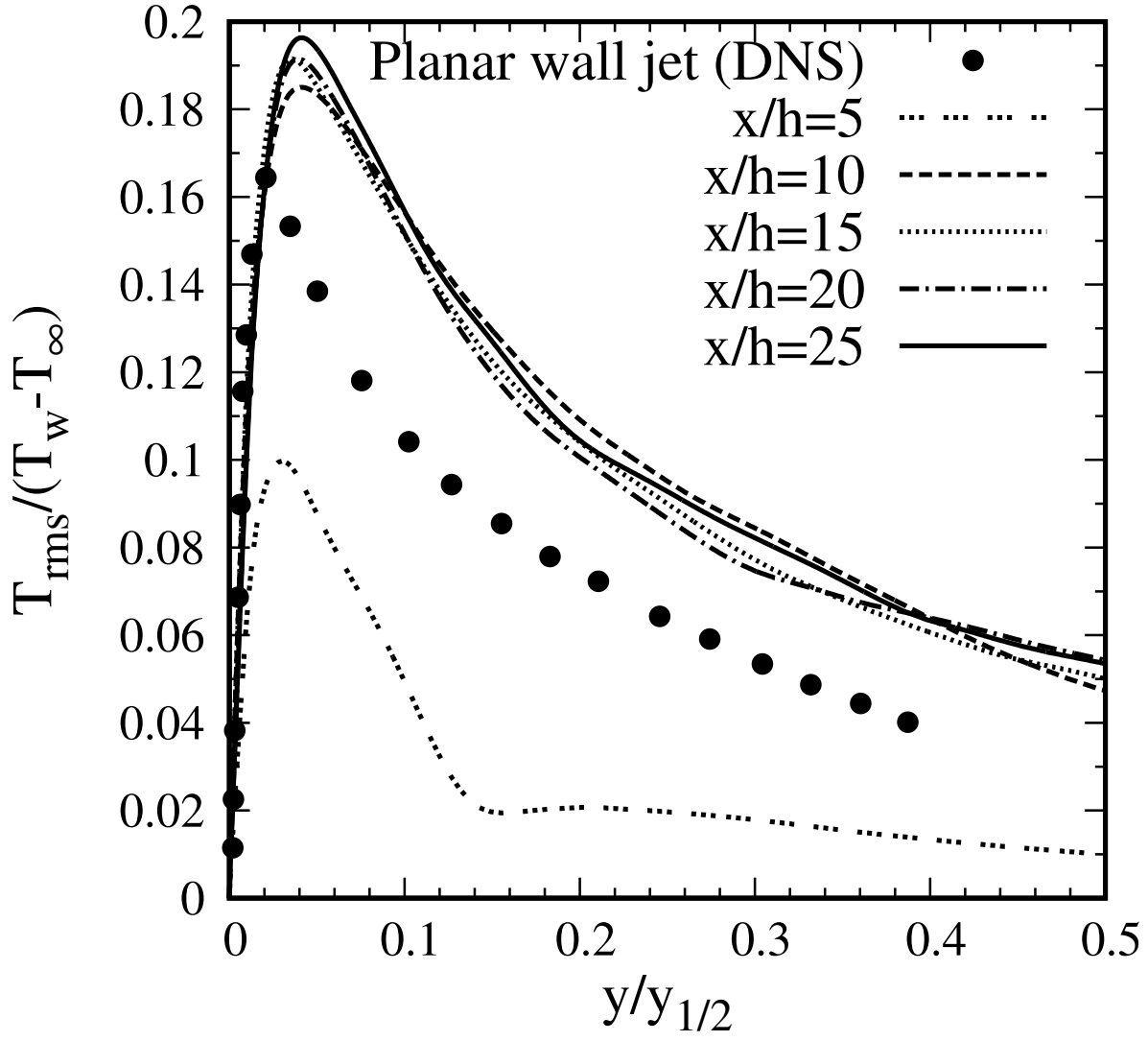


This is the author's peer reviewed, accepted manuscript. However, the online version of record will be different from this version once it has been copyedited and typeset.

PLEASE CITE THIS ARTICLE AS DOI: 10.1063/5.0031138

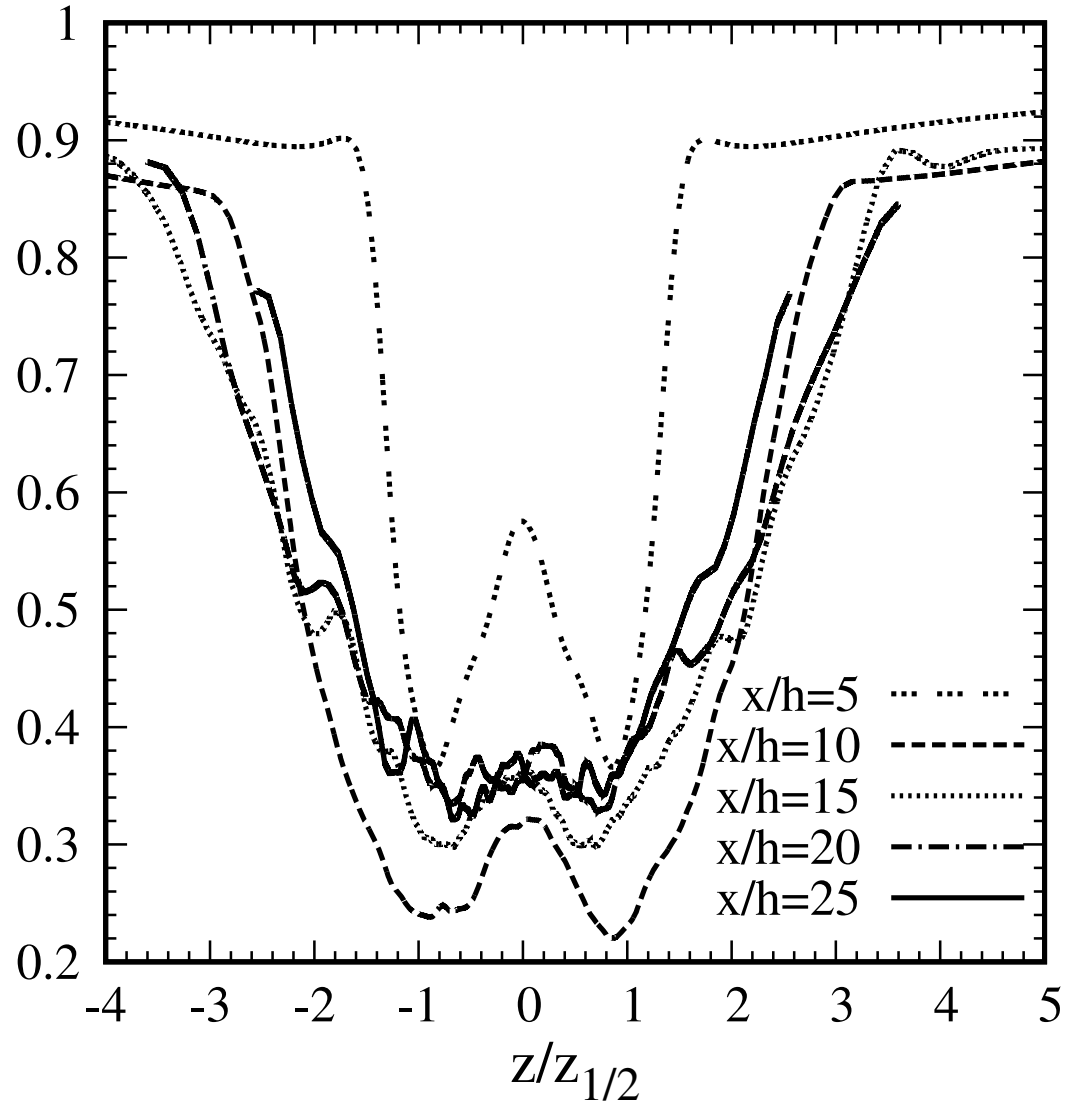
($\langle T \rangle - T_\infty$) / ($T_w - T_\infty$)





This is the author's peer reviewed, accepted manuscript. However, the online version of record will be different from this version once it has been copyedited and typeset.
PLEASE CITE THIS ARTICLE AS DOI: 10.1063/5.0031138

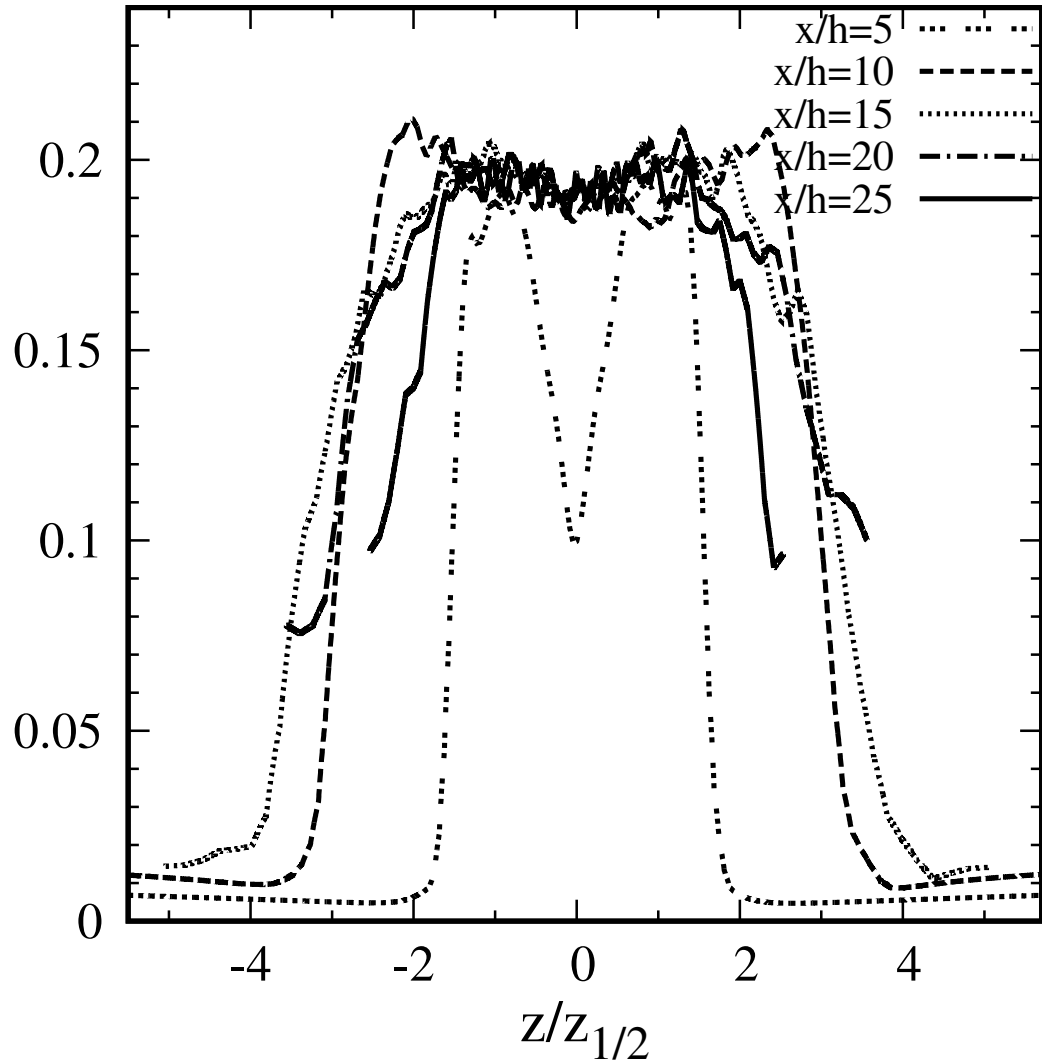
$$\langle T \rangle - T_\infty) / (T_w - T_\infty)$$



This is the author's peer reviewed, accepted manuscript. However, the online version of record will be different from this version once it has been copyedited and typeset.

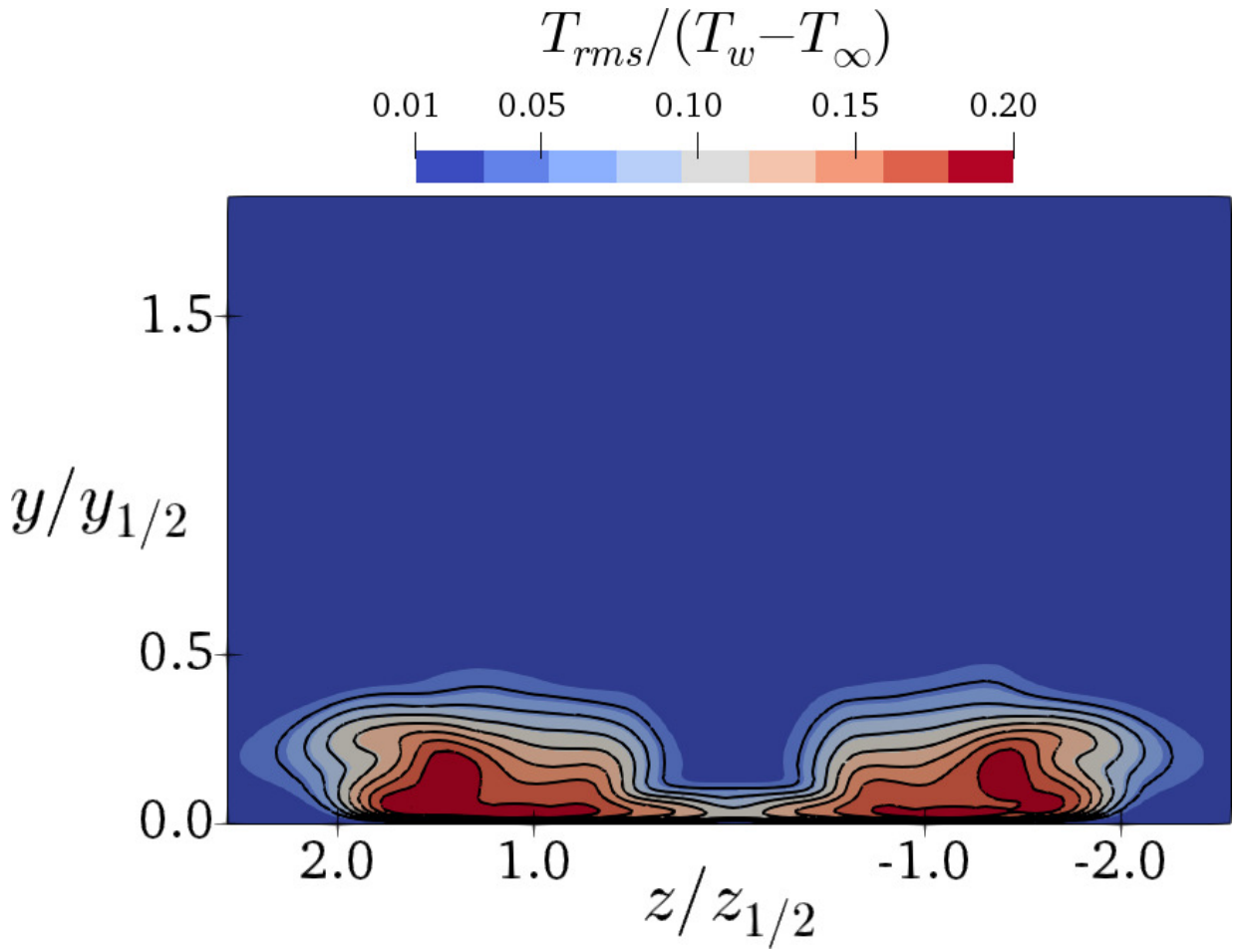
PLEASE CITE THIS ARTICLE AS DOI: 10.1063/5.0031138

$$T_{rms}/(T_w - T_\infty)$$



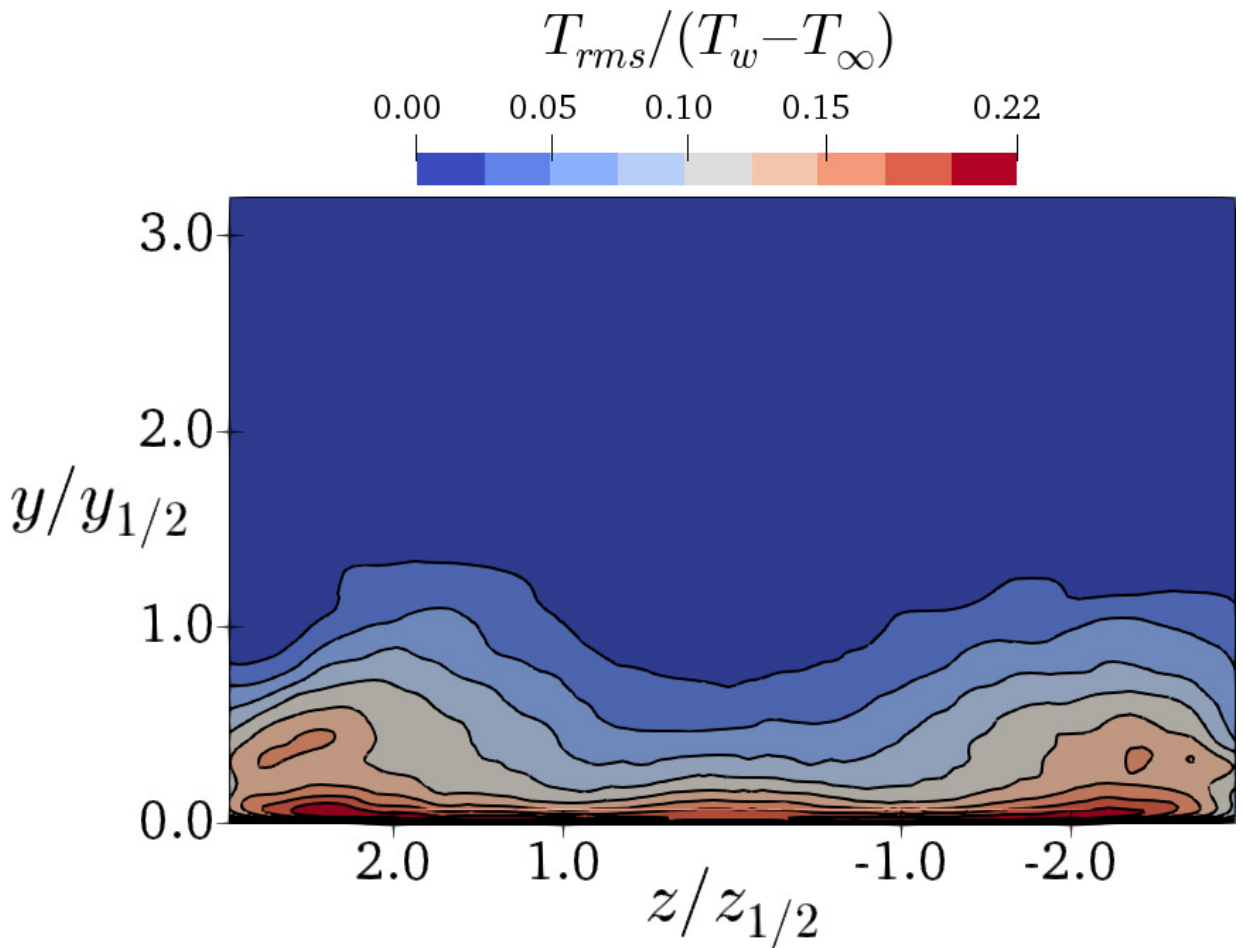
This is the author's peer reviewed, accepted manuscript. However, the online version of record will be different from this version once it has been copyedited and typeset.

PLEASE CITE THIS ARTICLE AS DOI: 10.1063/5.0031138



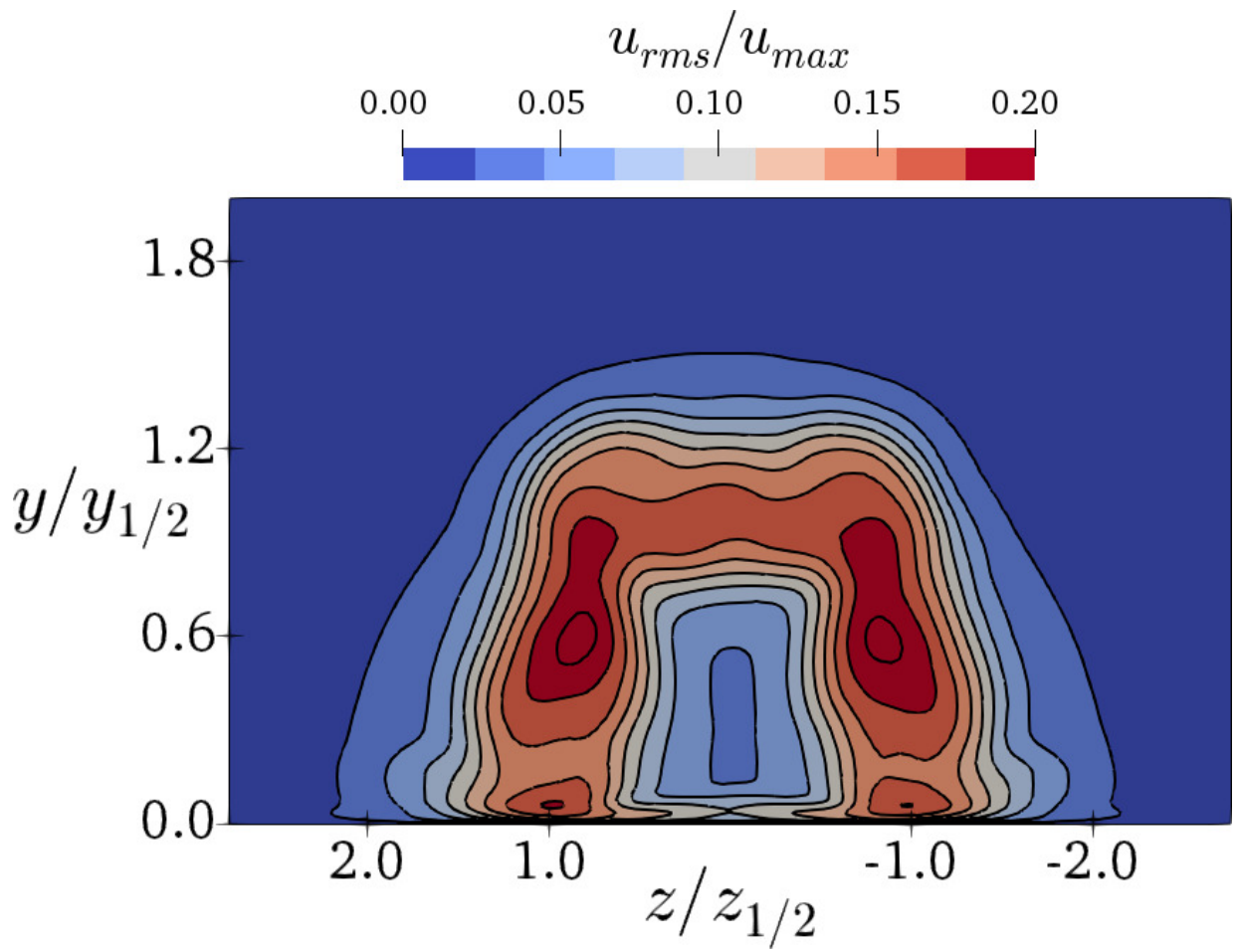
This is the author's peer reviewed, accepted manuscript. However, the online version of record will be different from this version once it has been copyedited and typeset.

PLEASE CITE THIS ARTICLE AS DOI: 10.1063/5.0031138



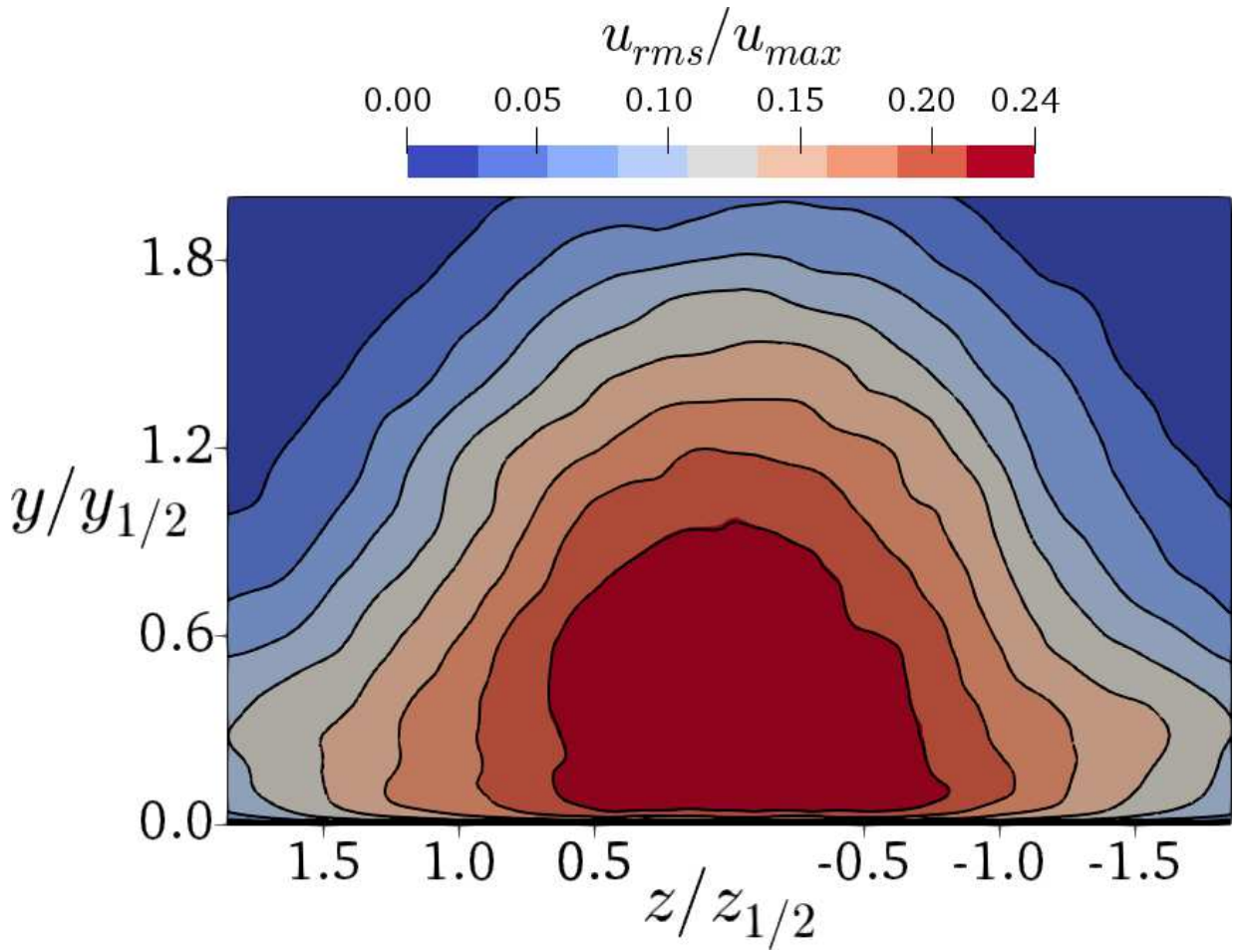
This is the author's peer reviewed, accepted manuscript. However, the online version of record will be different from this version once it has been copyedited and typeset.

PLEASE CITE THIS ARTICLE AS DOI: 10.1063/5.0031138



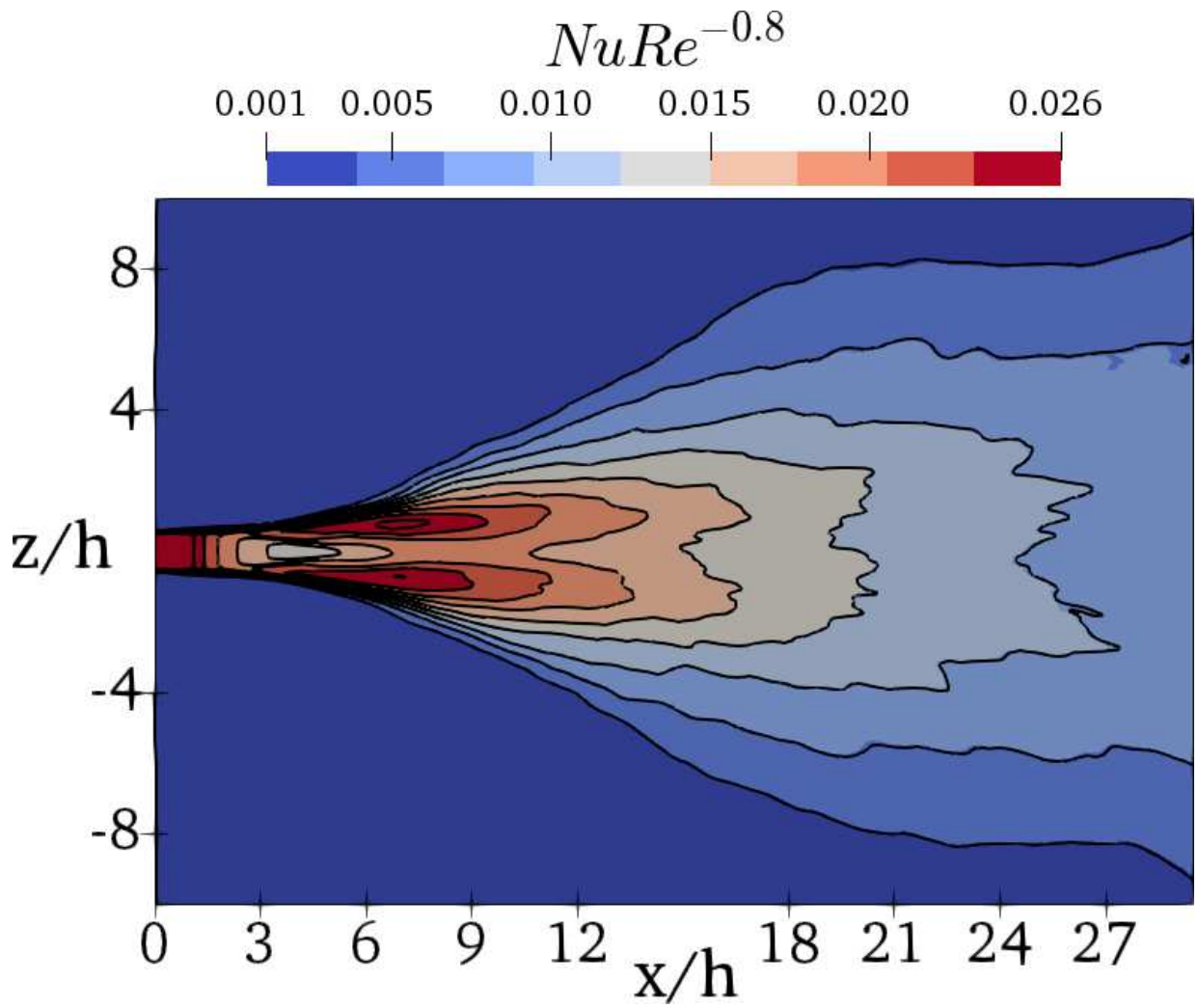
This is the author's peer reviewed, accepted manuscript. However, the online version of record will be different from this version once it has been copyedited and typeset.

PLEASE CITE THIS ARTICLE AS DOI: 10.1063/5.0031138



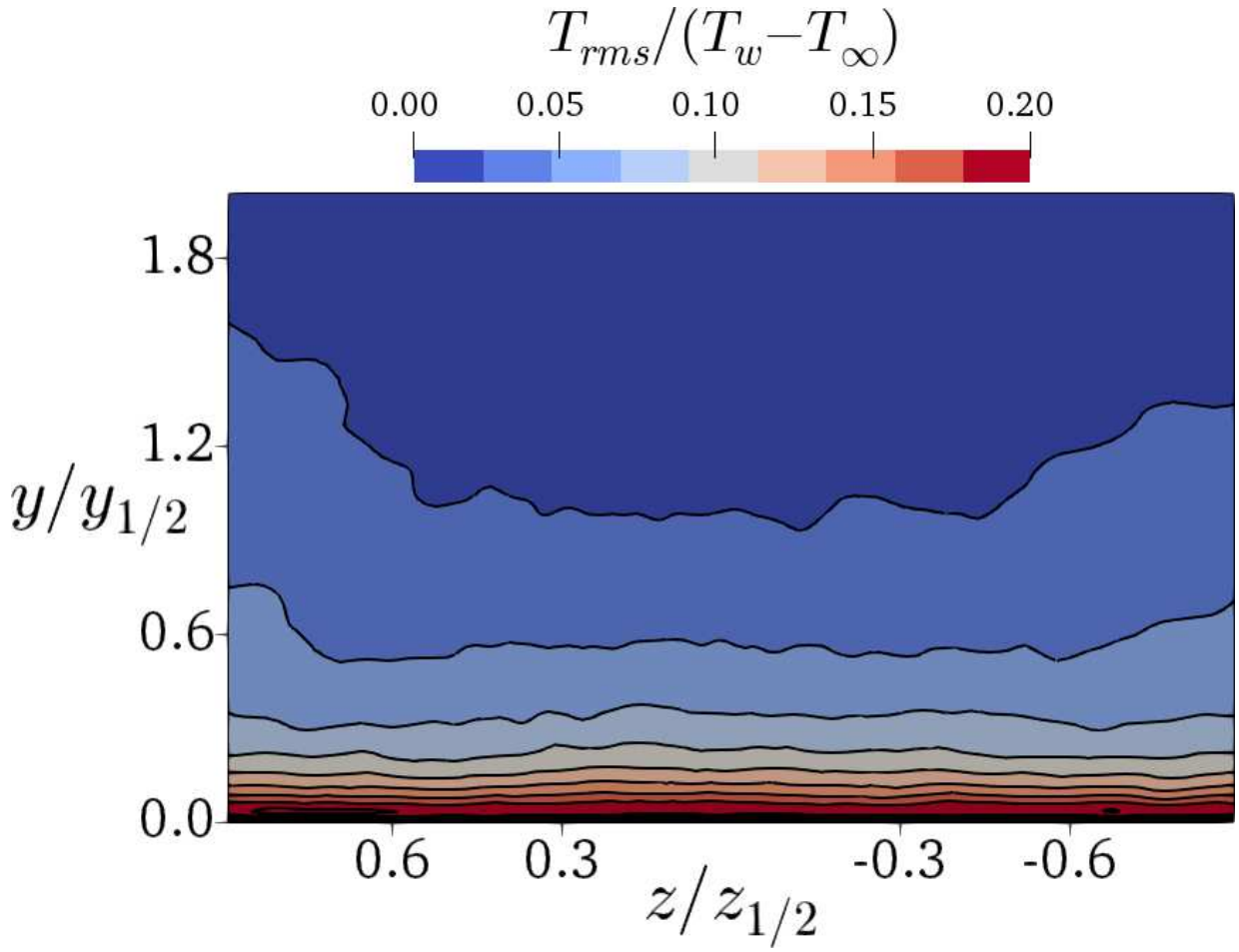
This is the author's peer reviewed, accepted manuscript. However, the online version of record will be different from this version once it has been copyedited and typeset.

PLEASE CITE THIS ARTICLE AS DOI: 10.1063/5.0031138

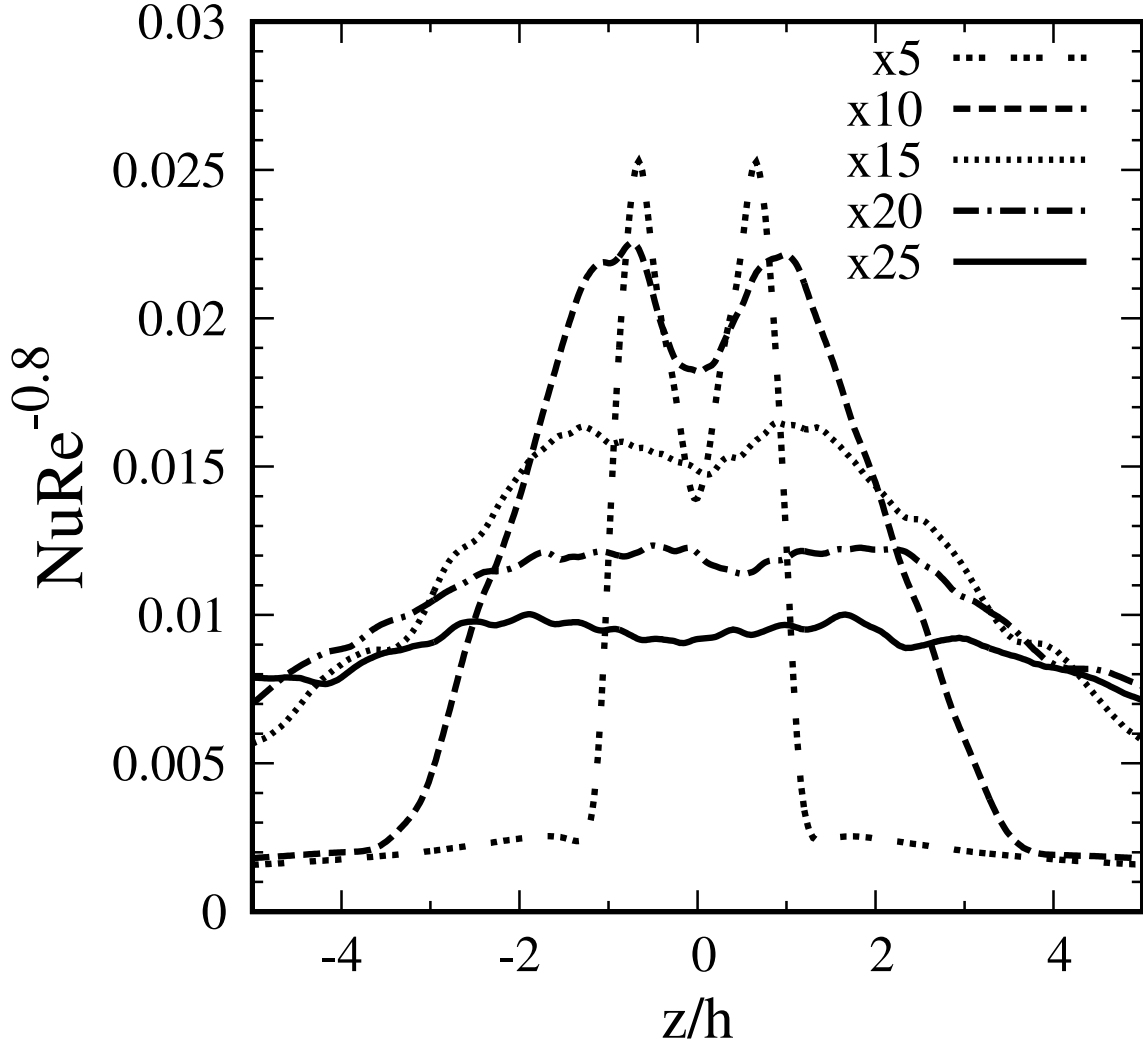


This is the author's peer reviewed, accepted manuscript. However, the online version of record will be different from this version once it has been copyedited and typeset.

PLEASE CITE THIS ARTICLE AS DOI: 10.1063/5.0031138

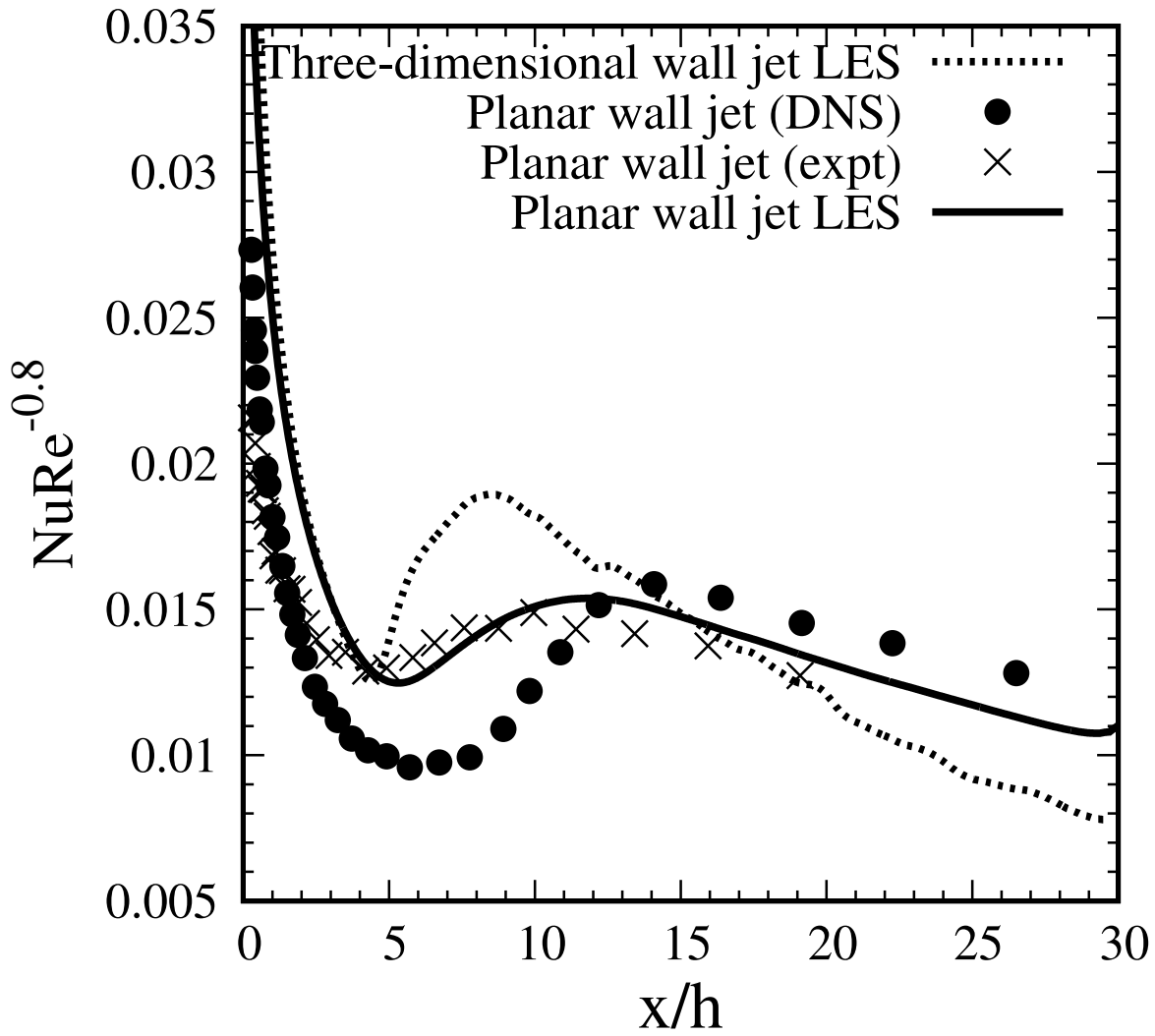


This is the author's peer reviewed, accepted manuscript. However, the online version of record will be different from this version once it has been copyedited and typeset.
PLEASE CITE THIS ARTICLE AS DOI: 10.1063/5.0031138



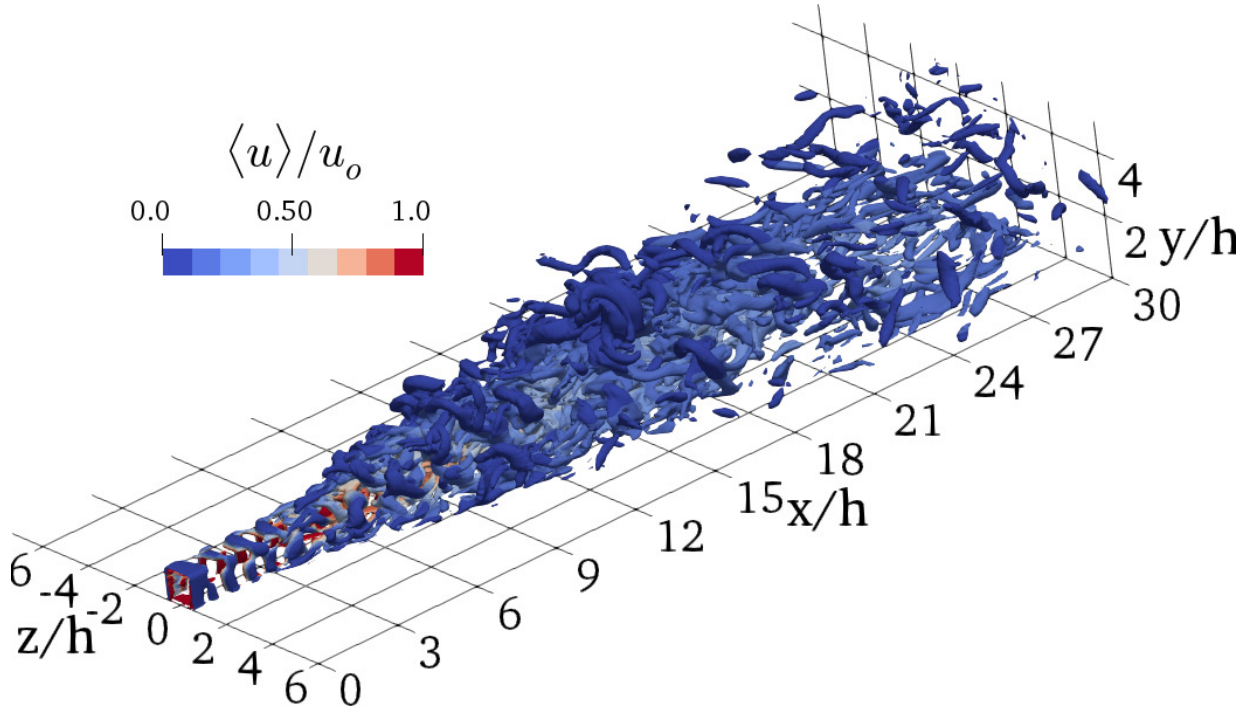
This is the author's peer reviewed, accepted manuscript. However, the online version of record will be different from this version once it has been copyedited and typeset.

PLEASE CITE THIS ARTICLE AS DOI: 10.1063/5.0031138



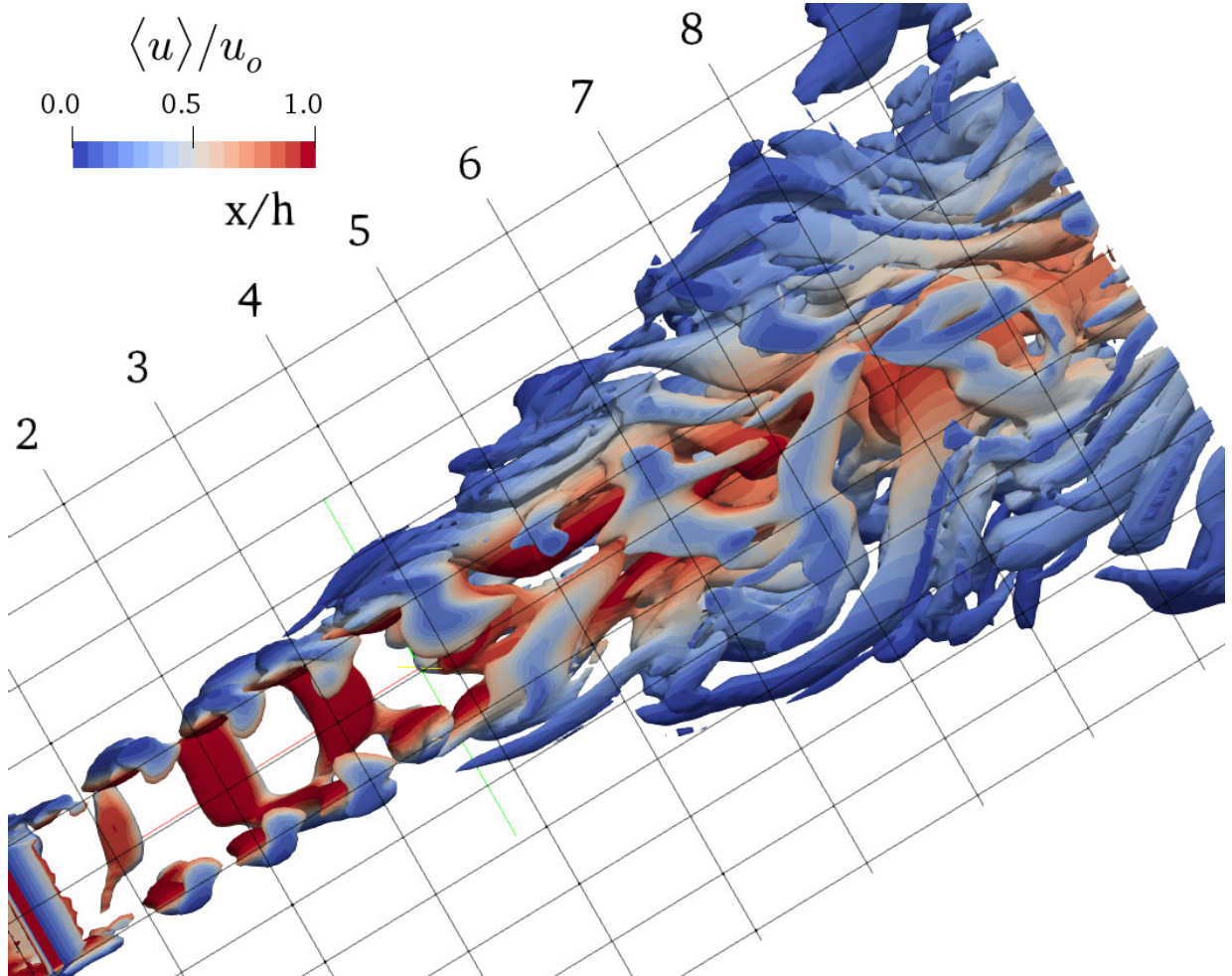
This is the author's peer reviewed, accepted manuscript. However, the online version of record will be different from this version once it has been copyedited and typeset.

PLEASE CITE THIS ARTICLE AS DOI: 10.1063/5.0031138



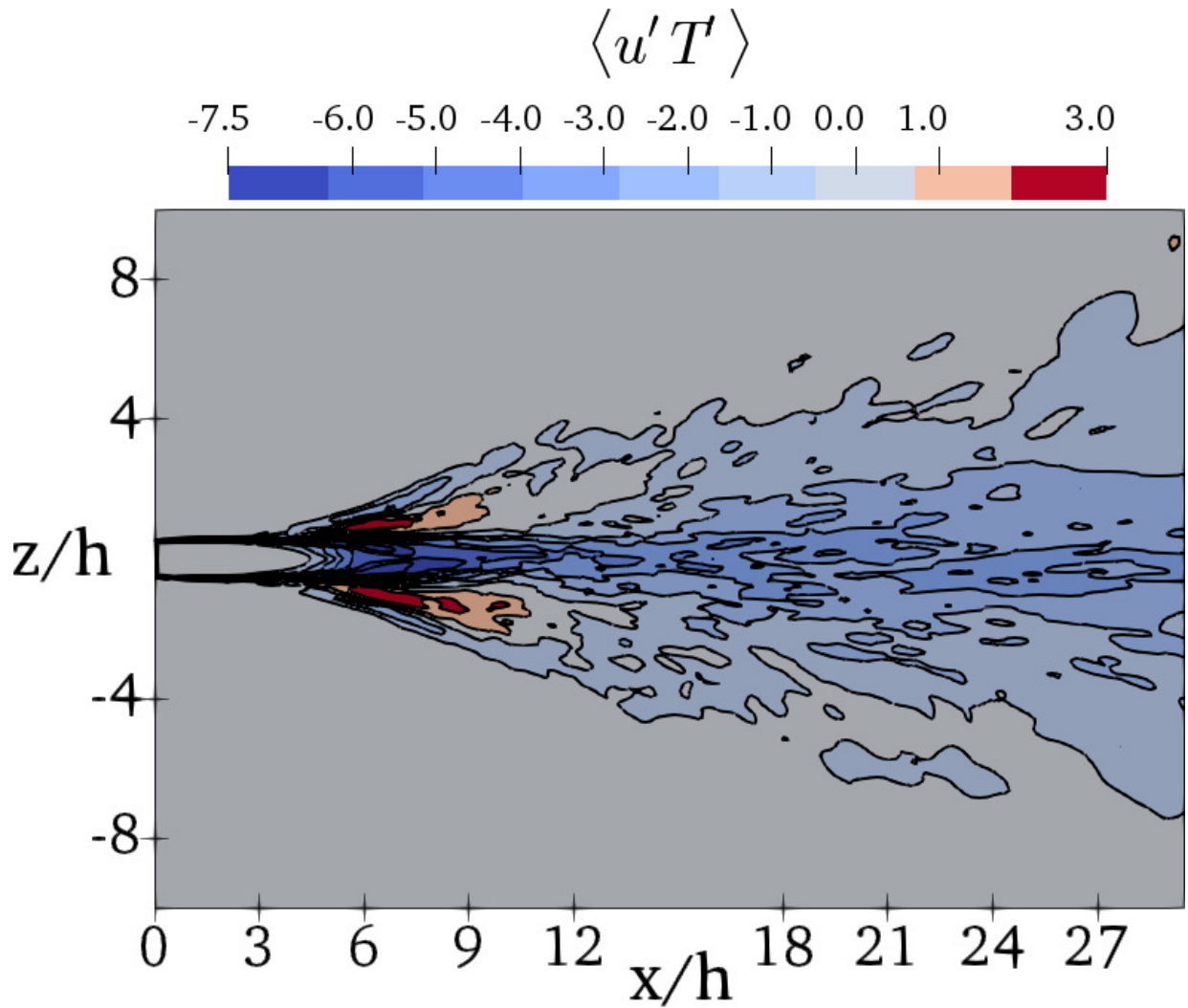
This is the author's peer reviewed, accepted manuscript. However, the online version of record will be different from this version once it has been copyedited and typeset.

PLEASE CITE THIS ARTICLE AS DOI: 10.1063/5.0031138



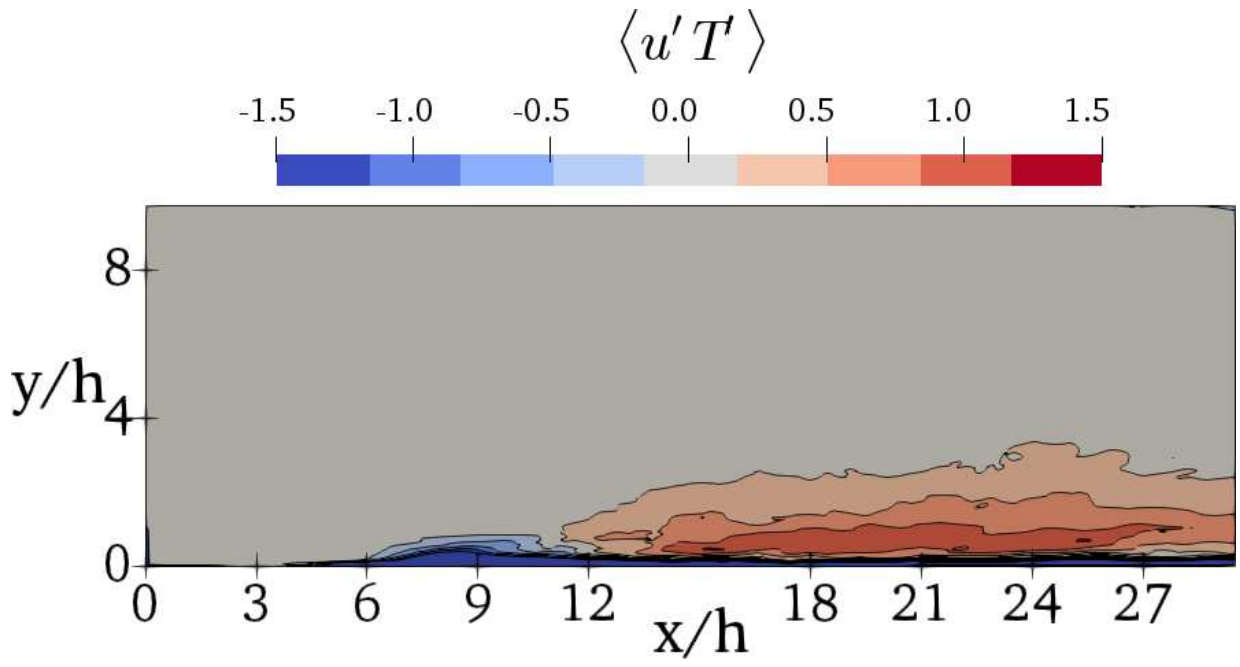
This is the author's peer reviewed, accepted manuscript. However, the online version of record will be different from this version once it has been copyedited and typeset.

PLEASE CITE THIS ARTICLE AS DOI: 10.1063/5.0031138



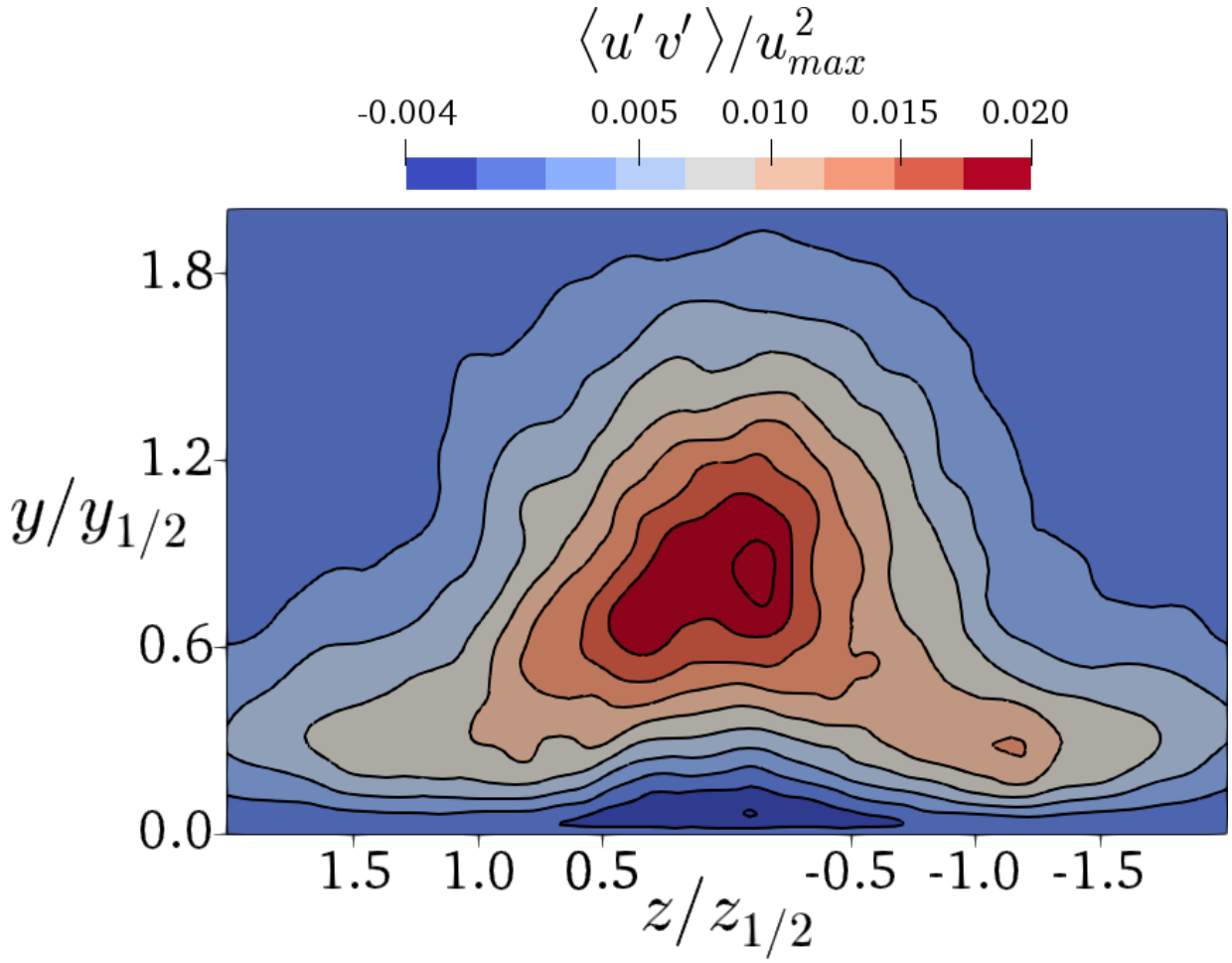
This is the author's peer reviewed, accepted manuscript. However, the online version of record will be different from this version once it has been copyedited and typeset.

PLEASE CITE THIS ARTICLE AS DOI: 10.1063/5.0031138



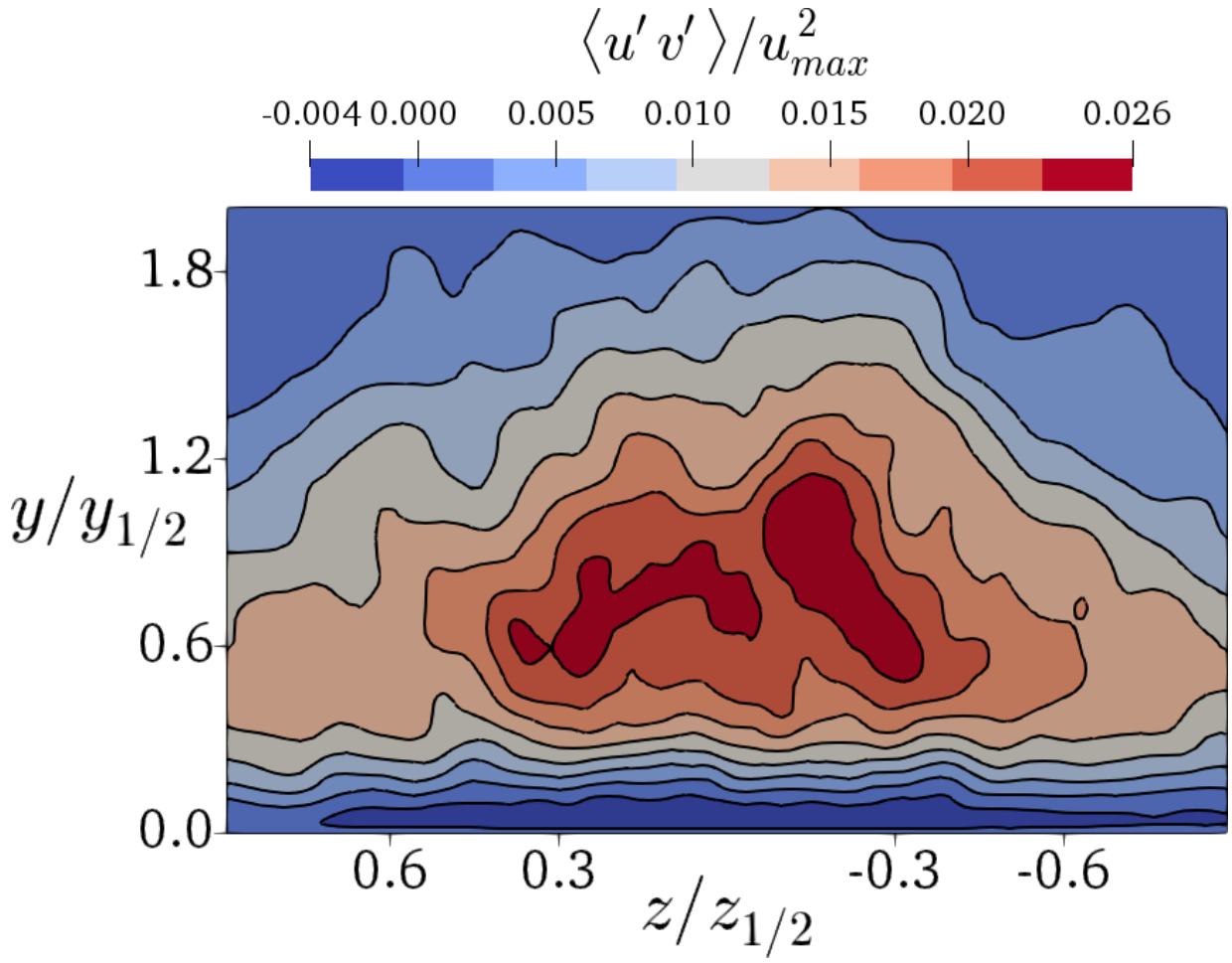
This is the author's peer reviewed, accepted manuscript. However, the online version of record will be different from this version once it has been copyedited and typeset.

PLEASE CITE THIS ARTICLE AS DOI: 10.1063/5.0031138



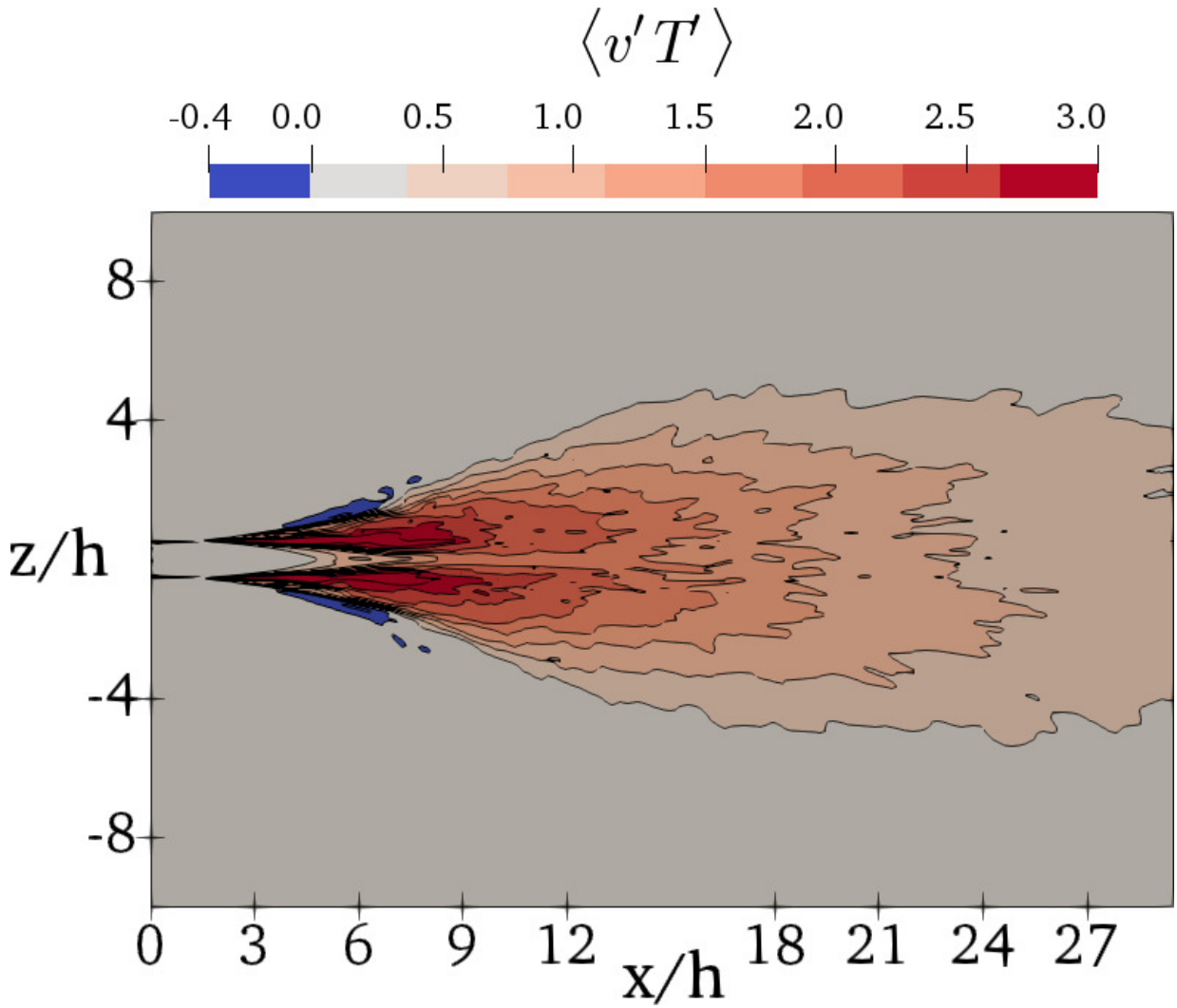
This is the author's peer reviewed, accepted manuscript. However, the online version of record will be different from this version once it has been copyedited and typeset.

PLEASE CITE THIS ARTICLE AS DOI: 10.1063/5.0031138



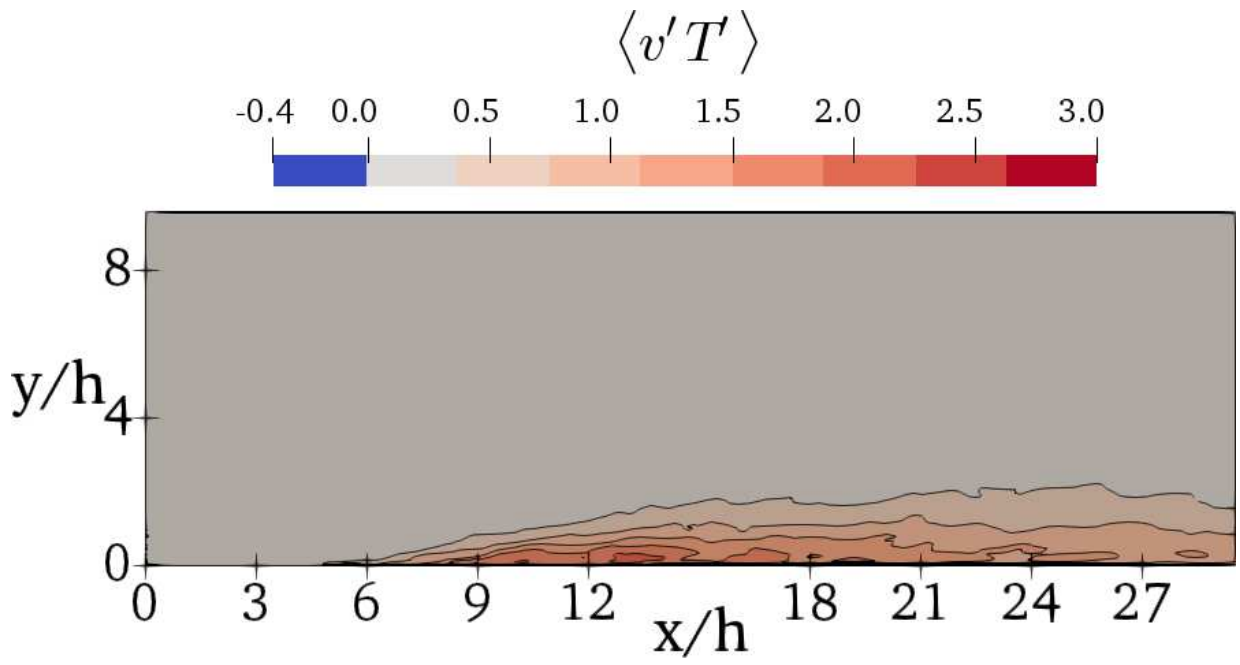
This is the author's peer reviewed, accepted manuscript. However, the online version of record will be different from this version once it has been copyedited and typeset.

PLEASE CITE THIS ARTICLE AS DOI: 10.1063/5.0031138



This is the author's peer reviewed, accepted manuscript. However, the online version of record will be different from this version once it has been copyedited and typeset.

PLEASE CITE THIS ARTICLE AS DOI: 10.1063/5.0031138



This is the author's peer reviewed, accepted manuscript. However, the online version of record will be different from this version once it has been copyedited and typeset.

PLEASE CITE THIS ARTICLE AS DOI: 10.1063/5.0031138

